MIT OpenCourseWare
http://ocw.mit.edu

Continuum Electromechanics

For any use or distribution of this textbook, please cite as follows:

Melcher, James R. *Continuum Electromechanics*. Cambridge, MA: MIT Press, 1981.
Copyright Massachusetts Institute of Technology. ISBN: 9780262131650. Also
available online from MIT OpenCourseWare at http://ocw.mit.edu (accessed MM DD,
YYYY) under Creative Commons license Attribution-NonCommercial-Share Alike.

For more information about citing these materials or our Terms of Use, visit:
http://ocw.mit.edu/terms.

9

Electromechanical Flows
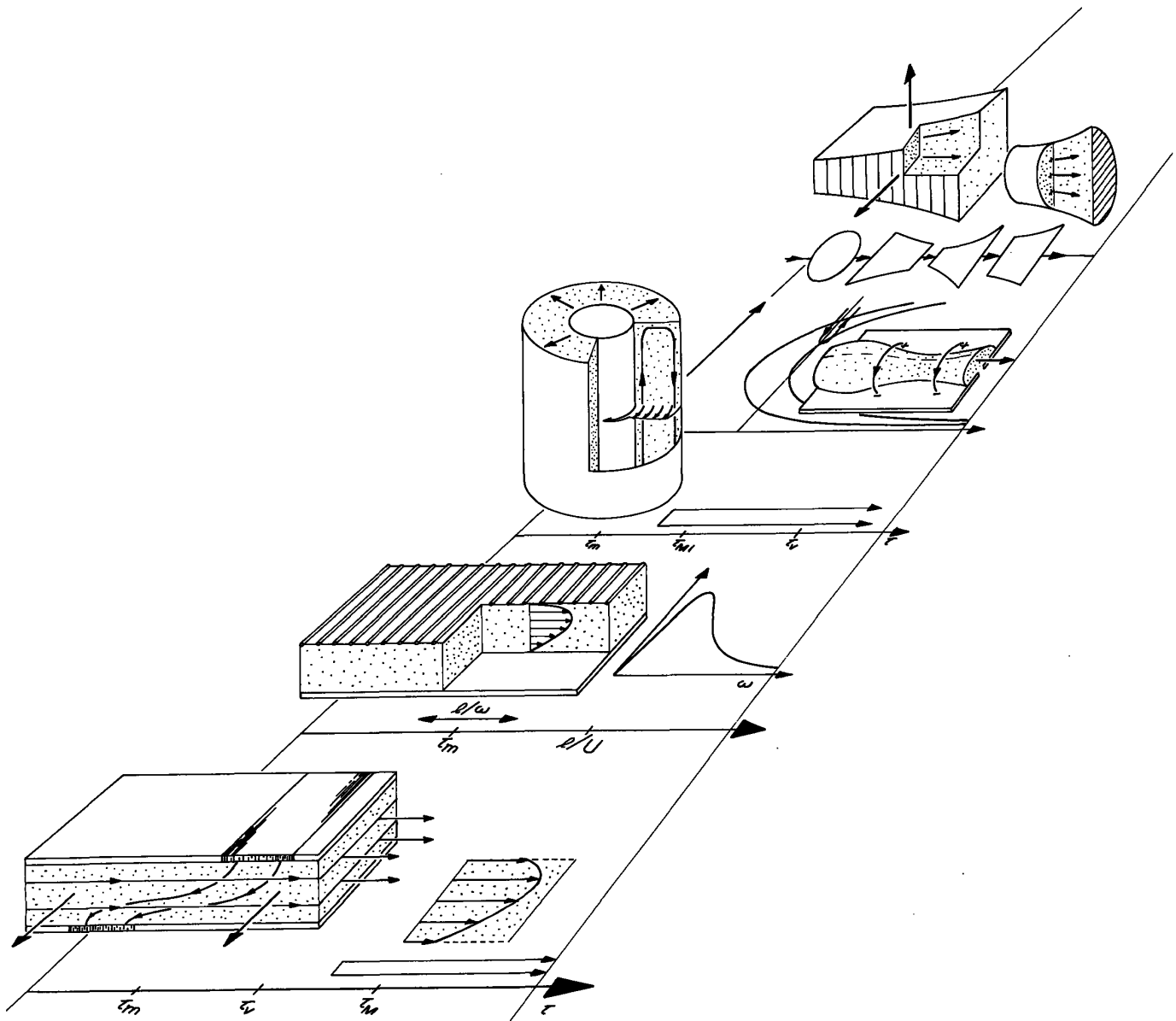
9.1 Introduction

The dynamics of fluids perturbed from static equilibria, considered in Chap. 8, illustrate mechanical and electromechanical rate processes. Identified with these processes are characteristic times. Approximations are then motivated by recognizing the hierarchy of these times and the temporal range of interest. For example, if the response to a sinusoidal steady-state drive having the frequency ω is of interest, the range is in the neighborhood of $\tau = 1/\omega$. Even for a temporal transient, where the natural frequencies are at the outset unknown, approximations are eventually justified by seeing where the reciprocal of a given natural frequency fits into the hierarchy of characteristic times.

In this chapter, it is steady flows and the establishment of such flows that is of interest. Typically, the characteristic times from Chap. 8 are now to be compared to a transport time, ℓ/u. The recognition of simplifying approximations becomes even more important, because nonlinear equations are likely to be an essential part of a model.

The requirement for a static equilibrium that force densities be irrotational is emphasized in Sec. 8.2. Taken up in Sec. 9.2 is the question, what types of flow can result from application of such force densities? This is the first of 11 sections devoted to homogeneous flows, where such properties as the mass density and electrical conductivity are uniform throughout the flow region.

Some of the most practical interactions between fields and fluids can be represented by a force density or surface force density that is determined without regard for the fluid motion or geometry. Such imposed surface and volume force density flows are the subject of Secs. 9.3-9.8. In Sec. 9.3, fully developed flows are described in such a way that their application to a wide range of problems should be evident. By way of illustration, surface coupled and volume coupled electric and magnetic flows are then discussed in Secs. 9.4 and 9.5. Liquid metal magnetohydrodynamic induction pumps usually fit the model of Sec. 9.5.

To appreciate a fully developed flow, it is necessary to consider the flow development. In Sec. 9.6, this is done by examining the temporal transient that results as a closed system is suddenly turned on and the steady flow allowed to establish itself. Then, in terms of boundary layers, the spatial transient is discussed. In addition to its application to surface coupled flows, illustrated in Sec. 9.7, the boundary layer model is applied to a self-consistent bulk coupled flow in Sec. 9.12. In Secs. 9.6 and 9.7, viscous diffusion is of interest, both fluid inertia and viscosity are important and times of interest are, by definition, on the order of the viscous diffusion time.

Illustrated in Sec. 9.8 are an important class of electromechanical models in which the bulk flow is described by linear equations. Here, transport times are long compared to the viscous diffusion time and "creep flow" prevails.

The self-consistent imposed field flows of Secs. 9.9-9.12 give the opportunity to broaden the range of dynamical processes. In the first two of these sections, magnetohydrodynamic processes are taken up. The magnetic diffusion time is short compared to the other times of interest, the viscous diffusion time and the magneto-inertial time. These sections first illustrate how the field alters fully developed flows and then considers how the electromechanics contributes to temporal flow development. The electrohydrodynamic approximation discussed and illustrated in the last two sections of this part is based on having a self-precipitation time for unipolar charges that is long compared to other times of interest, for example, an electroviscous time.

With the introduction of inhomogeneity come more characteristic dynamical times. These are illustrated for systems having a static equilibrium and abrupt discontinuities in properties in Secs. 8.9-8.16. Typically, the associated characteristic times represent propagation of surface waves. Smoothly distributed inhomogeneities, Secs. 8.17-8.18, give rise to related internal waves with their characteristic times. The flow models developed in Sec. 9.13 and illustrated in Sec. 9.14 incorporate wave phenomena similar to those from Chap. 8. The wave phenomena show up in steady flow situations through critical conditions, often expressed in terms of the ratio of a convective velocity to a wave velocity, i.e., as a Mach number. In essence these numbers are the ratio of transport times to wave transit times. <u>Times</u> of interest in these sections, which <u>reflect the existence</u> of waves, are a capillary time $\tau_\gamma = \sqrt{\gamma/\rho\ell^2}$ (Sec. 8.9), a gravity time $\tau_g = \sqrt{g\,(\rho_b - \rho_a)/(\rho_b + \rho_a)\ell}$ (Sec. 8.9) and various magneto- and electro-inertial times (Secs. 8.10-8.15).

In view of Sec. 8.8 on magneto-acoustic and electro-acoustic waves, it should be expected that additional times introduced in the remaining sections on compressible flow are the transit times for acoustic and acoustic related waves. Sections 9.15 and 9.17 bring into the discussion the additional physical laws required to represent interactions with the internal energy subsystem of a gas. Here, the energy equation is derived and thermodynamic variables needed in subsequent sections defined. These laws are not only necessary for the description of thermal-to-electrical energy conversion (to be taken

up in Secs. 9.21-9.23), but also can be used to describe convective heat transfer.

The quasi-one-dimensional model introduced in Sec. 9.19 is the basis for the various energy conversion systems discussed in the remaining sections. Once again, even in steady flows, the role of wave propagation is unavoidable. As in Sec. 9.14, flow through energy conversion devices is dependent on the fluid velocity relative to a wave velocity. This time, the waves are acoustic related.

In Secs. 9.21 and 9.23, the energy conversion process is again highlighted. These models, which include the thermodynamics as well as the electromechanics, hark back to the prototype magnetic and electric d-c machines introduced in Secs. 4.10 and 4.14. The MHD and EHD energy converters combine the functions of the turbine and a generator in a conventional power generating plant. Thus, they give the opportunity to understand the overall thermodynamic limitations of the energy conversion process.

To fully appreciate the steady flows of inhomogeneous fluids, Sec. 9.14, and of compressible fluids, Secs. 9.20-9.22, flow transients predicted by the same quasi-one-dimensional models should be studied. These are taken up in Chap. 12, where the method of characteristics is applied to nonlinear flows involving propagating wave phenomena. In this chapter, nonlinear processes represented by quasi-one-dimensional models are represented by systems of ordinary differential equations. Similarity solutions, introduced in Sec. 6.9, are now extended to nonlinear equations.

9.2 Homogeneous Flows with Irrotational Force Densities

The static equilibria of Secs. 8.1-8.5 illustrate electrical to mechanical coupling approximated by irrotational magnetic and electric force densities. In this section, yet another field configuration that can be represented by a force density of the form $\vec{F} = -\nabla \xi$ is introduced. But more important, steady flows are to be illustrated. The point in this section is that now, given boundary conditions stipulating the fluid velocity, an irrotational force density interacts with the flow of a homogeneous incompressible fluid to alter the pressure distribution, but not the flow pattern.

Inviscid Flow: Recall that for an irrotational inviscid flow, the velocity potential satisfies Laplace's equation (Eq. 7.8.10)

$$\nabla^2 \theta = 0; \quad \vec{v} = -\nabla\theta \tag{1}$$

With boundary conditions on $\vec{v}$ specified over the surface enclosing the volume of interest, the flow is therefore uniquely determined without regard for the force densities. However, through ξ, the force density does contribute to the pressure distribution. From Eq. 7.8.11,

$$p = -\frac{1}{2}\rho\vec{v}\cdot\vec{v} + \rho\vec{g}\cdot\vec{r} - \xi + \Pi \tag{2}$$

As an example of an irrotational force density, consider the MQS low magnetic Reynolds number flow in two dimensions (x,y) through a region where a perpendicular uniform magnetic field, $\vec{H} = H_0\vec{i}_z$, is imposed. The current density is solenoidal with components in the x-y plane only. It is therefore represented in terms of the z component of a vector potential (Cartesian coordinates, Table 2.18.1)

$$\vec{J} = \frac{\partial A}{\partial y}\vec{i}_x - \frac{\partial A}{\partial x}\vec{i}_y \tag{3}$$

Because current induced by the motion is negligible compared to that imposed, throughout a region of uniform electrical conductivity, $\vec{J}$ is also approximately irrotational. Hence, within such a region

$$\nabla^2 A = 0 \tag{4}$$

This expression is justified provided that $R_m \equiv \mu_0\sigma\ell u \ll 1$, as is evident from a normalization of Eq. 6.5.3 in the fashion of Eq. 6.2.9. The force density is expressed in terms of A by using Eq. 3 for $\vec{J}$ and approximating the field intensity as the imposed field:

$$\vec{F} = \vec{J} \times \mu_0 H_0\vec{i}_z = -\nabla\xi ; \quad \xi = \mu_0 H_0 A \tag{5}$$

Remember that H_0 is by assumption much greater than the field induced by $\vec{J}$. From Ampere's law, this requires that $|\vec{J}|\ell \ll H_0$, where ℓ is a typical length.

Uniform Inviscid Flow: The channel flow sketched in Fig. 9.2.1a has fluid entering at the left with a uniform velocity profile and leaving at the right with the same profile. A flow satisfying Eq. 1 and the additional boundary conditions that there be no normal velocity on the rigid upper and lower boundaries is simply a uniform velocity everywhere, $\theta = -Uy$.
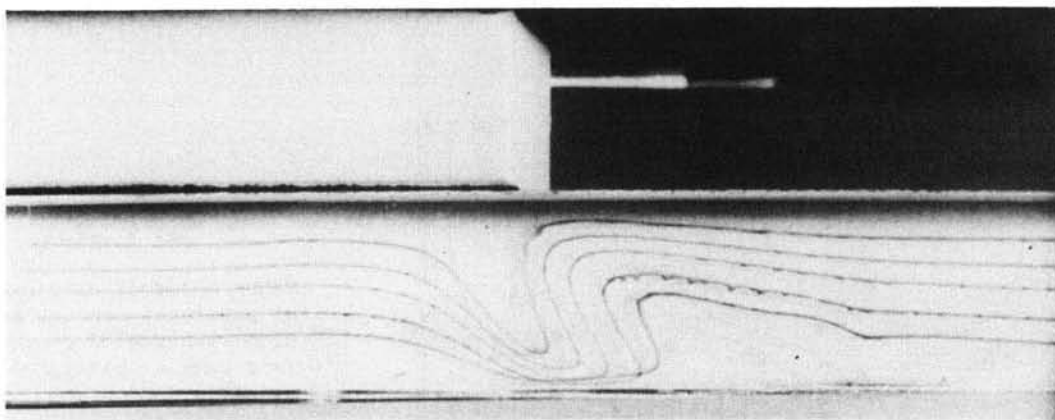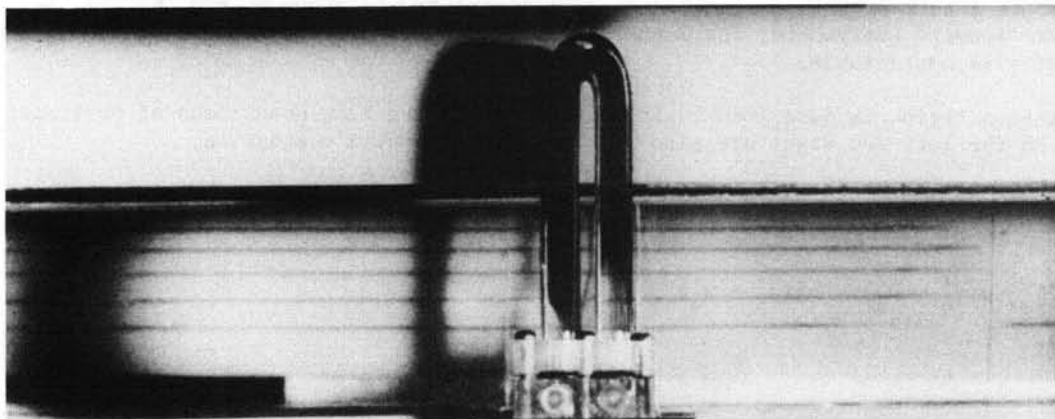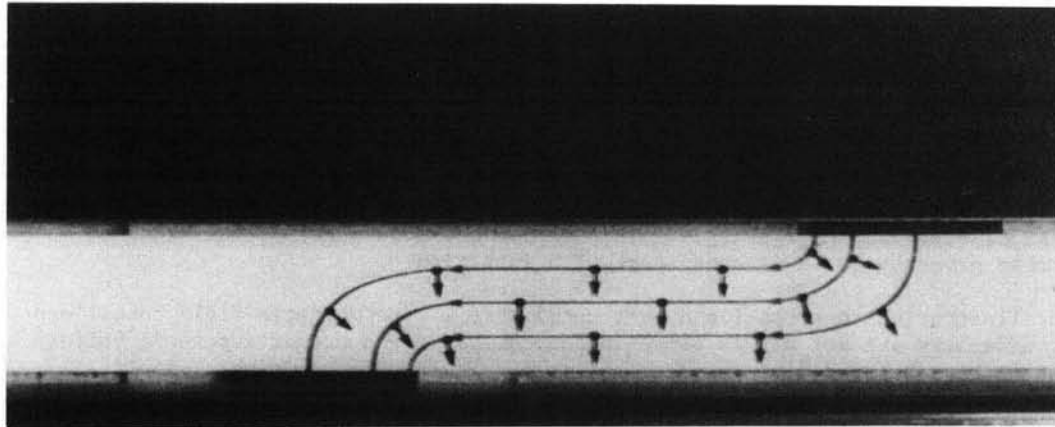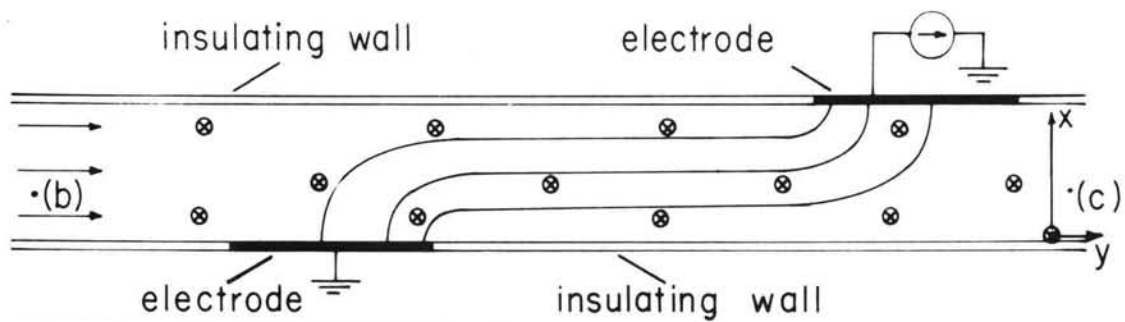
Fig. 9.2.1. (a) Electrolyte is channeled by insulating walls through region of uniform magnetic field perpendicular to flow (positive in the y direction). (b) From Reference 7, Appendix C, sketch of current and $\vec{J} \times \vec{B}$ densities in experiment with H_0 positive and I negative. (c) With H_0 uniform, extremely nonuniform but irrotational force distribution of (b) leaves plane flow undisturbed (shown by streamlines) but results in pressure rise (shown by manometer). (d) With H_0 nonuniform, strong acceleration caused by rotational force density is evident in the stirring of the flow.

Electrodes embedded in the lower and upper walls are used to pass a current through the flow. As sketched in Fig. 9.2.1b, the resulting force density, which has both vertical and horizontal components, is complicated and nonuniform. Yet, it has been asserted that the flow pattern observed in the absence of a current would be the same as seen after the current is applied. In the experiment shown in Fig. 9.2.1c, the streamlines are in fact not appreciably different after the current is applied. What does change is the pressure distribution, as suggested by the manometer. This is predicted by Eqs. 2 and 5, which show that for any two points (α) and (β),

$$P_\alpha - P_\beta = -\frac{1}{2}\rho(v_\alpha^2 - v_\beta^2) - \rho g(x_\alpha - x_\beta) - \mu_o H_o(A^\alpha - A^\beta) \tag{7}$$

Note that

$$A^\alpha - A^\beta = i \tag{8}$$

where i is the current linked by a surface having unit length in the z direction and edges at (α) and (β) (see Sec. 2.18). Thus, with α and β the locations c and b respectively in Fig. 9.2.1a, i is the total current (per unit length perpendicular to the paper) I, and Eq. 7 becomes

$$P_c - P_b = -\frac{1}{2}\rho(v_c^2 - v_b^2) - \rho g(x_c - x_b) - \mu_o H_o I \tag{9}$$

For the conditions of Fig. 9.2.1c, $v_c = v_b$, H_o is positive and I is negative (as sketched in Fig. 9.2.1b) so the pressure rise given by Eq. 9 is consistent with intuition.

A dramatic illustration that the fluid must accelerate if the magnetic field conditions for an irrotational force density are not met is shown in Fig. 9.2.1d. The magnet imposes a uniform H_0 over the region to the left, but the region to the right is in the nonuniform fringing field.

Inviscid Pump or Generator with Arbitrary Geometry: The generalization of the configuration to a channel flow through a duct of arbitrary two-dimensional geometry is shown by Fig. 9.2.2. To insure an irrotational force density everywhere, the magnetic field need only be uniform over the region where the current density is appreciable.

The interaction region is described by Eq. 9. To relate the flow conditions at positions (d) and (a), the "legs" to the left and right are also described by Bernoulli's equation,

$$P_d - P_c = -\frac{1}{2}\rho(v_d^2 - v_c^2) - \rho g(x_d - x_c) \tag{10}$$

$$P_d - P_a = -\frac{1}{2}\rho(v_b^2 - v_a^2) - \rho g(x_b - x_a) \tag{11}$$
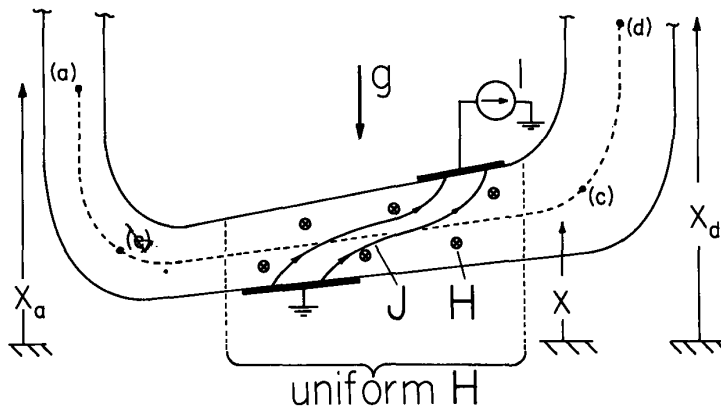

Fig. 9.2.2

Magnetohydrodynamic pump or generator configuration with region of current density permeated by uniform $\bar{H}$ out of paper.

Addition of these last three expressions gives the desired pressure-velocity relation for the entire system:

$$P_d - P_a = - \frac{1}{2} \rho (v_d^2 - v_a^2) - \rho g (x_d - x_a) - \mu_o H_o I \qquad (12)$$

Again, note that this simple relation applies regardless of electrode geometry.

   <u>Viscous Flow</u>: Finally, observe that if the force density is irrotational, and hence takes the form $\vec{F} = -\nabla \xi$, it can be lumped with the pressure gradient. For an incompressible homogeneous flow, the pressure appears only in the force equation.

   With the redefinition of the pressure, $p \rightarrow p + \xi$, the equations of motion are no different than in the absence of the field. Thus, if the boundary conditions do not involve the pressure, it is clear that the flow pattern must be the same with and without the field. In the experiment of Fig. 9.2.1, the flow is probably more nearly fully developed (as defined in Sec.9.3) than inviscid and hence has vorticity. Yet, the only effect of the irrotational magnetic force density is to revise the pressure distribution.

FLOWS WITH IMPOSED SURFACE AND VOLUME FORCE DENSITIES

9.3 <u>Fully Developed Flows Driven by Imposed Surface and Volume Force Densities</u>

   Fully developed flows are stationary equilibria established after either a temporal or a spatial transient. Flow established by setting the coaxial wall of a Couette viscometer into steady rotation is an example of the former. Typical of a spatial transient is steady flow through a conduit of uniform cross section. As the fluid first enters a pipe, the velocity profile is determined by the entrance conditions. But, as an element progresses, the viscous shear stresses from the walls penetrate into the flow until they are effective over the entire cross section. At this point, the flow becomes independent of longitudinal position and is said to be fully developed.

   For a region of rectangular cross section, with its x dimension much less than the y dimension, the fully developed flow is a special type of plane flow:

$$\vec{v} = v(x)\vec{i}_y \qquad (1)$$

Note that continuity is automatically satisfied, i.e., $\vec{v}$ is solenoidal.

   The objective of this and the next two sections is an illustration of how viscous forces can balance electric and magnetic forces imposed either at surfaces or throughout the fluid volume. By "imposed," it is meant that the fluid motion does not play a significant part in determining the electromagnetic force distribution. Sections 9.4 and 9.5 illustrate the flow itself.

   Because $\partial \vec{v}/\partial t = 0$ and (from Eq. 1) $\vec{v} \cdot \nabla \vec{v} = 0$, there is no acceleration. The Navier-Stokes equation, Eq. 7.16.6, becomes

$$\nabla p = \nabla (\rho \vec{g} \cdot \vec{r}) + \vec{F} + \eta \nabla^2 \vec{v} \qquad (2)$$

The force density is only a function of x, so a scalar ξ can always be found such that $F_x = -\partial \xi(x)/\partial x$. Thus, the x component of Eq. 2 becomes

$$\frac{\partial p'}{\partial x} = 0; \quad p' \equiv p - \rho \vec{g} \cdot \vec{r} + \xi(x) \qquad (3)$$

It follows that p' is uniform over the cross section. The x dependence of p is whatever it must be to balance the transverse gravitational and electromagnetic force components.

   In terms of p', the longitudinal component of Eq. 2 becomes

$$\frac{\partial p'}{\partial y} = F_y(x) + \eta \frac{\partial^2 v}{\partial x^2} \qquad (4)$$

Terms on the right are independent of z, so the longitudinal hybrid pressure gradient, $\partial p'/\partial z$, must also be independent of y.

   Because the force density F_y is independent of y, it can be written in terms of a tensor divergence which reduces to simply $F_y = \partial T_{yx}/\partial x$.

Integrated on x, Eq. 4 then represents the balance of electromagnetic and viscous shear stresses:

$$\frac{\partial p'}{\partial y} x = T_{yx}(x) - T_{yx}(0) + \eta[\frac{\partial v}{\partial x}(x) - \frac{\partial v}{\partial x}(0)] \qquad (5)$$

It is instructive to note the physical origins of this expression. It can also be obtained by writing the y component of force balance for the fluid within a control volume of incremental length in the y direction, unit depth in the z direction and with transverse surfaces at x = 0 and x = x, respectively. In the absence of a hybrid pressure gradient, the fully developed flow is simply a balance of viscous and electromagnetic shear stresses.

To determine the velocity profile, Eq. 5 is once again integrated from x = 0 where $v = v^\beta$ to x = x, and solved for v(x). The constant $\partial v/\partial x(0)$ is determined by evaluating v(x) at x = Δ where it equals v^α. The resulting velocity profile is the first of those given in Table 9.3.1.

The circulating flow and axial flow through a circular cylindrical annulus, also shown in the table are other examples where a fully developed flow is found by what amounts to the same stress balance as exploited in the planar case. Note that for the circulating flow, the pressure gradient in the flow direction is zero. Determination of the velocity profiles summarized in Table 9.3.1 is left for the problems.

Table 9.3.1. Three fully developed flows.

$$v(x) = v^\beta(1 - \frac{x}{\Delta}) + v^\alpha \frac{x}{\Delta}$$

$$+ \frac{\Delta^2}{2\eta} \frac{\partial p'}{\partial y}\left[(\frac{x}{\Delta})^2 - \frac{x}{\Delta}\right] - \frac{1}{\eta}\int_0^x T_{yx}dx + \frac{x}{\eta\Delta}\int_0^\Delta T_{yx}dx \qquad (a)$$

$$v = \frac{1}{(\frac{\alpha}{\beta} - \frac{\beta}{\alpha})}[v^\alpha(\frac{r}{\beta} - \frac{\beta}{r}) + v^\beta(\frac{\alpha}{r} - \frac{r}{\alpha})]$$

$$+ \alpha\frac{(\frac{r}{\beta} - \frac{\beta}{r})}{(\frac{\alpha}{\beta} - \frac{\beta}{\alpha})\eta}\int_\beta^\alpha \frac{T_{\theta r}}{r} dr - \frac{r}{\eta}\int_\beta^r \frac{T_{\theta r}}{r} dr \qquad (b)$$

$$v = v^\alpha\frac{\ln(\frac{r}{\beta})}{\ln(\frac{\alpha}{\beta})} + v^\beta\frac{\ln(\frac{\alpha}{r})}{\ln(\frac{\alpha}{\beta})}$$

$$+ \frac{1}{4\eta}\frac{\partial p'}{\partial z}\left[(r^2 - \beta^2) - (\alpha^2 - \beta^2)\frac{\ln(\frac{r}{\beta})}{\ln(\frac{\alpha}{\beta})}\right]$$

$$- \frac{1}{\eta}\int_\beta^r T_{zr}dr + \frac{\ln(\frac{r}{\beta})}{\eta\ln(\frac{\alpha}{\beta})}\int_\beta^\alpha T_{zr}dr \qquad (c)$$

where

$$p' \equiv p - \rho(\vec{g}\cdot\vec{r}) + \mathcal{E}(r); \quad F_r = -\frac{d\mathcal{E}}{dr}$$

9.4 Surface-Coupled Fully Developed Flows

Fully developed flows are often used in quasi-one-dimensional models. Examples in this section illustrate by using the results of Sec. 9.3 to describe liquid circulations. They also illustrate how shearing surface force densities can act in consort with viscous shear stresses to give rise to volume fluid motions. The example treated in detail is EQS, with the surface force density resulting from the combination of a monolayer of charge and a tangential electric field at a "free" interterface. If the magnetic skin depth is short compared to the depth of the fluid, similar flows can result from subjecting the interface of a liquid metal to a magnetic shear stress, as suggested by Sec. 6.8. Consider first a specific case study, after which it is appropriate to identify the general nature of the interactions that it illustrates.

Charge-Monolayer Driven Convection: A semi-insulating liquid fills an insulating container to a depth b. Electrodes to the right and left have the potential difference V_0. Provided the charge convection at the interface is not appreciable, the resulting current density in the liquid is uniformly distributed throughout the volume of the liquid. As discussed in Sec. 5.10, at least insofar as it can be described by an ohmic conduction model, the liquid does not support a volume free charge density. It also has a uniform permittivity. Hence, there is no volumetric electrical force. However, an electrical force does exist at the interface, where the conductivity is discontinuous. In this "Taylor Pump" the electrode above the interface is canted in just such a way as to make the resulting electric shearing surface force density tend to be uniform over most of the interface. To see that this is so, observe that, if effects of convection can be ignored, in the liquid

$$\Phi = V_o \frac{(y - \ell)}{\ell} \; ; \quad \vec{E} = - \frac{V_o}{\ell} \vec{i}_y; \quad 0 < x < b \tag{1}$$

Because $a \ll \ell$, the electric field between interface and slanted plate is essentially in the x direction and given by the plate-interface potential difference divided by the spacing:

$$\vec{E} = \frac{V_o y/\ell}{h(y)} \vec{i}_x = \frac{V_o}{a} \vec{i}_x; \quad b < x < \frac{ay}{\ell} + b \tag{2}$$

Note that, at the interface, the tangential electric field is continuous and there is no normal electric field on the liquid side. Thus, the interfacial surface force density is

$$\vec{T} = \frac{1}{2} [\![\varepsilon E_x^2 - \varepsilon E_y^2]\!] \vec{i}_x + [\![\varepsilon E_x E_y]\!] \vec{i}_y = \frac{1}{2} \left(\frac{V_o}{a} \right)^2 \left[\varepsilon_o + \frac{a^2}{\ell^2} (\varepsilon - \varepsilon_o) \right] \vec{i}_x - \varepsilon_o \frac{V_o^2}{a\ell} \vec{i}_y \tag{3}$$

and, as required for a fully developed model, both the normal and shear components are independent of y.

The normal component of $\vec{T}$ is equilibrated by the liquid pressure. With the pressure of the air defined as zero, normal stress balance at the interface, where $x = b + \xi$, requires that

$$T_x = -p(x = b + \xi) \tag{4}$$

In the liquid bulk, where the flow is modeled as fully developed, Eq. 9.3.3 shows that p' is only a function of y. Here, p' is determined by substituting p' evaluated at $x = b + \xi$ into Eq. 4. It follows that

$$p' = \rho g(b + \xi) - \frac{1}{2} \left(\frac{V_o}{a} \right)^2 \left[\varepsilon_o + \left(\frac{a}{\ell} \right)^2 (\varepsilon - \varepsilon_o) \right] \tag{5}$$

Here, $\xi(y)$ is yet to be determined. If this vertical deflection of the interface is much less than the depth of the liquid layer, insofar as the flow is concerned, the fluid depth can be approximated as simply b.

Three conditions are required to determine the variables v^α, v^β and $\partial p/\partial y$ in Eq. (a) of Table 9.3.1. Two of these come from the facts that the velocity at the tank bottom is zero and that the net flow through any x-y plane is zero:

$$v(x = 0) = 0 \tag{6}$$

$$\int_0^b v\,dx = 0 \tag{7}$$

The third follows from the shear stress equilibrium at the interface, where the electrical shear stress is balanced by the viscous shear stress,

$$\frac{-\epsilon_o V_o^2}{a\ell} = \eta \frac{\partial v}{\partial x} \quad (x = b) \tag{8}$$

It follows from Eq. 6 that $v^\beta = 0$. Then, substitution of Eq. (a) of Table 9.3.1 into Eq. 7 gives the longitudinal pressure gradient in terms of the surface velocity:

$$\frac{\partial p'}{\partial y} = \frac{6\eta}{b^2} v^\alpha \tag{9}$$

This result and Eq. 8 (evaluated using Eq. (a) of Table 9.3.1) then make it possible to evaluate the surface velocity:

$$v^\alpha = - \frac{\epsilon_o V_o^2 b}{4a\ell\eta} \tag{10}$$

This velocity results from a competition between electric and viscous stresses, so it is no surprise that the transport time b/v^α is found to be on the order of the electro-viscous time $\tau_{EV} = \eta/\epsilon_o (V_o^2/a\ell)$.

Evaluated using Eqs. 9 and 10, the velocity profile follows from Eq. (a) of Table 9.3.1 as

$$v = - \frac{\epsilon_o V_o^2 b}{2\eta a\ell} \left[\frac{3}{2}(\frac{x}{b})^2 - \frac{x}{b} \right] \tag{11}$$

This is the profile shown in Fig. 9.4.1a.

As a reminder of the vertical pressure equilibrium implied by the model, it is now possible to evaluate the small variation in the liquid depth caused by the horizontal flow. Integration of Eq. 9 with v^α from Eq. 11 gives

$$p' = - \frac{3}{2} \frac{\epsilon_o V_o^2}{a\ell} (\frac{y}{b}) + \text{constant} \tag{12}$$

where p' is also given by Eq. 5. The constant is set by equating these expressions and defining the position where $\xi = 0$ as being $y = 0$. It follows that the depth varies as

$$\xi = - \frac{3}{2} \frac{\epsilon_o V_o^2}{ab\rho g} (\frac{y}{\ell}) \tag{13}$$

That the liquid depth is greatest at the left reflects the fact that the pressure is greatest at the left. Thus, in the lower 2/3's of the liquid (where there is no horizontal force density to propel the liquid) the pressure propels the liquid to the right.

The field and charge distributions have been computed under the assumption that the effects of material motion are not important. This is justified only if the fluid conductivity is large enough that the interfacial convection of charge does not compete appreciably with the volume conduction in determining the interfacial charge distribution. In retrospect, an estimate of the implied condition is obtained by considering conservation of charge for a section of the interface near the left end. Here, the surface velocity falls from its peak value to zero in a horizontal distance on the order of the depth b. If the current convected at the interface is to be small compared to that conducted to the electrode from the bulk, then
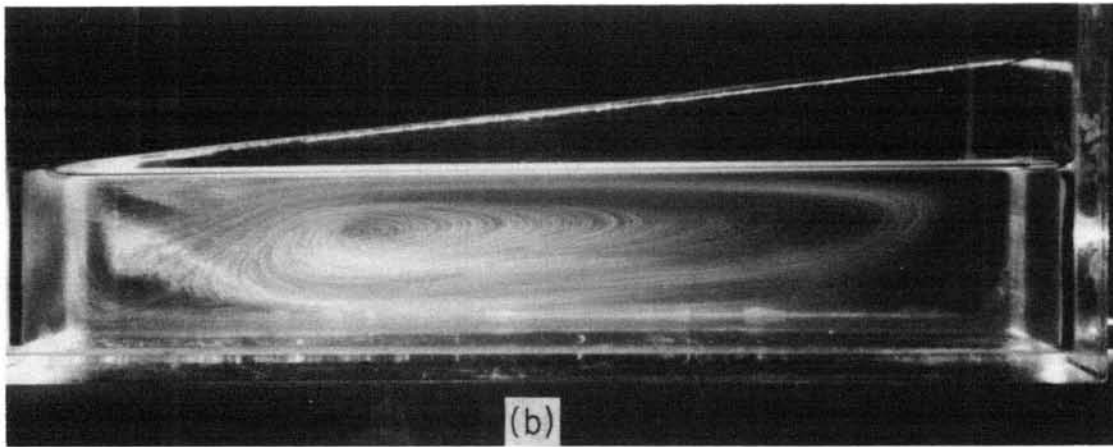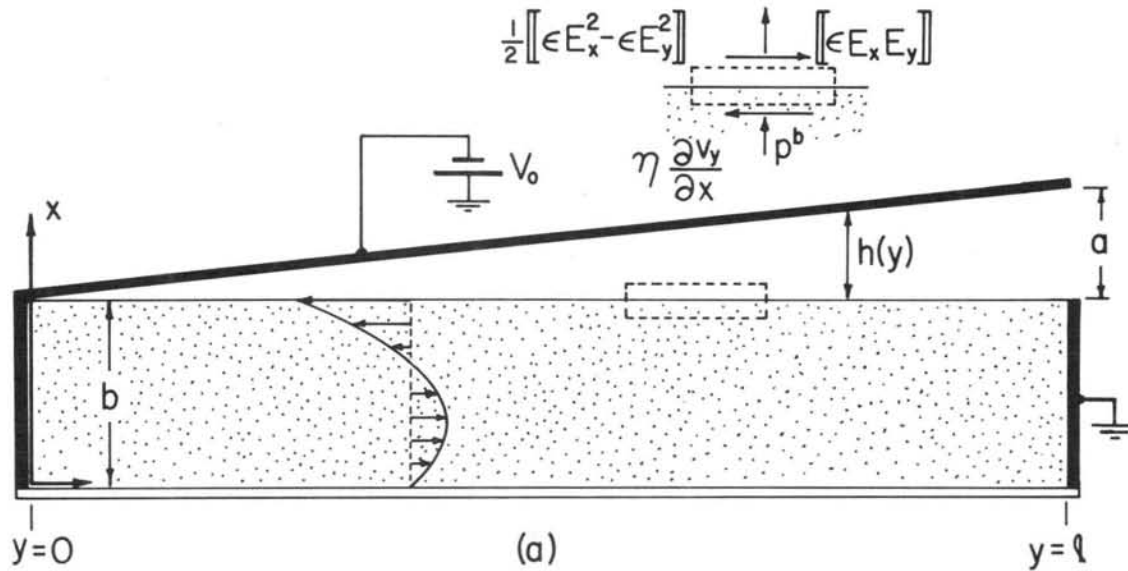
$$|\sigma_f v^\alpha| << |\frac{b\sigma V_o}{\ell}| \tag{14}$$

According to the approximate theory, the surface charge is given from Eq. 2 and Gauss' law as $\sigma_f = \epsilon_o V_o/a$, so that Eq. 14 is equivalent to

$$R_e \equiv \frac{\epsilon_o v^\alpha \ell}{ab\sigma} << 1 \tag{15}$$

Hence, the imposed stress model is valid in the low electric Reynolds number approximation. The physical significance of R_e, here the ratio of the charge relaxation time $(\epsilon_o/\sigma)(\ell/a)$ to the transport time b/v^α, is discussed in Sec. 5.10. Too great a velocity or too small a conductivity results in an electric stress in part determined by the fluid response.

Of course, the velocity in Eq. 15 is actually determined by the fields themselves, so a more explicit statement can be made. From Eq. 10, v^α is related to the fields so that R_e becomes

$$\tfrac{1}{2}\left[\!\!\left[\epsilon E_x^2-\epsilon E_y^2\right]\!\!\right] \qquad \left[\!\!\left[\epsilon E_x E_y\right]\!\!\right]$$

$$\eta\,\frac{\partial v_y}{\partial x} \qquad \uparrow p^b$$

Courtesy of Education Development Center, Inc. Used with permission.

Fig. 9.4.1.   (a) Cross section of liquid layer driven to the left at its interface by surface force
density. Electrodes at the left and above have zero potential relative to the electrode at
the right, which has potential V_o. The liquid is slightly conducting and contained by an in-
sulating tank.   (b) Time exposure of bubbles entrained in liquid show stream lines with experi-
mental configuration essentially that of (a). The liquid is corn oil, with depth of a few cm
and surface velocities at voltages in the range 10-20 kV on the order of 5 cm/sec. (For ex-
perimental correlation, see J. R. Melcher and G. I. Taylor, "Electrohydrodynamics: A Review
of the Role of Interfacial Shear Stresses," in Annual Review of Fluid Mechanics, Vol. 1,
W. R. Sears, Ed., Annual Reviews, Inc., Palo Alto, Calif.. 1969, pp. 111-146. The experi-
ment is shown in Reference 12, Appendix C.

$$H_e^2 \equiv \frac{\epsilon_o V_o^2}{4a^2\eta\sigma} \ll 1 \tag{16}$$

·This more useful expression of the approximation is in terms of what will be termed the electric
Hartmann number, H_e. As the square root of the ratio of the charge relaxation time ϵ_o/σ, to the elec-
tro-viscous time, $\eta/\epsilon(V_o/a)^2$, this number also appears in Sec. 8.6.

If the viscosity is too low, the fully developed flow is not observed. Rather, the shear force at
the interface cannot entrain the fluid near the bottom before an element has passed from one end of the
tank to the other. Then, only a boundary layer is set into motion. A suitable model is discussed in
Sec. 9.7.

At the ends, the "turn around" also involves accelerations. Under what conditions does the resulting inertial force density, $\rho \vec{v} \cdot \nabla \vec{v}$, compete significantly with that from viscosity? With the spatial derivatives characterized by the reciprocal length b^{-1}, the ratio of acceleration to viscous force density is of the order

$$R_y \equiv \frac{[\rho(v^\alpha)^2/b]}{\eta v^\alpha/b^2} = \frac{\rho v^\alpha b}{\eta} \ll 1 \tag{17}$$

Defined as the ratio of the viscous diffusion time, $\rho b^2/\eta$, to the transport time, b/v^α, the Reynolds number R_y is introduced in Sec. 7.18.

EQS Surface Coupled Systems: Two configurations that are very similar to the "Taylor pump" with fully developed flows providing quasi-one-dimensional models are shown by Figs. 9.4.2a and 9.4.2b. Note that the experiments to which these models apply are shown in Fig. 5.14.4.

MQS Systems Coupled by Magnetic Shearing Surface Force Densities: In pumping liquid metals with alternating fields, if the magnetic skin depth is short compared to the depth of the liquid, the surface-coupled model exemplified in this section again applies. In the configuration of Fig. 9.4.2c, a traveling wave is used to induce circulations in a liquid metal. Such a pump is useful in handling liquid metals in open conduits, perhaps in metallurgical processing.

The MQS system of Fig. 9.4.2d is in a way the counterpart of the "Taylor pump." In the air gap, the alternating magnetic field has essentially the same temporal phase throughout the air gap. However, because this field is nonuniform in the y direction, a time-average shearing surface force density is induced in the skin region of the liquid metal, with attendant circulations that can be modeled by the fully developed flow.
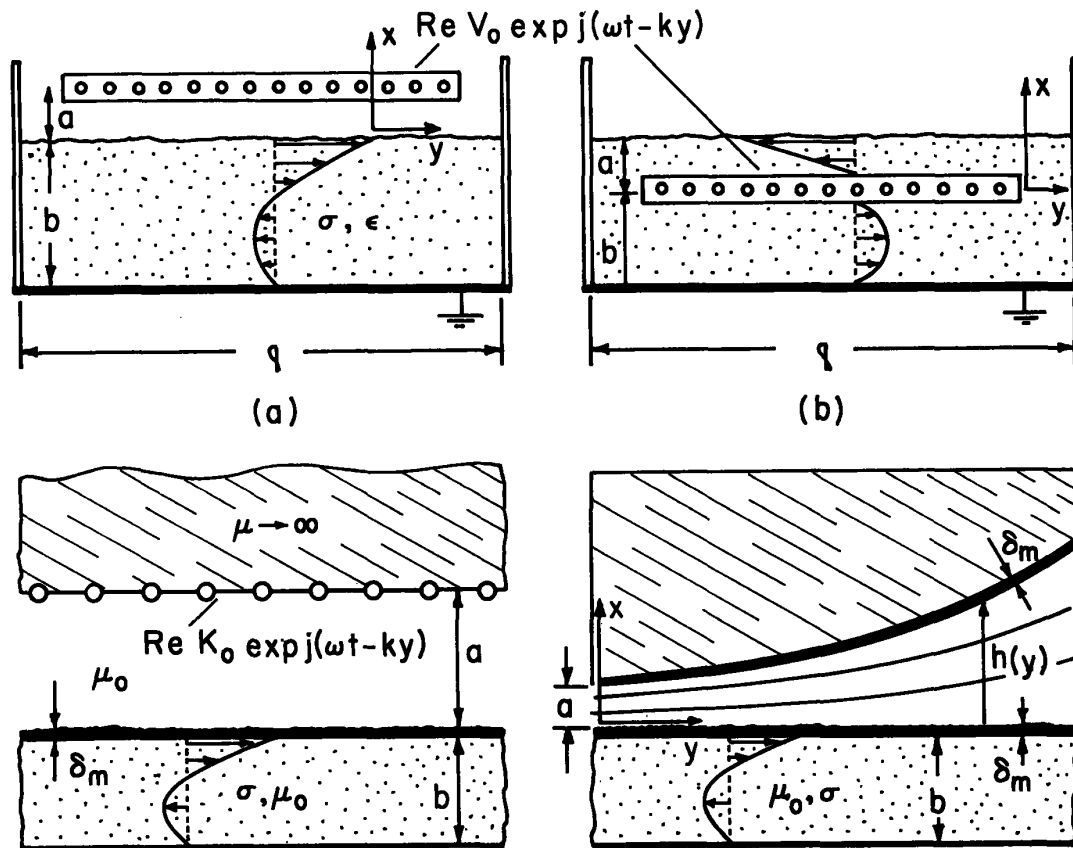

Fig. 9.4.2. (a) EQS traveling-wave-induced convection model for experiment shown in Fig. 5.14.4a.
(b) Model for experiment of Fig. 5.14.4b. (c) MQS MHD surface pump. Traveling wave of current imposed above air gap induces currents in liquid metal with magnetic skin depth much less than b.
(d) Surface current in skin layer has the same temporal phase as a function of y, but because the field is nonuniform there is a time-average surface force density driving liquid circulations.

9.5 Fully Developed Magnetic Induction Pumping

The magnetic induction motor discussed in Sec. 6.6 is readily adapted to pumping conducting liquids. The arrangement of driving current, magnetic material and fluid is typically like that of Fig. 9.5.1 in a class of pumps that has the advantage of not requiring mechanical moving parts or electrical contact with the liquid. The conduit can be insulating. A natural application is to the pumping of liquid metals such as sodium, which can react violently when exposed.[1]

In the liquid metal pump, each x-y layer of the fluid is analogous to the conducting sheet of Sec. 6.4. Induced currents result in both longitudinal and transverse traveling-wave forces. At a given position, these forces are composed of time-average and second-harmonic parts. With the traveling-wave frequency in the frame of the moving fluid ($\omega - k v_y$) sufficiently high, the liquid (limited as it is by its inertia and viscosity) usually can react only to the time-average part.

First, observe that the components of the magnetic stress have time averages that are independent of y. For example $\left\langle T_{yx} \right\rangle_t = \frac{1}{2} \text{Re} \mu_0 \hat{H}_x(x) \hat{H}_y^*(x)$. Hence, the time-average magnetic force density is simply

$$\left\langle \vec{F} \right\rangle_t = \frac{d}{dx} \left\langle T_{xx} \right\rangle_t \vec{i}_x + \frac{d}{dx} (\frac{1}{2} \mu_0 \text{Re} \hat{H}_x \hat{H}_y^*) \vec{i}_y \tag{1}$$

and takes the form assumed in Sec. 9.3, where

$$\mathcal{E} \rightarrow - \left\langle T_{xx} \right\rangle_t \quad \text{and} \quad T_{yx} \rightarrow \frac{1}{2} \mu_0 \text{Re} \hat{H}_x \hat{H}_y^*$$

$\mu \rightarrow \infty$

(a)

$K_z = \text{Re } K_0 \exp j(\omega t - ky)$

(b)

$\mu \rightarrow \infty$

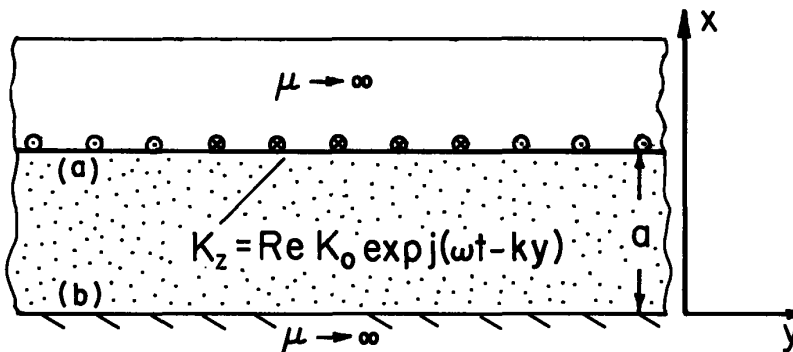Fig. 9.5.1

Planar magnetohydrodynamic induction pump.

At the walls, where x = 0 and x = a, the no-slip condition requires that $v_y \equiv v$ vanish, and hence with the identification of $\Delta \rightarrow a$, the velocity profile of Eq. (a) from Table 9.3.1 becomes

$$v = \frac{\partial p'}{\partial y} (x^2 - x) + V(x, \omega, k) \tag{2}$$

where

$$V(x, \omega, k) \equiv - \int_0^x \text{Re} \hat{H}_x \hat{H}_y^* dx + x \int_0^1 \text{Re} \hat{H}_x \hat{H}_y^* dx$$

and variables are normalized such that

$$\vec{H} = \underline{\vec{H}} K_0 \qquad k = \underline{k}/a$$

$$p = \underline{p} \mu_0 K_0^2 \qquad \omega = \underline{\omega}/\mu_0 \sigma a^2$$

$$v = (a\mu_0 K_0^2/2\eta) \underline{v} \qquad (x,y) = (a\underline{x}, a\underline{y})$$

Implicit is the assumption that the magnetic field distribution is not altered by the liquid motion. In fact, to some extent, it must be. But, if the fluid velocity at all points is small compared to the wave velocity, ω/k, then the fields are not dependent on the motion. This is suggested by the example of the moving sheet in Sec. 6.4, where the sheet represents a liquid layer. The liquid velocity enters in determining the time average force of Eq. 6.4.11 through S_m, as expressed by Eq. 6.4.7. Currents responsible for the force are induced because a magnetic diffusion time $\tau_m = \mu_0 \sigma \ell^2$ is on the order of ω^{-1}, whereas convective effects on this induction are ignorable because the magnetic Reynolds number based on

---

1. For extensive treatment, see E. S. Pierson and W. D. Jackson, "The MHD Induction Machine," Tech. Rep. AFAPL-TR-65-107, Air Force Aero Propulsion Laboratory, Research and Technology Division, Air Force Systems Command, Wright-Patterson Air Force Base, Dayton, Ohio, 1966.

The convection velocity, $R_m = \mu_o \sigma v \ell$, is still small compared to unity. Note that of the two possible lengths, a and $2\pi/k$, the latter is used here to represent rates of change in the y direction.

In this limit of small R_m, the transfer relations (b) from Table 6.5.1 with $U \to 0$ and $\Delta \to a$ give the magnetic field distribution. Identification of $\alpha \to a$ and $\beta \to b$ and use of the boundary conditions $\hat{H}_y^a = -\hat{K}_o, \hat{H}_y^b = 0$ specializes the relations to

$$\begin{bmatrix} \hat{A}^a \\ \\ \hat{A}^b \end{bmatrix} = + \frac{\mu_o \hat{K}_o}{\gamma} \begin{bmatrix} \coth \gamma a \\ \\ \dfrac{1}{\sinh \gamma a} \end{bmatrix} \tag{3}$$

where $\gamma \equiv \sqrt{k^2 + j\omega\mu\sigma}$. Substituted into Eqs. 6.5.6, these coefficients give the distribution of $\hat{A}$ and hence of $\hat{H}_x$ and $\hat{H}_y$. In normalized form

$$\hat{H}_x = \frac{-jk}{\gamma} \left[\coth \gamma \frac{\sinh \gamma x}{\sinh \gamma} - \frac{\sinh \gamma(x-1)}{\sinh^2 \gamma} \right] \tag{4}$$

$$-\hat{H}_y = \coth \gamma \frac{\cosh \gamma x}{\sinh \gamma} - \frac{\cosh \gamma(x-1)}{\sinh^2 \gamma}; \quad \gamma \equiv \sqrt{k^2 + j\omega} \tag{5}$$

Substituted into Eq. 2, these expressions determine the velocity profile as a function of the pressure gradient and the driving current.

Although now reduced to a straightforward integration, the explicit evaluation of the x dependence is conveniently done numerically. The profiles shown in Fig. 9.5.2 reflect the tendency for the velocity to peak near the driving windings. This results for two reasons. If the wavelengths are short compared to the channel width, the fields decay exponentially in the x direction even if the frequency is sufficiently low to give no induced currents. But even more, as the frequency is raised, the induced currents shield the magnetic field out of the lower fluid regions to further enhance this decay of the force density. The details of the magnetic field diffusion are represented in Figs. 6.6.3 and 6.6.4. Note that δ'/a as defined there is $\sqrt{2/\omega}$. For a pump having a width w in the z direction, the volume rate of flow, Q_v, is the integral of v over the x-y cross section. The relation between pressure gradient and volume rate of flow thus follows by integrating Eq. 2,

$$Q_v = \int_0^1 v\,dx = -\frac{1}{6} \frac{\partial p'}{\partial y} + Q(\omega,k); \quad Q \equiv \int_0^1 V(x,\omega,k)\,dx \tag{6}$$
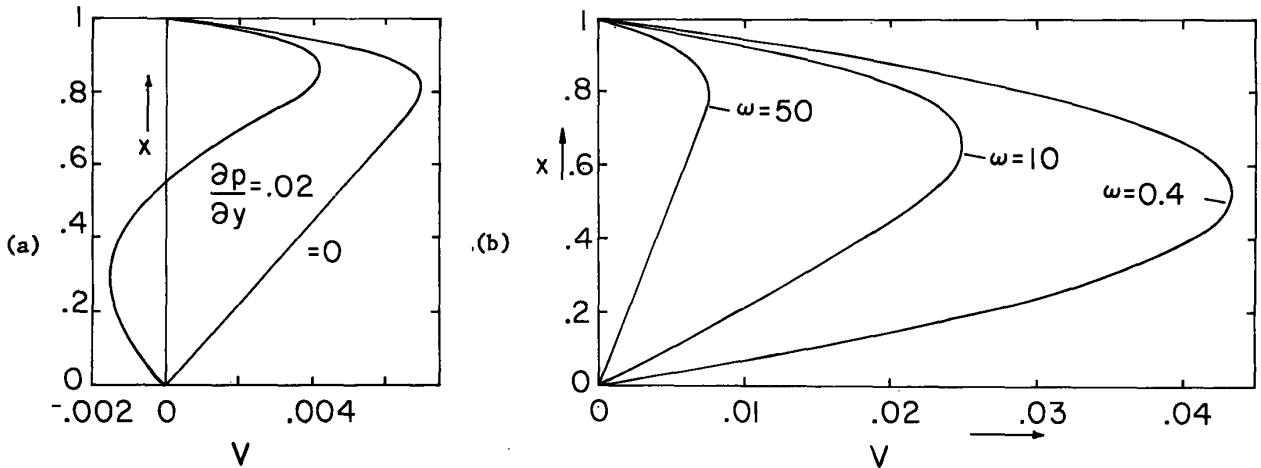
where

$$Q_v = Q_v wa^2 \mu_o K_o^2 / 2\eta$$

Fig. 9.5.2. (a) Normalized velocity profile with pressure gradient as parameter. $\omega = 50$ ($\delta'/a = 0.2$) and $k = 1$. (b) Normalized velocity profile with zero pressure gradient showing effect of frequency ω. For $\omega = 50$, the force density is confined to upper 20% of layer so that profile in the region below is the linear one typical of Couette flow.

The pump characteristic therefore has the general form illustrated by Fig. 9.5.3. The intercepts are functions of (ω, k). The dependence on $\underline{\omega}$ is typically that of the induction machine developed in Secs. 6.4 and 6.6 and is illustrated in Fig. 9.5.4.

To achieve pumping over the entire cross section, the design calls for making the wavelength and skin depth large compared to the channel depth a. Mathematically, this is the limit $\gamma a \ll 1$, and the limiting forms taken by Eqs. 4 and 5 show that $\hat{H}_x$ is then uniform over the cross section, while $\hat{H}_y$ decays in a linear fashion from the current sheet to the magnetic wall below:

$$\hat{H}_x \to -j \frac{k}{\gamma^2}; \qquad \hat{H}_y = x \qquad (6)$$

The integrations in Eqs. 2 and 6 are now carried out to give

$$V(x,\omega,k) = \frac{\omega k}{2(k^4 + \omega^2)} (x - x^2) \qquad (7)$$

$$Q(\omega,k) = \frac{\omega k}{12(k^4 + \omega^2)} \qquad (8)$$

The approximate magnetic force density implied by the magnetic field of Eq. 6 is uniform over the channel cross section. This is why the approximate long-wavelength long-skin-depth velocity profile has the same parabolic x dependence as if the flow were driven by a negative pressure gradient.

In practice, "end effects" are likely to be important. Such effects result from the spatial transient needed to establish the spatial sinusoidal steady state described in this section. In the imposed force density approximation used here, this transient is akin to those illustrated in Sec. 9.7, superimposed on a magnetic diffusion spatial transient.

Windings that could be used to drive the system are illustrated in Sec. 4.7. The electrical terminal relations are then found following the same approach taken in Sec. 6.4.

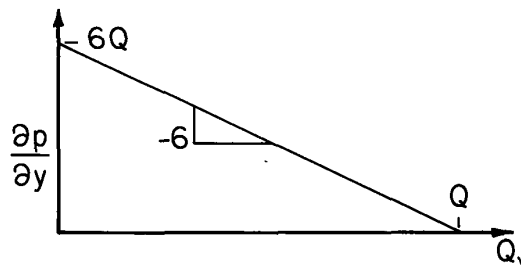## 9.6 Temporal Flow Development with Imposed Surface and Volume Force Densities

Fig. 9.5.3. Normalized pressure gradient as a function of normalized volume rate of flow.
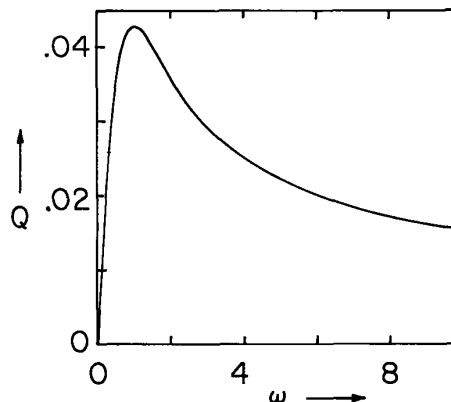
Fig. 9.5.4. Dependence of normalized Q (Fig. 9.5.3 and Eq. 6) on normalized frequency with $\underline{k} = 1$.

Under what conditions is a flow fully developed? The answer to this question can either be one of "when?" or "where?" If the configuration is reentrant, as for example in the Couette geometry of Table 9.3.1, and volume and surface force densities which are uniformly distributed with respect to the longitudinal directions are suddenly turned on, the question is one of, when? On the other hand, if a steady state prevails in a system having a finite length and the fluid enters with some velocity profile other than the fully developed one, the question is one of, where? In either case, the development is governed by viscous diffusion.

In this section, the temporal transient is considered. The spatial transient is taken up in Sec. 9.7.

Turn-On Transient of Reentrant Flows: Suppose that the plane flow considered in Sec. 9.3 (first of the configurations in Table 9.3.1) is reentrant, so that there is no longitudinal pressure gradient, $\partial p'/\partial y = 0$. Boundaries (or surface stresses) and volume force densities are applied when $t = 0$. How long before the fully developed flow described by Eq. (a) of Table 9.3.1 pertains?

The incompressible mass conservation and momentum force equations can be satisfied by a time-varying plane flow: $\vec{v} = v(x,t)\vec{i}_y$. The longitudinal force equation is then

$$\rho \frac{\partial v}{\partial t} = F_y(x) + \eta \frac{\partial^2 v}{\partial x^2} \qquad (1)$$

for $t > 0$. Fully developed flow can be regarded as a particular solution, $v_{fd}(x)$. This solution both balances the force distribution in the volume and satisfies the boundary conditions $v(\Delta) = v^\alpha$ and $v(0) = v^\beta$. With the understanding that the total solution is $v = v_{fd} + v_h(x,t)$, it follows that

$$\rho \frac{\partial v_h}{\partial t} = \eta \frac{\partial^2 v_h}{\partial x^2} \tag{2}$$

where v_h satisfies the boundary conditions $v = 0$ at $x = \Delta$ and $x = 0$.

In the terminology introduced in Sec. 5.15, the required solutions to Eq. 2 are the temporal modes $Rev_n(x)exps_n t$ (with no longitudinal dependence and hence with $k_y = 0$). Substitution converts Eq. 2 to

$$\frac{d^2 v_n}{dx^2} + \gamma_n^2 v_n = 0; \quad \gamma_n^2 = - \frac{\rho s_n}{\eta} \tag{3}$$

Solutions to Eq. 3 that satisfy the homogeneous boundary conditions are

$$v_n = V_n \sin \gamma_n x \tag{4}$$

where because $\sin \gamma_n \Delta = 0$,

$$\gamma_n = \frac{n\pi}{\Delta}; \quad s_n = - \frac{\eta}{\rho}(\gamma_n)^2$$

Thus, the velocity distribution evolves at a rate determined by the sum of modes, each having a time constant $\tau_n = \rho(\Delta/n\pi)^2/\eta$, the viscous diffusion time based on a length $\Delta/n\pi$. The total solution is in general

$$v = v_{fd}(x) + \sum_{n=1}^{\infty} V_n \sin (\frac{n\pi}{\Delta} x)e^{s_n t} \tag{5}$$

The coefficients V_n are determined by the initial conditions on the flow, $v(x,0) = 0$,

$$-v_{fd} = \sum_{n=1}^{\infty} V_n \sin (\frac{n\pi}{\Delta} x) \tag{6}$$

The temporal modes are orthogonal, in this case simply Fourier modes, so the coefficients are determined from Eq. 5, much as explained in Sec. 2.15.

As an example, suppose that when $t = 0$, the upper boundary is set into motion with velocity U, that the lower one is fixed and that there is no volume force density. Then, $v_{fd} = (x/\Delta)U$ and it follows that the sum of the fully developed and homogeneous solutions gives

$$\frac{v}{U} = \frac{x}{\Delta} + \sum_{n=1}^{\infty} \frac{2(-1)^n}{n\pi} \sin (\frac{n\pi}{\Delta} x)e^{s_n t} \tag{7}$$

This developing flow is shown in Fig. 9.6.1.

The boundary conditions satisfied by the temporal modes are determined by the way in which the transverse drive is applied. Suppose that the upper boundary is a "free" surface to which an electric stress is suddenly applied when $t = 0$. An example would be the electrically driven flow of Fig. 5.14.4a, but closed on itself in the longitudinal direction. (It is assumed that the traveling-wave velocity is much greater than that of the interface, and that, in terms of variables used in that section, the flow responds to the time-average surface force density $T_o \equiv \langle T_z \rangle_z$ which is suddenly turned on when $t = 0$.)

The fully developed flow is again simply $(x/\Delta)U$. However, the surface velocity is in general a function of time, $U = U(t)$, and for the fully developed flow is determined by the condition that the interfacial viscous shear stress balance the applied surface force density: $\eta \partial v/\partial x(x=\Delta) = T_o u_{-1}(t)$. Because the driving condition is balanced by the fully developed part, the homogeneous solution to Eq. 3 must now satisfy homogeneous boundary conditions: $\partial v_h/\partial x(x=\Delta) = 0$ and $v_h(0) = 0$. Thus, the temporal modes are determined. The resulting solution is

$$v/(\Delta T_o/\eta) = \frac{x}{\Delta} - \sum_{n=0}^{\infty} \frac{2(-1)^n}{[\pi(n + \frac{1}{2})]^2} \sin[(n + \frac{1}{2})\frac{\pi x}{\Delta}]e^{s_n t} \tag{8}$$
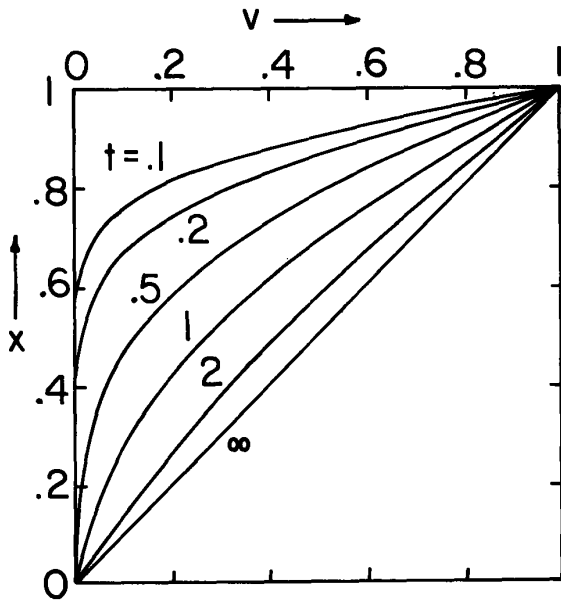
Fig. 9.6.1

Temporal transient leading to fully developed plane Couette flow as velocity in plane $x=\Delta$ is suddenly constrained to be U. v,x and t respectively, normalized to U, Δ, and $\rho\Delta^2/\eta\pi^2$.
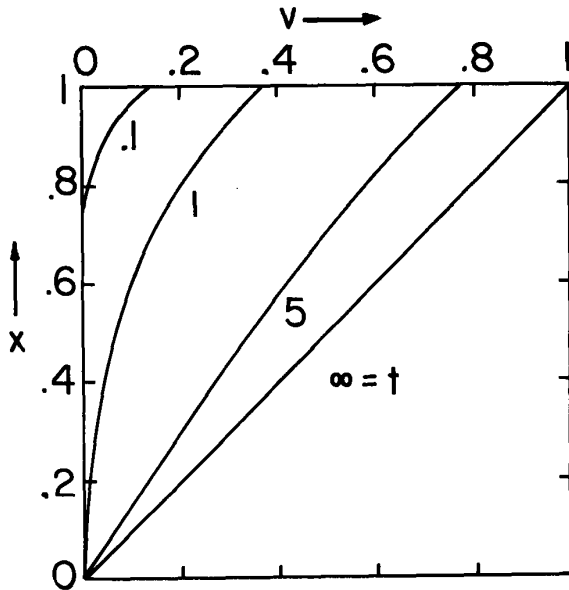

Fig. 9.6.2

Temporal transient leading to fully developed plane Couette flow initiated by application of constant surface force density, T_0, at free upper interface. v,x and t respectively, normalized to $\Delta T_0/\eta$, Δ, and $\rho\Delta^2/\eta\pi^2$.

where

$$s_n = - \frac{\eta\pi^2}{\rho\Delta^2} \left(n + \frac{1}{2}\right)^2$$

This transient, shown in Fig. 9.6.2, shows how both the interface and the fluid beneath approach the fully developed plane Couette flow.

9.7 Viscous Diffusion Boundary Layers

It is clear from the temporal viscous diffusion transients considered in Sec. 9.6 that in the early stages of development, motions imparted by a boundary are confined to the adjacent fluid. Examples are shown by Figs. 9.6.1 and 9.6.2. For times short compared to the viscous diffusion time based on the channel width Δ, the second boundary is of no influence and the diffusion phenomenon effectively picks out its own natural length. For the temporal transients considered, this length increases with time until the diffusion reaches another boundary.

With increasing time, the viscous process remains confined to the neighborhood of a boundary in two important situations. One is encountered in Sec. 7.19. There, boundary excitations are in the sinusoidal steady state and motions are confined to within a viscous skin depth of the boundary. In the second situation, there is a mean flow involved having a transport time through the volume of interest that is short compared to the viscous diffusion time based on a typical dimension of that volume. Thus, the distance into the flow that boundary effects can diffuse is limited to a viscous skin depth (based on the reciprocal transport time). Thus, there are two spatial scales. One, characterized by ℓ, describes variations in the longitudinal (dominant flow) direction y. The other scale is typified by the boundary layer thickness, which represents variations in the transverse direction. What makes the subject of boundary layers require some foresight is that this characteristic transverse length, d, is at the outset unknown.

The approach now taken is akin to that introduced in Sec. 4.12, a space-rate-parameter expansion is made in the ratio of lengths, $\gamma \equiv (d/\ell)^2$. The Navier-Stokes's equations (in two dimensions) and the continuity equation are written in normalized form as

$$\gamma\left(\frac{\partial v_x}{\partial t} + v_x \frac{\partial v_x}{\partial x} + v_y \frac{\partial v_x}{\partial y}\right) + \frac{\partial p}{\partial x} = \frac{\eta}{\rho\ell U}\left(\frac{\partial^2 v_x}{\partial x^2} + \gamma \frac{\partial^2 v_x}{\partial y^2}\right) + F_x \tag{1}$$

$$\frac{\partial v_y}{\partial t} + v_x \frac{\partial v_y}{\partial x} + v_y \frac{\partial v_y}{\partial y} + \frac{\partial p}{\partial y} = \frac{1}{\gamma}\left(\frac{\eta}{\rho\ell U}\right)\left(\frac{\partial^2 v_y}{\partial x^2} + \gamma \frac{\partial^2 v_y}{\partial y^2}\right) + F_y \tag{2}$$

$$\frac{\partial v_x}{\partial x} + \frac{\partial v_y}{\partial y} = 0 \tag{3}$$

where

$$
\begin{array}{lll}
x = \underline{x}d & v_x = \underline{v}_x U \frac{d}{\ell} & F_x = \underline{F}_x \frac{\rho U^2}{d} \\[2ex]
y = \underline{y}\ell & v_y = \underline{v}_y U & F_y = \underline{F}_y \frac{\rho U^2}{\ell} \\[2ex]
t = \underline{t}(\ell/U) & p = \underline{p}\rho U^2 &
\end{array}
\tag{4}
$$

Formally, an expansion is now made of the normalized variables in powers of γ. However, not only is this space-rate parameter small, so also is the reciprocal Reynolds number based on the longitudinal length: $\eta/\rho\ell U$. That is, the viscous diffusion time $\rho\ell^2/\eta$ is long compared to the transport time ℓ/U. Thus, to zero order, Eq. 1 is simply

$$\frac{\partial p}{\partial x} = F_x \tag{5}$$

This means that the transverse pressure distribution is determined without regard for the inertial and viscous force densities. The flow outside the boundary layer, which is essentially inviscid, determines the exterior pressure distribution. Because F_x is imposed, from Eq. 13 it is deduced that the pressure distribution, $p(y,t)$, within the layer is therefore a __given__ function. In ordinary fluid mechanics, $p(y,t)$ is usually determined by solving for the inviscid fluid motion in the volume subject to boundary conditions appropriate to an inviscid model.

In Eq. 2, it is clear that, to zero order in γ, the second term on the right can be dropped compared to the first. But, because both γ and $\eta/\rho\ell U$ are small, the parameter $(\eta/\rho\ell U)/\gamma$ is of the order of unity, so that the first term on the right is retained. The continuity equation contains no parameters. Hence, the boundary layer equations are Eq. 5 and

$$\frac{\partial v_y}{\partial t} + v_x \frac{\partial v_y}{\partial x} + v_y \frac{\partial v_y}{\partial y} + \frac{1}{\rho}\frac{\partial p}{\partial y} = \frac{\eta}{\rho}\frac{\partial^2 v_y}{\partial x^2} + \frac{1}{\rho}F_y \tag{6}$$

$$\frac{\partial v_x}{\partial x} + \frac{\partial v_y}{\partial y} = 0 \tag{7}$$

In these last two expressions, p is to be regarded as a predetermined function. If $\vec{F}$ is known, they comprise two equations for determining v_y and v_x.

Linear Boundary Layer: Suppose that liquid fills the half-space $x < 0$, has a "free surface" in the plane $x = 0$ and, in the absence of electrical excitations, undergoes a uniform translation to the right with velocity U. An electric or magnetic structure, sketched in Fig. 9.7.1, is used to impose a surface force density that is turned on when $t = 0$ and extends from $y = 0$ to the right. There is no bulk imposed force density. What is the perturbation in velocity or viscous stress distribution induced in the liquid by this excitation? Effects of the gas above the liquid will be ignored.
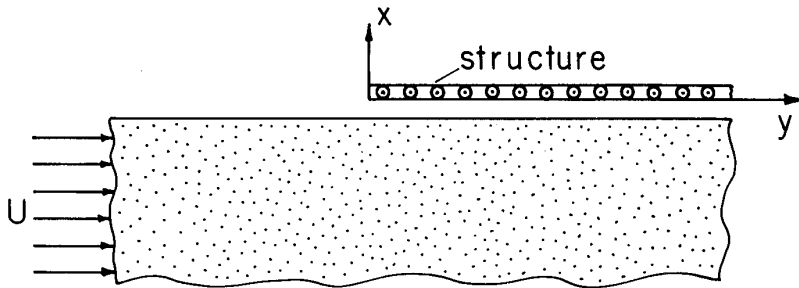

Fig. 9.7.1

Fluid moving uniformly to right encounters imposed surface force density where $y > 0$. Structure might induce electric or magnetic surface force density, as suggested in Secs. 5.14 and 6.8, respectively.

The imposed pressure is zero. The velocity can be written as $\vec{v} = v_x'\vec{i}_x + (U + v_y')\vec{i}_y$, where primes indicate perturbations. Thus, for small amplitudes, Eq. 6 reduces to a linear expression in v_y alone:

$$\left(\frac{\partial}{\partial t} + U\frac{\partial}{\partial y}\right)v_y' = \frac{n}{\rho}\frac{\partial^2 v_y'}{\partial x^2} \tag{8}$$

and Eq. 7 determines v_x' once v_y' is known.

The boundary condition at $x = 0$ is that $\eta\partial v_y/\partial x \equiv S_{yx} = T_o u_{-1}(t)u_{-1}(y)$, so it is convenient to take the derivative of Eq. 8 and introduce the stress as the dependent variable:

$$\frac{\partial S_{yx}}{\partial t'} = \left(\frac{\partial}{\partial t} + U\frac{\partial}{\partial y}\right)S_{yx} = \frac{n}{\rho}\frac{\partial^2 S_{yx}}{\partial x^2} \tag{9}$$

Here, t' is the rate of change with respect to time for an observer moving with the velocity U. This expression and the associated initial value and boundary value problem is the viscous analogue of the magnetic diffusion example treated in Sec. 6.9. Compare Eqs. 6.9.3 for example. Thus, the picture of temporal and finally spatial boundary layer evolution given there, for example by Fig. 6.9.3 with $H_y \to S_{yx}$, pertains equally well here.

The notion of an electric or magnetic surface force density implies that the coupling is confined to a region that is thin compared to that of the viscous boundary layer. In the case of a magnetic skin-effect coupling, the magnetic skin depth must be short compared to the viscous skin depth if the model suggested here is to be appropriate.

Stream-Function Form of Boundary Layer Equations: So that the continuity equation, Eq. 7, is automatically satisfied, it is convenient to introduce the stream function (from Table 2.18.1)

$$\vec{v} = \frac{\partial A_v}{\partial y}\vec{i}_x - \frac{\partial A_v}{\partial x}\vec{i}_y \tag{10}$$

Substitution converts the longitudinal force equation, Eq. 6, to

$$\frac{\partial^2 A_v}{\partial t\partial x} + \frac{\partial A_v}{\partial y}\frac{\partial^2 A_v}{\partial x^2} - \frac{\partial A_v}{\partial x}\frac{\partial^2 A_v}{\partial x\partial y} - \frac{n}{\rho}\frac{\partial^3 A_v}{\partial x^3} = \frac{1}{\rho}\frac{\partial p}{\partial y} - \frac{1}{\rho}\vec{F}_y \tag{11}$$

This expression is now applied to two examples in the remainder of this section.

<u>Irrotational Force Density; Blasius Boundary Layer</u>: Suppose that, as in Sec. 9.2, the imposed force density is irrotational; $\vec{F} = -\nabla\xi$. Also, steady conditions prevail, so $\partial(\ )/\partial t = 0$. Thus, the boundary layer describes the first stages of steady-state flow development adjacent to a planar boundary. Perhaps the fluid makes an entrance with uniform velocity profile (at $y = 0$) to the region of interest, as shown in Fig. 9.7.2.

Conditions in the core of the flow are determined from the inviscid laws. Given that the flow enters free of vorticity, Bernoulli's equation, Eq. 7.8.11, shows that

$$p + \xi \equiv P = \Pi - \frac{1}{2}\rho v^2 \qquad (12)$$

where Π is a constant.

Fig. 9.7.2. Viscous diffusion boundary layer near entrance to channel.

The transverse component of the boundary layer equation, Eq. 9.7.5, requires that across the boundary layer

$$\frac{\partial}{\partial x}(P) = 0 \qquad (13)$$

so it follows that within the boundary layer, $P = P(y)$. From Eq. 12, the particular dependence of $P(y)$ is determined by the bulk flow velocity distrubtion.

Because it follows from Eq. 10 that $p = P - \xi$ and $F_y = -\nabla\xi$, the longitudinal force equation, Eq. 11, reduces to

$$\frac{\partial A_v}{\partial y}\frac{\partial^2 A_v}{\partial x^2} - \frac{\partial A_v}{\partial x}\frac{\partial^2 A_v}{\partial x \partial y} - \frac{\eta}{\rho}\frac{\partial^3 A_v}{\partial x^3} = \frac{1}{\rho}\frac{dP}{dy} \qquad (14)$$

Consider now a flow that enters at $y = 0$ in Fig. 9.7.2 with a uniform velocity profile $\vec{v} = U\vec{i}_y$. In the core, where the inviscid laws apply, the flow remains uniform with this same velocity. Thus, because v in Eq. 12 is independent of y, it follows that the pressure gradient on the right in Eq. 14 is zero. By introducing a similarity parameter, such as illustrated for magnetic diffusion in Sec. 6.9 it is then possible to reduce Eq. 14 to an ordinary differential equation.

By way of motivating the similarity parameter, observe that at a location y fluid has had the transit time $\tau = y/U$ for viscous diffusion. The rate of this process is typified by the viscous diffusion time, $\tau_v = \rho(x/2)^2/\eta$, based on half of the transverse position x of interest. Thus, it is plausible that viscous diffusion will have proceeded to the same degree at locations (x,y) preserving the ratio

$$\xi = \sqrt{\frac{\tau_v}{\tau}} = \frac{x}{2}\sqrt{\frac{\rho U}{\eta y}} \qquad (15)$$

This similarity parameter is the analogue of the magnetic diffusion parameter given by Eq. 6.9.9.

With a function $f(\xi)$ defined such that $A_v = -f(\xi)\sqrt{\eta U y/\rho}$, Eq. 14 then reduces to the ordinary differential equation

$$\frac{d^3 f}{d\xi^3} + f\frac{d^2 f}{d\xi^2} = 0 \qquad (16)$$

This third order expression is equivalent to the three first-order equations

$$\frac{d}{d\xi}\begin{bmatrix} f \\ g \\ h \end{bmatrix} = \begin{bmatrix} g \\ h \\ -fh \end{bmatrix} \qquad (17)$$

Appropriate boundary conditions for flow over the flat plate are

$$v_x(0,y) = 0 \Rightarrow f(0) = 0, \quad v_y(0,y) = 0 \Rightarrow g(0) = 0, \quad v_y(\infty,y) \to U \Rightarrow g(\infty) \to 2 \qquad (18)$$

Numerical integration of Eqs. 18 subject to these boundary conditions is conveniently carried out using standard library subroutines. (Used here was the IMSLIB routine DVERK.) To satisfy the condition as $\xi \to \infty$, $h(0)$ is used as an iteration parameter and found to be 1.328.
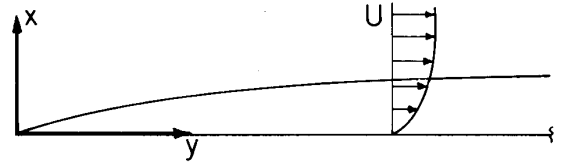
The velocity profile $v_y = -(U/2)df/d\xi$ is shown in Fig. 9.7.3. Note that eighty-five percent of the free stream velocity is obtained at $\xi = 1.5$. (For demonstration of this boundary layer, as well as exposition of layers with free stream pressure gradients, their transition to turbulence and turbulent boundary layers, see Reference 5, Appendix C.)[1]

The viscous stress on the flat plate then follows as

$$S_{yx}(0,y) = \frac{1}{4} U\eta \sqrt{\frac{\rho U}{\eta y}} h(0) = 0.332 U\eta \sqrt{\frac{\rho U}{\eta y}} \tag{19}$$

This y dependence is shown in Fig. 9.7.4a. Stream lines are illustrated by Fig. 9.7.4b. Even though the boundary layer approximation breaks down at the leading edge, the total viscous force, f_y, on a plate of width w and length L, found by integrating Eq. 19, is well behaved:

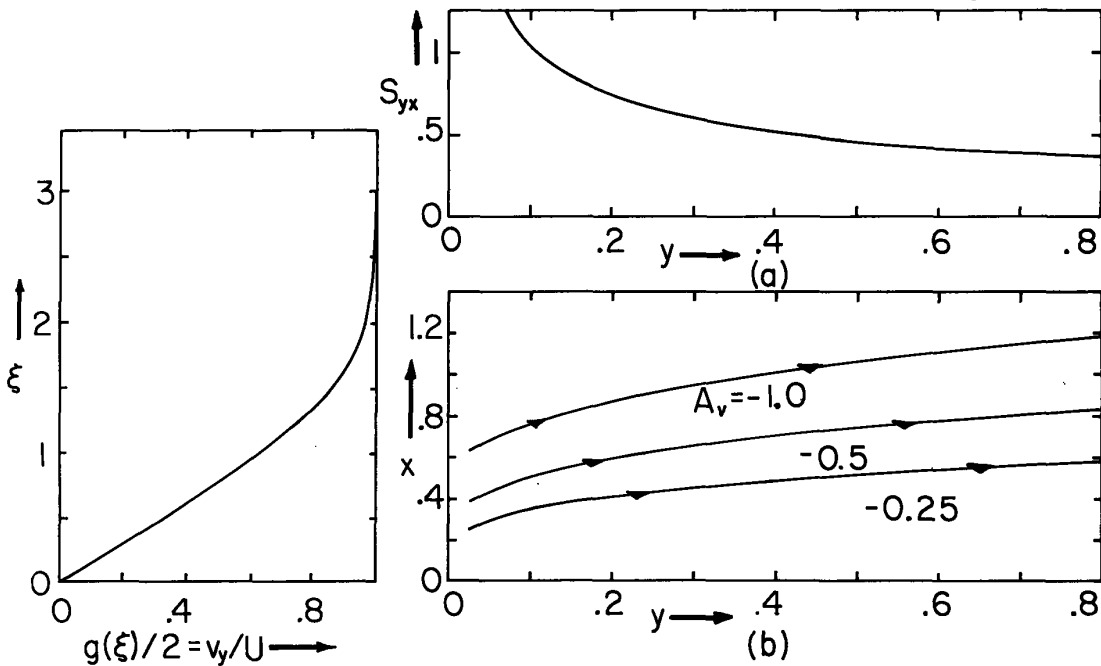$$f_y = w \int_0^L S_{yx}(0,y)dy = 0.664 w U \sqrt{\rho \eta U L} \tag{20}$$

Fig. 9.7.3. Velocity profile of
Blasius boundary layer as
function of similarity
parameter ξ, defined by
Eq. 15.

Fig. 9.7.4. (a) Distribution of viscous stress with longi-
tudinal position $\underline{y} = y/L$. $\underline{S}_{yx} \equiv S_{yx} U\eta \sqrt{\rho U/\eta L}$.
(b) Streamlines with $\underline{A}_v \equiv A_v/\sqrt{\eta U L/\rho}$, $\underline{x} \equiv (x/2)\sqrt{\rho U/L\eta}$.

What is there to be learned from this classical similarity solution that can serve as a guide in attacking the next example? First, observe that the similarity parameter can be thought of as an alternative coordinate. Lines of constant ξ form a family of parabolas in the x-y plane. One similarity coordinate is perpendicular to this family. In the x-y plane this similarity coordinate has the shape of an ellipse, as exemplified by Fig. 9.7.5. Not only does the boundary layer equation become an ordinary differential equation in this coordinate, but the boundary conditions are also a function of ξ alone.

---

1. Standard references on boundary layers are: A. Walz, Boundary Layers of Flow and Temperature, The MIT Press, Cambridge, Mass., 1969; and H. Schlichting, Boundary Layer Theory, McGraw-Hill Book Company, New York, 1960.

In Fig. 9.7.5, boundary conditions at A (the flat plate) and C
(the free stream) are the same as at A' and C'. Otherwise, the
solution found by integrating Eq. 17 along AC and A'C' would
not give the same result at B as at B'. Because $f = f(\xi)$, the
value of f must be the same at these two points.

A rational procedure for seeking a similarity parameter
as well as the y dependence of A_v would begin by letting
$\xi = c_1 x y^n$ and $A_v = c_2 f(\xi) y^m$, where n and m are to be determined.
It follows from the assumed form for A_v that $v_y = -c_2 y^{m+n} df/d\xi$.
If this velocity is to be the same constant, U, in the free
stream regardless of the trajectory in the x-y plane, it follows
that $m = -n$. To make the boundary layer equation reduce to an
ordinary differential equation, it is then necessary that
$m = -1/2$. Thus, the assumed forms for ξ and A_v are deduced.

<u>Stress-Constrained Boundary Layer</u>: Typical of boundary
layer development with an imposed surface force density is the
system shown in Fig. 9.7.6. The electrode structure imposes a
time-average surface force density T_o at the interface to the
right of $y = 0$. Well below the interface, the fluid is essen-
tially quiescent, and so the only motion is the result of the
electromechanical drive. A typical electromechanical coupling
is that of Fig. 5.14.4a, where a time-average surface force den-
sity acts on that part of the interface under the electrode struc-
ture. For the boundary layer model now developed to apply, the
fluid should be doped Freon, which is about 100 times less vis-
cous than the fluid shown (see Reference 12, Appendix C).

Fig. 9.7.5. Lines of constant
similarity parameter, ξ,
in (x-y) plane.

First observe that, in terms of the normali-
zation given by Eq. 9.7.4, the viscous stress is

$$S_{yx} = \frac{\eta U}{d}\left(\gamma \frac{\partial v_x}{\partial y} + \frac{\partial v_y}{\partial x}\right) \qquad (21)$$

Thus, in the boundary layer approximation (γ small),
the viscous stress is approximated by the second of
the two derivatives. In terms of the stream func-
tion, the stress then becomes

$$S_{yx} = -\eta \frac{\partial^2 A_v}{\partial x^2} \qquad (22)$$

What is desired is a similarity parameter and
stream function defined so that the condition
that S_{yx} be constant at $x = 0$ for all $y > 0$ is
met by evaluating $f(\xi)$ at one value of ξ. Thus,
S_{yx} must be a function of the similarity parameter

Fig. 9.7.6. A uniform surface force density is
applied to interface for $0 < y$. Develop-
ing velocity profile is v_y.

alone. With m and n at the outset unknown and c_1 and c_2 normalizing parameters, trial forms are

$$\cdot \ \xi = c_1 x y^n; \qquad A_v = c_2 f(\xi) y^m \qquad (23)$$

It follows from Eq. 22 that if S_{yx} is to be a function of the similarity parameter alone, $m + 2n = 0$.
Substitution into Eq. 14 then shows that $n = -1/3$. Thus, the boundary layer equation, Eq. 14 with
$dP/dy = 0$, reduces to

$$\frac{d}{d\xi}\begin{bmatrix} f \\ g \\ h \end{bmatrix} = \begin{bmatrix} g \\ h \\ \frac{1}{3}g^2 - \frac{2}{3}fh \end{bmatrix} \qquad (24)$$
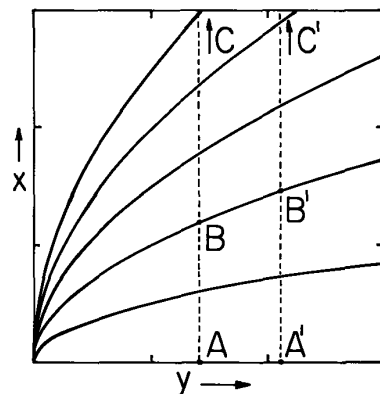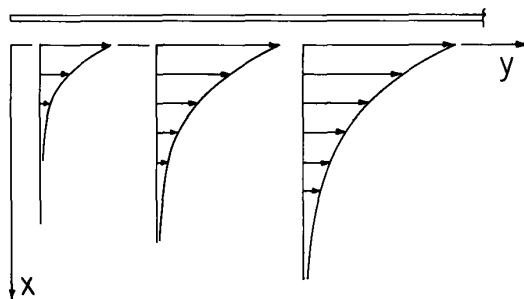
where S_{yx} is normalized to T_o so that (this similarity solution was identified for the author by Mr. Richard M. Ehrlich while a graduate student)

$$\xi = \left(\frac{\rho T_o}{\eta^2}\right)^{1/3} x y^{-1/3} \tag{25}$$

$$A_v = -\left(\frac{\rho T_o}{\rho^2}\right)^{1/3} f(\xi) y^{2/3} \tag{26}$$

Boundary conditions consistent with having a constant surface force density T_o acting in the y direction, no vertical velocity at the interface and a stagnant-free stream are

$$v_x(0,y) = 0 \Rightarrow f(0) = 0, \quad S_{yx}(0,y) = T_o \Rightarrow h(0) = -1, \quad v_y(\infty,y) \to 0 \Rightarrow g(\infty) \to 0 \tag{27}$$

To match the boundary conditions as $\xi \to \infty$, $g(0)$ is used as an iteration parameter which is adjusted to make $g \to 0$ as $\xi \to \infty$ with the other two conditions at $\xi = 0$ satisfied. From this iteration it follows that $g(0) = 1.296$. The universal profiles $f(\xi)$ and $g(\xi)$ are shown in Fig. 9.7.7. The velocity profile, recovered by using the relation $v_y = (T_o^2/\rho\eta)^{1/3} g(\xi) y^{1/3}$, is as exemplified in Fig. 9.7.6. With increasing longitudinal position y, the interface has increasing velocity and the motion penetrates further into the bulk.

The velocity of the interface is simply

$$v_y = \left(\frac{T_o^2}{\rho\eta}\right)^{1/3} (1.296) y^{1/3} \tag{28}$$

and is shown in Fig. 9.7.8.

Streamlines help to emphasize that the fluid is being drawn into the boundary layer from below. These lines of constant A_v, given by Eq. 26, are illustrated in Fig. 9.7.9.

In retrospect, what is the physical origin of the difference between similarity parameters for the constant velocity and the imposed stress boundary layers? In fact ξ as defined by Eq. 25 is again the ratio of a time for viscous diffusion in the x direction to a transport time in the y direction. However, with the stress at the interface constrained, the transport velocity in fact varies as $y^{1/3}$. Based on a transport time consistent with this variation in velocity, it is again found that ξ is the square root of the ratio of the viscous diffusion time to the transport time.
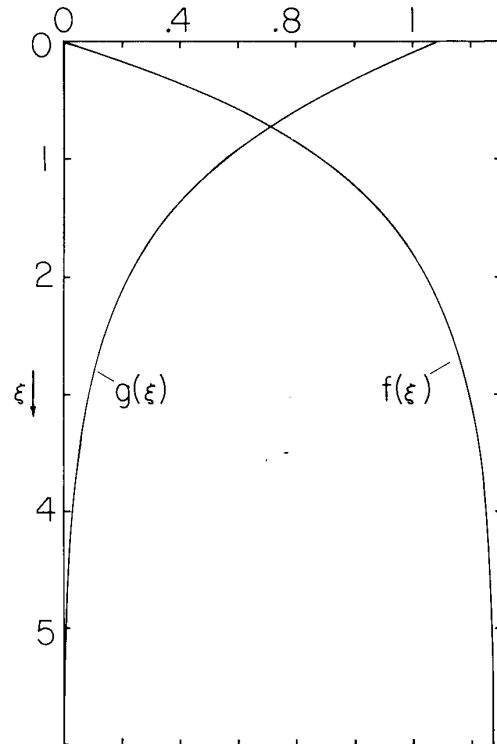

Fig. 9.7.7. Universal profiles of $f(\xi)$ and $g(\xi)$ as function of similarity parameter for boundary layer with uniform surface force density.
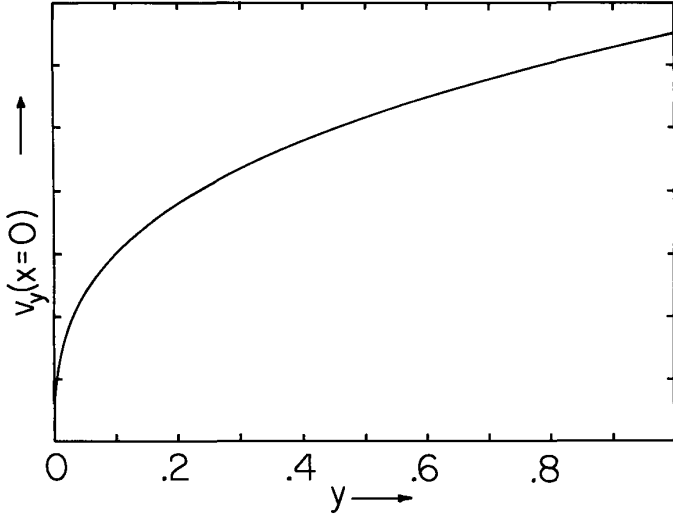
Fig. 9.7.8. Interfacial velocity of interface subject to uniform surface force density T_0. v_y and y normalized to $(T_0^2 L/\rho\eta)^{1/3}$ and L respectively.
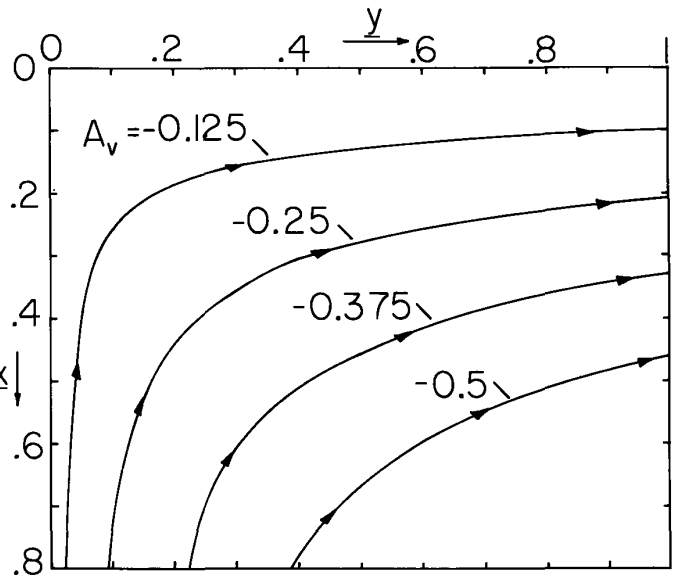
Fig. 9.7.9. Streamlines for stress-constrained boundary layer, as would result in configuration of Fig. 9.7.6. Variables are normalized.

9.8 Cellular Creep Flow Induced by Nonuniform Fields

Low-Reynolds-number models are often used to describe fluid circulations where, if it were not for a relatively high viscosity or for a relatively low velocity, the nonlinear acceleration term would make the mathematical description difficult. The main virtue of this approximation, which is discussed in Secs. 7.18 and 7.20, is that the flow is then described by linear differential equations. Thus, a Fourier-type decomposition of surface force densities results in a flow that can be represented by responses, in a way exemplified by many spatially periodic examples from previous chapters.

Illustrated in this section are such circulating imposed surface density flows. They are of interest in their own right, but also are useful in developing models where the surface force density is in fact dependent on the flow.

Magnetic Skin-Effect Induced Convection: The layer of liquid metal shown in Fig. 9.8.1 rests on a rigid bottom and has a "free" interface. Separated from the interface by an air gap, windings backed by a perfectly permeable material impose a tangential magnetic field that takes the form of a standing wave. The frequency ω is high enough that the magnetic skin depth δ in the liquid (Eq. 6.2.10) is much less than the liquid depth b. Associated with this skin region are both normal and shearing time-average surface force densities acting on the material within the layer (Eqs. 6.8.8 and 6.8.10). At relatively low applied fields, gravity maintains an essentially flat interface in spite of the normal surface force density. However, the shearing component establishes cellular motions, as now derived.

First, the imposed time-average magnetic shearing surface force density is computed. A region having thickness of the order of δ near the interface is pictured as subject to a force per unit area which is the time average of the force density $\vec{J} \times \mu_0\vec{H}$ integrated over the thickness of the layer. Because the magnetic field below the layer is zero, this shearing surface force density is

$$\left\langle T_y \right\rangle_t = \left\langle B_x^d H_y^d - B_x^e H_y^e \right\rangle_t = \left\langle B_x^d H_y^d \right\rangle_t \tag{1}$$

Because the excitation is a standing wave, there is no net force on a section of the skin region one wavelength long in the y direction. Rather, there is a spatially periodic distribution of the time-

average surface force density that has twice the periodicity of the imposed field.

To exploit the complex-amplitude transfer relations, observe that the excitation surface current can be written as the sum of two traveling waves:

$$K_z = Re\hat{K}_o \cos \beta y e^{j\omega t} = Re(\hat{K}_+ e^{-j\beta y} + \hat{K}_- e^{j\beta y})e^{j\omega t}; \quad \hat{K}_\pm \equiv \hat{K}_o/2 \tag{2}$$

The backward wave is gotten from the forward one by replacing $\beta \rightarrow -\beta$. Using this decomposition, Eq. 1 becomes

$$\langle T_y \rangle_t = Re \frac{1}{2}(\hat{B}^d_{x+} e^{-j\beta y} + \hat{B}^d_{x-} e^{j\beta y})(\hat{H}^{d*}_{y+} e^{+j\beta y} + H^{d*}_{y-} e^{-j\beta y})$$

$$= \frac{1}{2} Re[\hat{B}^d_{x+}\hat{H}^{d*}_{y+} + \hat{B}^d_{x-}\hat{H}^{d*}_{y-} + \hat{B}^d_{x-}\hat{H}^{d*}_{y+} e^{j2\beta y} + \hat{B}^d_{x+}\hat{H}^{d*}_{y-} e^{-j2\beta y}] \tag{3}$$

The normal and tangential fields above the interface are related by the skin-effect transfer relations, Eq. 6.8.5. The upper sign is appropriate because it is assumed that the peak interfacial velocity is still much less than ω/β. Thus, substitution for $\hat{B}^d_{x+}$ and $\hat{B}^d_{x-}$ shows that the space average part of Eq. 3 cancels out while the remaining terms give

$$\langle T_y \rangle_t = \frac{1}{4} Re[-(1 + j)\beta\mu_o\delta\hat{H}^d_{y-}\hat{H}^{d*}_{y+} e^{j2\beta y} + (1 + j)\beta\mu_o\delta\hat{H}^d_{y+}\hat{H}^{d*}_{y-} e^{-j2\beta y}] \tag{4}$$

μ or μ_o
$\times$

Use can be made of the air-gap transfer relation to represent $\hat{H}^d_y$ in terms of the driving current $\hat{K}_o$. For simplicity it is assumed that $\beta d \ll 1$, so that the tangential field imposed by the surface current at (c) is essentially experienced at (d) as well:

$\times$

$\times$

$$\hat{H}^d_{y\pm} \simeq \hat{H}^c_{y\pm} = -\frac{\hat{K}_o}{2} \tag{5}$$

Thus, the time-average magnetic surface force density of Eq. 4 is simply

$$\langle T_y \rangle_t = \frac{\mu_o\beta\delta|\hat{K}_o|^2}{8} \sin 2\beta y \tag{6}$$

This is the distribution sketched at the interface of Fig. 9.8.1.

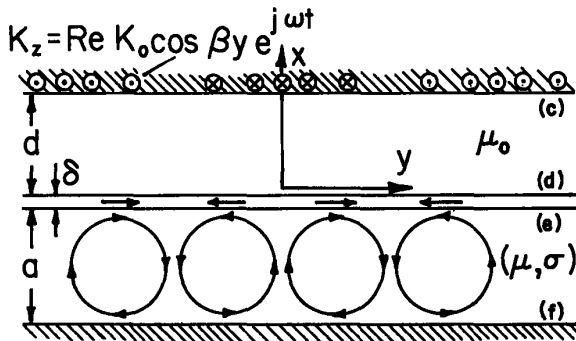$K_z = Re\ K_o \cos \beta y\ e^{j\omega t}$

Fig. 9.8.1

Cross section of liquid metal layer set into cellular convection by spatially periodic a-c magnetic field inducing magnetic shear stress in skin layer at interface.

Now that the imposed magnetic surface force density has been determined, the flow response can be computed. In Sec. 7.20, this too is represented in terms of complex amplitudes, so the drive, Eq. 7, is again decomposed into traveling-wave parts:

$$\langle T_y \rangle_t = Re(\tilde{T}_+ e^{-j2\beta y} + \tilde{T}_- e^{j2\beta y}); \quad \tilde{T}_\pm \equiv \pm j\mu_o\beta\delta|K_o|^2/16 \tag{7}$$

That the interface, modeled here as having a thickness several times δ, be in shear stress equilibrium requires that

$$\tilde{S}^e_{yx\pm} = \tilde{T}_\pm \tag{8}$$

With the assumption that gravity holds the interface essentially flat in spite of the normal magnetic surface force density goes the boundary condition

$$\tilde{v}_x^e = 0 \tag{9}$$

At the rigid lower boundary, both velocity components are zero:

$$\tilde{v}_x^f = 0; \quad \tilde{v}_y^f = 0 \tag{10}$$

The stress-velocity relations for the layer, Eq. 7.20.6, can now be used to represent the bulk fluid mechanics. In particular, Eq. 7.20.6c is evaluated using Eq. 8 on the left and Eqs. 9 and 10 on the right. Solved for the interfacial shear velocity, that expression becomes:

$$\tilde{v}_{y\pm}^e = \tilde{T}_\pm / \eta P_{33}; \quad P_{33} \equiv \frac{[\frac{1}{4}\sinh(4\beta a) - \beta a](8\beta)}{[\sinh^2(2\beta a) - (2\beta a)^2]} \tag{11}$$

Note that P_{33} is an even function of k and hence the same number whether evaluated with $k\Delta = 2\beta a$ or $k\Delta = -2\beta a$.

The last three equations specify all of the velocity amplitudes, so that equations 7.20.4 and 7.20.5 can be used to reconstruct the x-y dependence of the flow field if that is required. At the interface, it follows from Eq. 11 that the y dependence is

$$\tilde{v}_y = \text{Re} \frac{1}{\eta P_{33}} (\tilde{T}_+ e^{-2j\beta y} + \tilde{T}_- e^{2j\beta y}) = \frac{\mu_o \beta \delta |\tilde{K}_o|^2}{8\eta P_{33}} \sin 2\beta y \tag{12}$$

Thus, the flow pattern is as sketched in Fig. 9.8.1.

The hydromagnetic convection modeled here is akin to that obtained in the quasi-one-dimensional configuration of Fig. 9.4.2d. There the field nonuniformity is obtained by using a shaped bus. Here, the windings are used to shape the field.

Charge-Monolayer Induced Convection: Surface charge induced convection, akin to that of Fig. 9.4.1, takes a cellular form in the EQS experiment of Figs. 9.8.2 and 9.8.3. In the model developed in Prob. 9.8.1, the flow is slow enough that it has negligible effect on the field.[1]
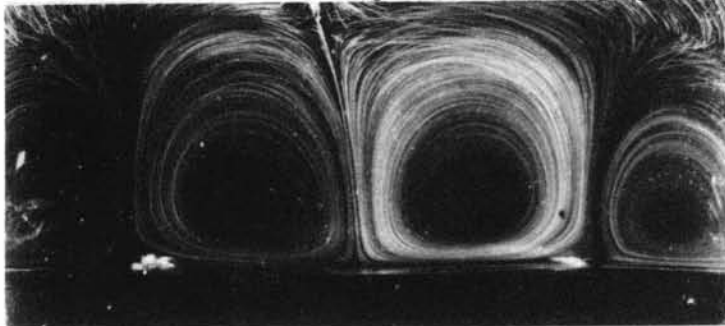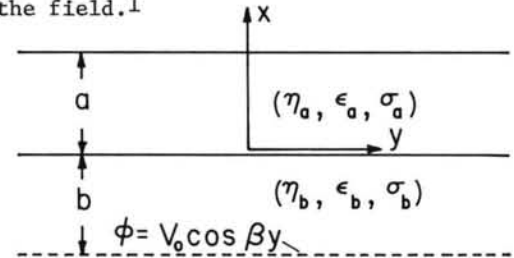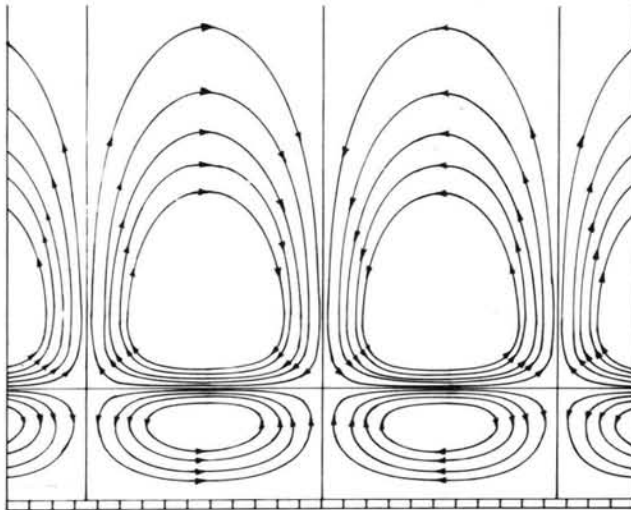
(a)

Fig. 9.8.2. Semi-insulating liquid layers stressed by static spatially periodic potential.

Fig. 9.8.3

(a) Streak lines of bubbles entrained in flow induced in configuration shown in Fig. 9.8.2. Upper fluid has properties $\varepsilon = 3.1\varepsilon_o$, $\sigma = 5\times10^{-11}$ mhos/m while lower one has $\varepsilon = 6.9\varepsilon_o$, and $\sigma = 3\times10^{-9}$. (b) Theoretical streamlines in limit where upper boundary is at infinity. In the experiment shown in (a), the cells in the upper region actually interact appreciably with the upper wall.

(b)

---

1. See C. V. Smith and J. R. Melcher, "Electrohydrodynamically Induced Spatially Periodic Cellular Stokes-Flow," Phys. Fluids 10, No. 11, 2315 (1967).

9.9 Magnetic Hartmann Type Approximation and Fully Developed Flows

Approximation: In typical laboratory situations involving the flow of electrolytes, liquid metals or even some plasmas through a magnetic field, magnetic diffusion times are short compared to times of interest. Nevertheless currents induced by the motion can make an appreciable contribution to the magnetic force density. The magnetic field associated with induced currents is then small compared to the imposed field.

The appropriate approximations to the magnetohydrodynamic equations are seen by writing those equations in normalized form:

$$\nabla \times \vec{E} = -\frac{\partial \vec{H}}{\partial t} \tag{1}$$

$$\nabla \times \vec{H} = \frac{\tau_m}{\tau} \not{/}(\vec{E} \not{+} \vec{v} \times \vec{H}) \tag{2} \qquad \times$$

$$\nabla \cdot \vec{H} = 0 \tag{3}$$

$$\frac{\partial \vec{v}}{\partial t} + \vec{v} \cdot \nabla \vec{v} + \nabla p = \frac{\tau_m}{\tau_{MI}} \frac{\tau}{\tau_{MI}} \ (\vec{E} + \vec{v} \times \vec{H}) \times \vec{H} + \frac{\tau}{\tau_V} \nabla^2 \vec{v} \tag{4}$$

$$\nabla \cdot \vec{v} = 0 \tag{5}$$

It is assumed that the fluid is an ohmic conductor with characteristic conductivity σ_o and essentially the permeability of free space. The normalization used here, summarized by Eqs. 2.3.4b, takes the electric field as being of the order $\mu_o \ell \mathcal{H}/\tau$, as it would be if induced by the motion. The three characteristic times

$$\tau_V = \frac{\rho \ell^2}{\eta}; \quad \tau_m = \sigma_o \mu_o \ell^2; \quad \tau_{MI} = \sqrt{\rho \ell^2 / \mu_o \mathcal{H}^2} \tag{6}$$

are the viscous diffusion time, magnetic diffusion time and the magneto-inertial time, respectively, familiar from Sec. 8.6.

In the imposed field approximation, these times have the order shown in Fig. 9.9.1, and times of interest, τ, are long compared to τ_m but arbitrary relative to τ_{MI} and τ_V. Of course, for steady flows the characteristic time is a transport time ℓ/u. Then, the approximation requires that the magnetic Reynolds number be small, but that the Reynolds number $\tau_V/\tau = \rho\ell u/\eta$ and the ratio of fluid velocity to Alfvén velocity $\tau_{MI}/\tau = u/\sqrt{\mu_o \mathcal{H}/\rho}$ be arbitrary.

Because τ_m/τ is small, the induced currents on the right in Eq. 2 are negligible. The magnetic field is imposed by means of currents in external windings. (More generally, there might be contributions from imposed volume currents which would arise from an electric field greater in order than $\mu_o \ell \mathcal{H}/\tau$, as presumed in the normalization of Eq. 2.)
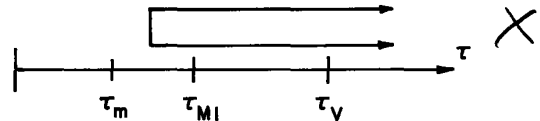

Fig. 9.9.1. Ordering of characteristic times in magnetic imposed field approximation.

Note that to zero order in τ_m/τ, the divergence of Eq. 2 still requires that the divergence of the induced current density vanish. Thus, Eqs. 2 and 3 reduce to expressions that determine $\vec{H}$,

$$\nabla \times \vec{H} = 0 \tag{7}$$

$$\nabla \cdot \mu_o \vec{H} = 0 \tag{8}$$

and with the understanding that $\vec{H}$ is the imposed field only,

$$\nabla \times \vec{E} = -\mu_o \frac{\partial \vec{H}}{\partial t} \tag{9} \qquad \times$$

$$\nabla \cdot \vec{J} = 0; \quad \vec{J} = \sigma(\vec{E} + \vec{v} \times \mu_o \vec{H}) \tag{10}$$

$$\rho(\frac{\partial \vec{v}}{\partial t} + \vec{v} \cdot \nabla \vec{v}) + \nabla p = \vec{J} \times \mu_o \vec{H} + \eta \nabla^2 \vec{v} \tag{11}$$

9.25

$$\nabla \cdot \vec{v} = 0 \tag{12}$$

The simple dimensional arguments given here presume that there is only one characteristic length ℓ. In general, more lengths and perhaps more than one characteristic time might be involved, and then approximations must hinge on a more detailed knowledge of the physical situation. The fully developed flow now considered involves one characteristic length, the transverse dimension d of the channel.

Fully Developed Flow: The magnetohydrodynamic pumping or generating configuration of Fig. 9.9.2 is an adaptation of the d-c kinematic (rotating machine) interaction from Sec. 4.10 and a refinement of the model introduced in Sec. 9.2. What is new is the internal redistribution of velocity caused by the magnetic force density.
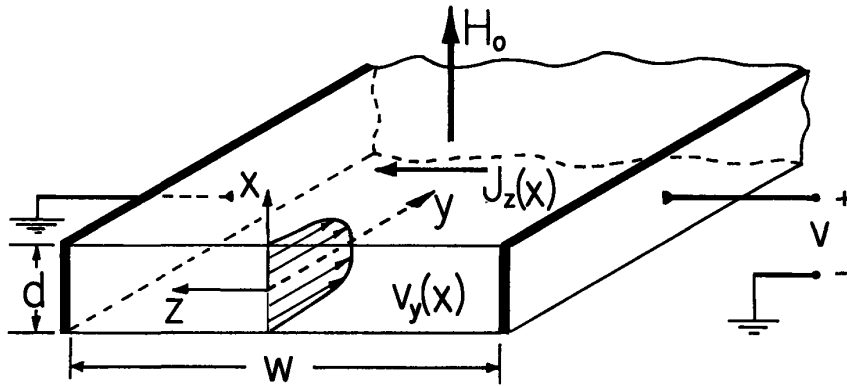

Fig. 9.9.2

Configuration for Hartmann flow. The aspect ratio $d/w \ll 1$ so that the velocity is essentially a function only of x: thus so also is the current density J_z.

A conducting fluid moves in the y direction through the rectangular channel (Fig. 9.9.2) having a width w much greater than the depth d. Hence, the viscous shear from the upper and lower walls dominates that due to the side walls and the velocity profile can be considered a function of x alone.

The side walls are conducting electrodes that make electrical contact with the fluid and are connected to an external load or excitation. With the application of a transverse magnetic field H_0 in the x direction, there is a magnetic force density $\vec{J} \times \vec{B}$ in the y direction tending to retard or accelerate the flow. Effects of gravity are absorbed in the pressure p. In this configuration, external currents generate the imposed $\vec{H}$ which is uniform and the constant H_0. Thus, Eqs. 7 and 8 are satisfied and the right-hand side of Eq. 9 is zero. Even if the flow is time-varying, the electric field is irrotational. If flow and field quantities are to be independent of z, it follows from the y component of Faraday's law that

$$E_z = E_z(t) = \frac{v}{w} \tag{13}$$

independent of x.

With the objective of finding a plane flow solution, $\vec{v} = v_y(x,t)\vec{i}_y$, note that the current density is

$$J_z = \sigma(E_z - \mu_o v_y H_o) \tag{14}$$

so that the y component of Eq. 11 reduces to

$$\rho \frac{\partial v_y}{\partial t} + \frac{\partial p}{\partial y} = \mu_o \sigma H_o E_z - (\mu_o H_o)^2 \sigma v_y + \eta \frac{\partial^2 v_y}{\partial x^2} \tag{15}$$

Also, Eq. 12 is automatically satisfied. The x component of the force equation, Eq. 11, shows that p is independent of x. In fully developed flow, the longitudinal pressure gradient, $\partial p/\partial y$, is also independent of y.

Temporal flow development is considered in the next section. For the remainder of this section, consider the flow to be steady, so that Eq. 15 reduces to

$$\frac{d^2 v_y}{dx^2} - \frac{\sigma(\mu_o H_o)^2 v_y}{\eta} = -\frac{\mu_o \sigma H_o}{\eta} E_z + \frac{1}{\eta}\frac{\partial p}{\partial y} \tag{16}$$

where the terms on the right are independent of x.

Boundary conditions for the configuration of Fig. 9.10.2 require that the velocity vanish at $x = \pm d/2$. Solution of Eq. 16 then gives

$$v_y = \left[\frac{1}{H_m^2} \frac{d^2}{4\eta} \frac{\partial p}{\partial y} - \frac{E_z}{\mu_o H_o} \right] \left[\frac{\cosh(H_m 2x/d)}{\cosh H_m} - 1 \right] \tag{17}$$

where the Hartmann[1] number, H_m, is defined as

$$H_m = \mu_o H_o \frac{d}{2} \sqrt{\frac{\sigma}{\eta}} \tag{18}$$

The velocity profile given by Eq. 17 is illustrated in Fig. 9.9.3. In the absence of a magnetic field, plane-Poiseuille flow prevails and the profile is a parabola. The tendency of the magnetic field to flatten the profile should have been expected. The current density has a direction determined by E_z', the term in brackets in Eq. 14. Wherever the velocity is so great that the "speed" field $\mu_o H_o v_y$ exceeds E_z, the force density tends to retard the motion. Thus, there is a tendency for the fluid bulk to suffer a rigid-body motion, with the strain rate confined to fully developed boundary layers. It follows from Eq. 16 that this "Hartmann layer" has an exponential profile with a thickness $\delta = d/2H_m$.

The Hartmann number indicates the degree to which the field competes with the viscosity in determining the fully developed profile. By one definition, the magnetic Hartmann number is the square root of the ratio of that part of the magnetic force density attributable to the material motion to the viscous force density. From Eq. 14, the motion-dependent part of $J \approx \sigma \mu_o v_y H_o$, so that the magnetic force density is of the order $(\sigma \mu_o v_y H_o)(\mu_o H_o)$. Using as a typical length $d/2$, the viscous force density is of the order $\eta v_y/(d/2)^2$. The square root of the ratio of these two quantities is H_m as defined by Eq. 18. This dimensionless number is alternatively defined in Sec. 8.6 as the square root of the ratio of a magnetic diffusion time to a magneto-viscous time.

Fig. 9.9.3. Velocity profile of Hartmann flow ($H_m = 10$) and plane-Poiseuille flow ($H_m = 0$).

The Hartmann flow was originally studied as a model for a liquid metal pump. The electromechanical terminal relations help to emphasize the energy conversion issues.

In practice, it is difficult to make an electrical contact between a liquid metal and a metallic electrode that does not have an appreciable contact resistance. However, with the understanding that v is the voltage across the fluid (the contact resistance might then be included in the external circuit equations), $E_z = v/w$. On the mechanical side, the pressure gradient is the pressure rise Δp divided by the length of the system in the flow direction, ℓ. Thus, Eq. 17 can be used to deduce the electromechanical terminal relations for the system by integrating over the x-z cross section to obtain the volume rate of flow Q_v:

$$Q_v \equiv w \int_{-\frac{d}{2}}^{\frac{d}{2}} v_y dx = \frac{d^3 w}{4\eta H_m^2} \left(\frac{\tanh H_m}{H_m} - 1 \right) \frac{\Delta p}{\ell} - \frac{d}{\mu_o H_o} \left(\frac{\tanh H_m}{H_m} - 1 \right) v \tag{19}$$

The electrical counterpart of this relation between the "terminals" of the system is obtained by using Eq. 17 in Eq. 14 to evaluate v_y and integrating the latter expression over the area of the input electrode:

$$i = \frac{\sigma \ell d}{w} v - \frac{\sigma \mu_o H_o \ell}{w} Q_v \tag{20}$$

With the volume rate of flow, Q_v, and voltage, v, constrained, it is convenient to solve Eq. 19 for the pressure rise and express the mechanical power output of the flow as

---

1. J. Hartmann and F. Lazarus, Kgl. Danske Videnskab. Selskab., Mat.-Fys. Medd. 15, Nos. 6 & 7 (1937)

$$\Delta p Q_v = \frac{4\eta \ell}{wd^3} \, Q_v^2 H_m \left(\frac{H_m^2}{\tanh H_m - H_m} + \underline{V} \right)$$ (21)

where $\underline{V} \equiv (v/Q_v) d^2 \sqrt{\sigma/\eta}/2$.

The electrical power input is similarly expressed by using Eq. 20:

$$vi = \frac{2\sigma \ell}{wd} \sqrt{\frac{\eta}{\sigma}} \, v Q_v (\underline{V} - H_m)$$ (22)

In these last two expressions, H_m represents the magnetic field. It plays the role of the field current, i_f, in the d-c machine of Sec. 4.10. The modes of energy conversion obtained by varying the field are seen from the dependences given by Eqs. 21 and 22 and illustrated by Fig. 9.9.4. The energy conversion regimes are as would be expected from those for the prototype machine from Sec. 4.10 (Fig. 4.10.5). The new brake regime to the left and the expanded one to the right reflect the new loss mechanism, the viscous dissipation.
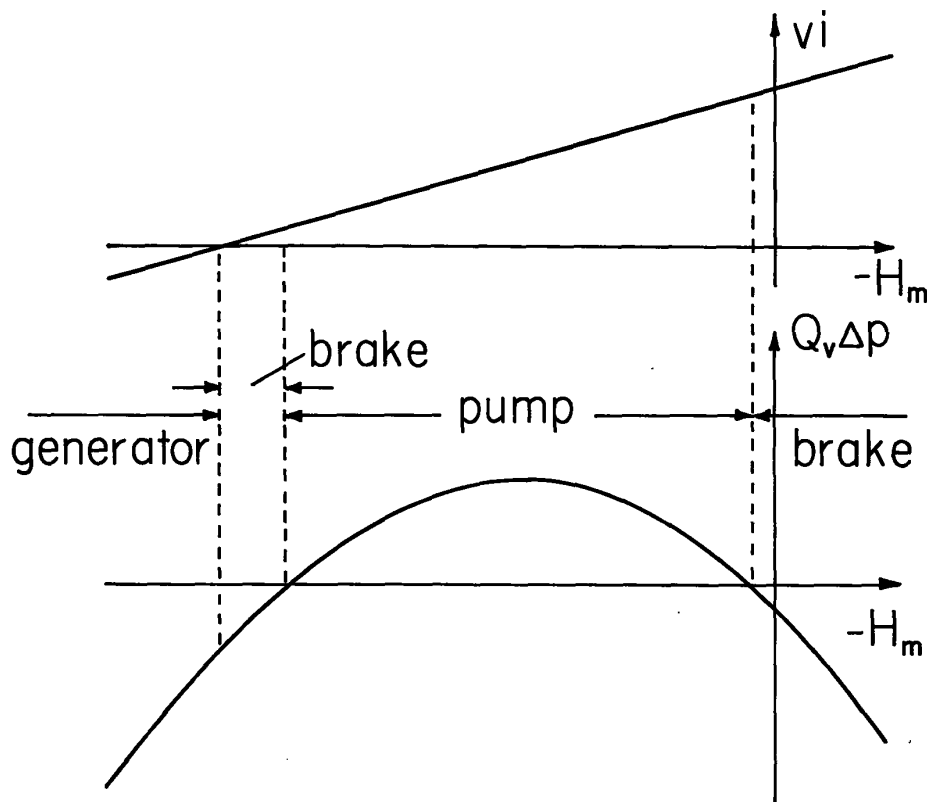

Fig. 9.9.4. Regimes of energy conversion for fully developed Hartmann flow with $\underline{V} = 10$.

9.10 Flow Development in the Magnetic Hartmann Approximation

In the absence of electromechanical interactions, the viscous diffusion time determines the time (or distance) for flow development. With the imposition of a magnetic field come processes characterized by the magneto-inertial time (Fig. 9.9.1). Because $\tau_{MI} < \tau_V$, there is now a stronger mechanism than viscous diffusion for establishing a fully developed flow.

To illustrate how induced currents can result in the establishment of fully developed flow at a rate that can be more rapid than would be expected on the basis of viscous diffusion alone, consider the configuration shown in Fig. 9.10.1. The system of Fig. 9.9.2 is essentially "wrapped around on itself" in the y direction. The annulus is thin enough compared to the radius ($a - b \equiv d \ll a$) that the planar model from Sec. 9.9 can be used. The annulus of what amounts to a Couette viscometer is filled with a liquid metal and subjected to a radial magnetic field, H_o. Motion is imparted by the rotation of the inner wall, which has a velocity U. Azimuthal fluid motion therefore induces currents in the z direction as shown in the figure.
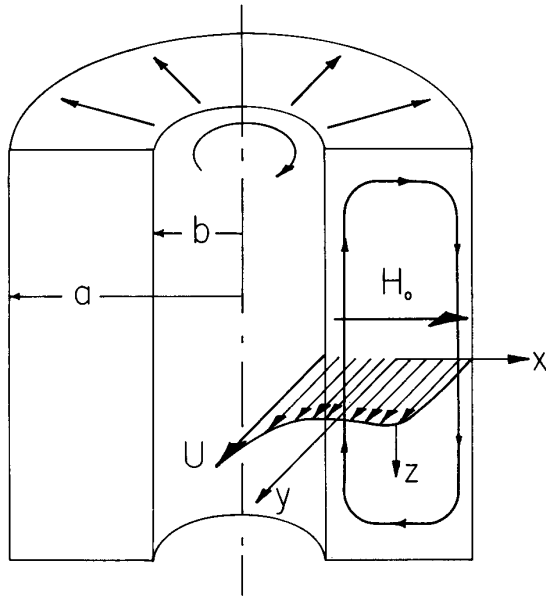
Fig. 9.10.1. Couette Hartmann flow. Inner wall rotates while outer one is fixed.
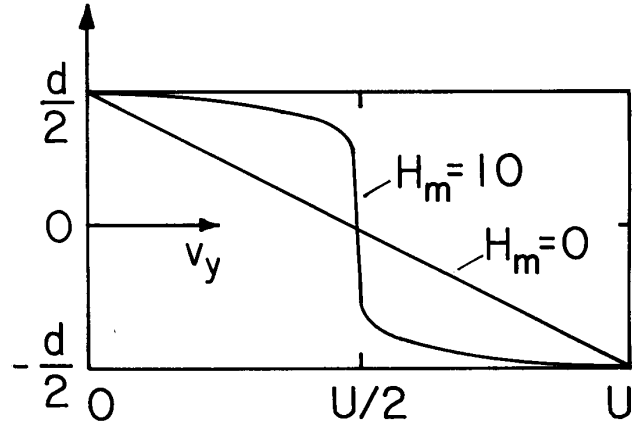
Fig. 9.10.2. Fully developed profile in Couette Hartmann flow of Fig. 9.10.1.

A filmed experiment (Reference 7, Appendix C) shows how the liquid responds as the inner wall is suddenly set into steady motion. Because the upper and lower surfaces of the annular region of liquid metal are bounded by insulators, the current that flows in the z direction over the region of the annulus well removed from the end circulates through the end regions. Thus, the net current in the z direction at any instant is zero. Questions to be answered here include, what is the fully developed velocity profile and what characteristic times govern in its establishment?[1]

The channel closes on itself in the azimuthal direction, and hence the pressure gradient in that direction is zero. This is the y direction in the planar model, and hence Eq. 9.9.15 reduces to

$$\rho \frac{\partial v_y}{\partial t} = \mu_o \sigma H_o E_z - (\mu_o H_o)^2 \sigma v_y + \eta \frac{\partial^2 v_y}{\partial x^2} \tag{1}$$

Because the net current in the z direction must be zero, the integral of J_z over the cross section must be zero. With J_z given by Eq. 9.9.14, it follows that E_z is related to v_y by the condition

$$E_z = \frac{\mu_o H_o}{d} \int_{-\frac{d}{2}}^{\frac{d}{2}} v_y d\cancel{x} \tag{2}$$

Representation of the temporal transient leading to the fully developed flow is carried out as in Sec. 9.6. The fully developed flow plays the role of a particular solution. It follows from Eq. 1 with $\partial v_y/\partial t \to 0$ and Eq. 2 together with the boundary conditions that $v_y(d/2) = 0$ and $v_y(-d/2) = U$, that

$$v_y = \frac{U}{2} \left[1 - \frac{\sinh(H_m 2x/d)}{\sinh H_m} \right] \tag{3}$$

where $H_m \equiv \mu_o H_o (d/2)\sqrt{\sigma/\eta}$. (This expression follows using the same steps as lead to Eq. 9.9.17.) The profile is shown in Fig. 9.10.2.

To satisfy the initial conditions, superimposed on this fully developed flow are the temporal modes. These are solutions to Eqs. 1 and 2 with the homogeneous boundary conditions $v_y(\pm d/2) = 0$.

---

1. For model in circular geometry, see W. H. Heiser and J. A. Shercliff, "A Simple Demonstration of the Hartmann Layer," J. Fluid Mech. 22, 701-707 (1965).

The temporal modes are assumed to take the form $v_y = \text{Re } \hat{v}_y(x)\exp(st)$. Thus, Eq. 1 becomes

$$\frac{d^2\hat{v}_y}{dx^2} - \gamma^2\hat{v}_y = -\frac{\mu_o\sigma H_o}{\eta}\hat{E}_z \tag{4}$$

where

$$\gamma^2 \equiv \frac{s\rho}{\eta} + \frac{\mu_o^2 H_o^2 \sigma}{\eta}$$

Solutions to Eq. 4 are the sum of a particular solution and two homogeneous solutions

$$\hat{v}_y = \frac{\mu_o\sigma H_o}{\eta\gamma^2}\hat{E}_z + A \sinh \gamma x + C \cosh \gamma x \tag{5}$$

This expression is substituted into Eq. 2 to find E_z in terms of the coefficient C:

$$\hat{E}_z = C \frac{\mu_o H_o \sinh(d\gamma/2)}{(\frac{d\gamma}{2})\left[1 - H_m^2/(\frac{d\gamma}{2})^2\right]} \tag{6}$$

Thus, Eq. 5 becomes

$$\hat{v}_y = A \left\{\sinh \gamma x\right\} + C \left\{\frac{H_m^2 \sinh(d\gamma/2)}{(d\gamma/2)^3\left[1 - H_m^2/(d\gamma/2)^2\right]} + \cosh \gamma x\right\} \tag{7}$$

The coefficients A and C are now adjusted to insure that $v_y = 0$ at $x = \pm\, d/2$. Because these coefficients can respectively be identified with the odd and even temporal modes, it is possible to determine the eigenvalues and associated eigenmodes by inspection. Odd modes can be made to satisfy the boundary conditions by having C = 0 and the coefficient of A vanish at either of the boundaries:

$$\sinh\left(\frac{d\gamma_o}{2}\right) = 0 \tag{8}$$

Here, o is used to denote the odd eigenvalues. Similarly, the even modes follow from Eq. 7 as resulting if A = 0 and the coefficient of C vanishes at either of the boundaries:

$$\frac{H_m^2 \sinh\left(\frac{d\gamma_e}{2}\right)}{\left(\frac{d\gamma_e}{2}\right)^3\left[1 - H_m^2/\left(\frac{d\gamma_e}{2}\right)^2\right]} + \cosh\left(\frac{\gamma_e d}{2}\right) = 0 \tag{9}$$

Thus, the total solution, the sum of the fully developed profile from Eq. 3 and the transient solution given by Eq. 7, is

$$v_y = \frac{U}{2}\left[1 - \frac{\sinh(H_m\frac{2x}{d})}{\sinh H_m}\right] + \text{Re } \sum_{o=1}^{\infty} A_o \sinh(\gamma_o x)e^{s_o t} + \text{Re } \sum_{e=1}^{\infty} C_e\left[\cosh(\gamma_e x) - \cosh(\frac{\gamma_e d}{2})\right]e^{s_e t} \tag{10}$$

Here, the coefficient of C has been simplified by using Eq. 9. The eigenfrequencies s_o and s_e of the even and odd modes follow from the definition of γ given with Eq. 4. Roots of Eq. 8 are simply $\gamma_o d/2 = jo\pi$, and hence the odd modes have the eigenfrequencies

$$\omega_o = \frac{1}{\tau_v}[H_m^2 + (o\pi)^2]; \quad o = 1,2,\cdots \tag{11}$$

where τ_v is the viscous diffusion time $(\rho/\eta)(d/2)^2$ based on the annulus half-width. These modes are so simply described because the condition on E_z is automatically satisfied by the odd modes with $E_z = 0$. Thus it is that temporal modes found here are a limiting case of those found in Sec. 8.6. That is, in the limit $\tau_m \ll \tau_{MI}$, Eq. 8.6.15 reduces to Eq. 11, where $H_m^2 \equiv \tau_m\tau_v/\tau_{MI}^2$.

To find the eigenvalues, γ_e, and eigenfrequencies, s_e, of the even modes, it is convenient to replace $\gamma_e \to j\beta_e$ and write Eq. 9 as
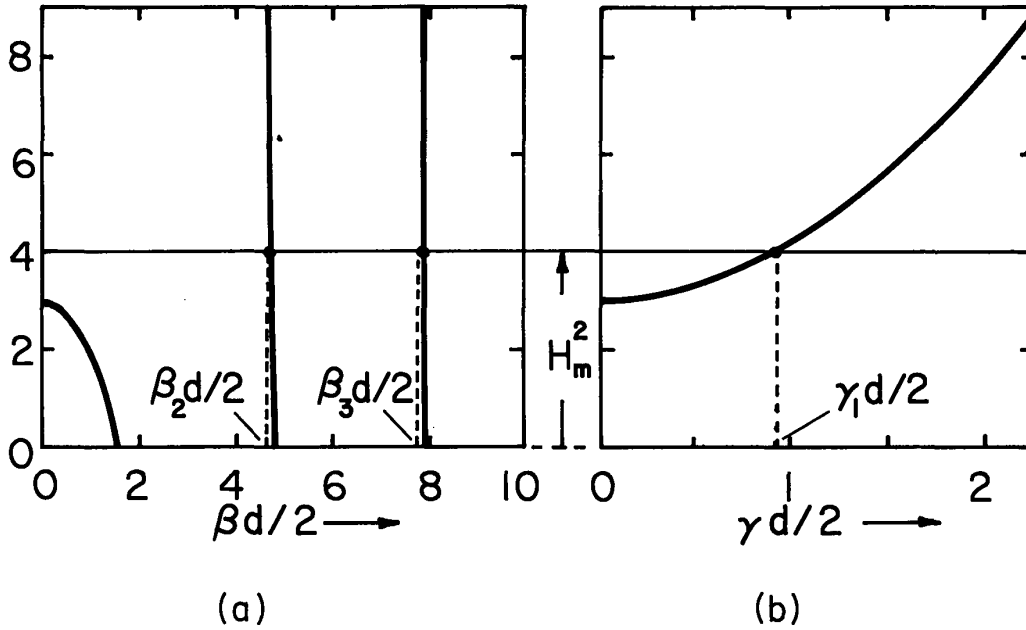
Fig. 9.10.3. Graphical solution of Eq. 12 for eigenvalues $\gamma_e d/2 \equiv j\beta_e d/2$ of even temporal modes.

$$H_m^2 = - \left(\frac{\beta_e d}{2}\right)^3 / \left[\left(\frac{\beta_e d}{2}\right) - \tan\left(\frac{\beta_e d}{2}\right)\right]$$

(12)

so that a graphical solution, Fig. 9.10.3a, gives the required modes. For these modes, the eigenvalues are themselves a function of H_m^2. From the definition of γ^2 (Eq. 4) the even-mode eigenvalues thus determined then give the eigenfrequencies:

$$s_e = - \frac{1}{\tau_v} \left[H_m^2 - \left(\frac{\gamma_e d}{2}\right)^2\right]$$

(13)

The even modes, $e \neq 1$, have eigenvalues that are essentially independent of H_m: $\beta_e d/2 \simeq 3\pi/2$, $5\pi/2, \cdots$. These even modes therefore have characteristic times having much the same nature as for the odd modes. With the magnetic field raised to a level such that H_m exceeds several multiples of π, the lower order modes have decay rates that are of the order $\tau_v/H_m^2 = \tau_{MI}(\tau_{MI}/\tau_m)$. These modes represent the relative adjustment of the profile so that the core of the fluid suffers essentially rigid-body translation. One way to envision the magnetic damping represented by these eigenfrequencies is to select a contour of fixed identity as shown in Fig. 9.10.4. Any vorticity results in an increasing flux linkage for such a loop. The current induced in response to the resulting rate of change of flux linkage results in a force tending to flatten the profile.
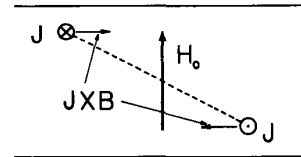
Although the magnetic field has a strong effect on the rate at which rigid-body motion is seen in the fluid bulk, the fluid nevertheless comes up to speed at a much slower rate. This process is represented by the lowest even mode, $e=1$. As H_m^2 is raised, the eigenvalue decreases to zero (at $H_m^2 = 3$) and then becomes purely real with a graphical solution gotten by plotting Eq. 12 with $j\beta_e \rightarrow \gamma_e$. The graphical solution is illustrated in Fig. 9.10.3b. As H_m becomes large, this root can be approximated by $(d\gamma/2)^2 \rightarrow H_m^2 - H_m$. Then the associated eigenfrequency is

Fig. 9.10.4. Contour of fixed identity in fluid.

$$s = - \frac{H_m}{\tau_v} = - \frac{\mu_o H_o \sqrt{\sigma\eta}}{\rho(d/2)}$$

(14)

Thus, the time required to get the rigid translating core of the fluid up to its steady velocity $U/2$ is τ_v/H_m, which is longer than the dominant time for the relative motion to establish itself, τ_v/H_m^2.

There is a simple picture to go with the transient represented by this lowest even mode. With H_m large, the profile consists of Hartmann boundary layers connected by a uniform profile. In the neighbor-

hood of the boundary, the steady profile is exponential with a decay length

$$\delta = d/2H_m \tag{15}$$

The viscous stress imparted to the fluid by the wall is of the order $\eta v_{wall}/\delta$. This stress must accelerate the core of the fluid to half of the velocity at the wall, and hence must be equal to $s\rho d v_{wall}/2$. Balancing of the inertial and viscous stresses results in a characteristic frequency consistent with Eq. 14.

Because currents circulate within the fluid, there is no net magnetic force on the fluid to contribute directly to its acceleration. The magnetic field plays a role in Eq. 14 only because it determines the thickness of the boundary layer, and hence the shear rate and the viscous stress.

9.11 Electrohydrodynamic Imposed Field Approximation

With the material motion prescribed, the imposed field approximation with unipolar conduction is as introduced in Sec. 5.3. In the region of interest, the electric field is largely due to external charges, perhaps on electrodes bounding the volume. The validity of the approximation hinges on the self-precipitation time τ_e being longer than the charge migration time τ_{mig}. This characteristic time interpretation of the approximation is discussed in Sec. 5.6. It can be stated formally by observing that the pertinent EQS equations of motion (Eqs. 11, 10 and 9 of Sec. 5.2, written for one species and no diffusion), together with the force and continuity equation for an incompressible fluid, take the normalized form

$$\nabla \times \vec{E} = 0; \quad \vec{E} = -\nabla \Phi \tag{1}$$

$$\nabla \cdot \vec{E} = \frac{\tau_{mig}}{\tau_e} \rho_f \tag{2}$$

$$\frac{\partial \rho_f}{\partial t} + (\frac{\tau}{\tau_{mig}} \vec{E} + \vec{v}) \cdot \nabla \rho_f + \frac{\tau}{\tau_e} \rho_f^2 = 0 \tag{3}$$

$$\frac{\partial v}{\partial t} + \vec{v} \cdot \nabla \vec{v} + (\frac{\tau}{\tau_{EI}})^2 \nabla p = (\frac{\tau}{\tau_{EI}})^2 \rho_f E + \frac{\tau}{\tau_V} \nabla^2 \vec{v} \tag{4}$$

$$\nabla \cdot v = 0 \tag{5}$$

Here, the normalization is as used in connection with Eqs. 4a, ρ_o and $\mathscr{E}$ are typical of the free charge density and imposed electric field, and the times that have been identified are

$$\tau_e \equiv \frac{\varepsilon_o}{\rho_o b}; \quad \tau_{mig} = \frac{\ell}{b\mathscr{E}}; \quad \tau_V = \frac{\rho \ell^2}{\eta}; \quad \tau_{EI} = \sqrt{\frac{\rho \ell}{\rho_o \mathscr{E}}} \tag{6}$$

In the imposed field approximation, times of interest, τ, are short compared to the self-precipitation time τ_e. If processes involve viscous diffusion, particle migration and electromechanical coupling to the fluid, then for the imposed approximation to be appropriate, the associated characteristic times must all be shorter than τ_e. But, regardless of the ordering of times, τ_{mig} must be shorter than τ_e if the approximation is to apply (Fig. 9.11.1). This means that the volume charge density term on the right in Eq. 2 is also ignorable, as is also the last (self-precipitation) term in Eq. 3.

In summary, the electric field is approximated as being both irrotational and solenoidal. The charge density is governed by the same rules as outlined in Sec. 5.3. Thus, ρ_f is constant along characteristic lines (Eqs. 5.3.3 and 4.3.4). Unless processes represented by the viscous diffusion and electro-inertial times can be ignored, the mechanical laws are represented by the Navier-Stokes equation, with the force density $\rho_f \vec{E}$, and the condition that $\vec{v}$ be solenoidal.
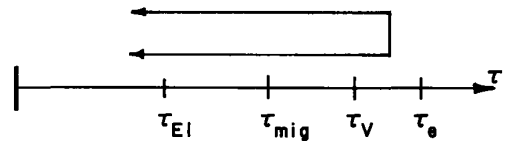

Fig. 9.11.1. Ordering of characteristic times in the EQS imposed field approximation.

9.12 Electrohydrodynamic "Hartmann" Flow

The competition between viscous and magnetic stresses that establishes the fully developed Hartmann flow illustrated in Sec. 9.11 has as an EQS analogue the fully developed flow in the "ion drag" configuration of Fig. 9.12.1. Charged particles, uniformly injected at the inlet where z = 0, might be ions generated upstream by a corona discharge, or might be charged macroscopic particles. They are collected by a screen electrode at z = ℓ. Although it might be used as a pump in the conventional sense, practical interest in the interaction illustrated would more likely come from a need to account for fluid-mechanical effects on the transport of macroscopic particles. Without a self-consistent representation of the effect of the field on the material motion, the interaction is developed in Sec. 5.7. There, space-charge effects are included, whereas here the electric field is approximated by the imposed field. The objective here is to illustrate the reaction of the field on the flow.

The conduction law and force density for charge carriers that individually transmit the electrical force to a neutral medium are discussed in Secs. 3.2, 3.3 and 5.2. In terms of the mobility b, the current density in the z direction is

$$J_z = \rho_f(bE_z + v_z) \tag{1}$$

where bE_z is the particle velocity relative to the air, and the fluid is itself moving at the velocity v_z. There is only one species of particles, and effects of diffusion and generation are negligible.

Because the electric field induced by charges in the fluid is negligible compared to that imposed by means of the electrodes,

$$\vec{E} \approx E_o \vec{i}_z = \frac{V}{\ell} \vec{i}_z \tag{2}$$

and Gauss' law is ignored in further developments. Note that Eq. 2 is consistent with there being no current density normal to the insulating walls. Fully developed solutions are of the form

$$\vec{v} = v_z(r)\vec{i}_z; \quad \rho_f = \rho_f(r)$$
$$\vec{J}_f = J_z(r)\vec{i}_z; \quad \frac{\partial p}{\partial z} = \text{constant} \tag{3}$$

and hence $\vec{v}$ and $\vec{J}_f$ are automatically solenoidal so that mass and charge conservation are insured. Effects of gravity are lumped with the pressure, and therefore only the z component of the Navier-Stokes equation remains to be satisfied:

$$\frac{\partial p}{\partial z} = \rho_f E_o + \frac{\eta}{r}\frac{\partial}{\partial r}\left(r\frac{\partial v_z}{\partial r}\right) \tag{4}$$

The current density, J_f, has a radial dependence determined at the inlet. Here, $J_f = J_o$ is taken as uniform over the cross section so that Eq. 1 is solved for the charge density and substituted into Eq. 4 to obtain a differential equation for the velocity profile:

$$\frac{\partial p}{\partial z} = \frac{J_o E_o}{(bE_o + v_z)} + \frac{\eta}{r}\frac{d}{dr}\left(r\frac{dv_z}{dr}\right) \tag{5}$$

This nonlinear expression is reduced to a linear one by restricting attention to circumstances when $bE_o \gg v_z$ so that $(bE_o + v_z)^{-1} \approx (bE_o)^{-1} - v_z(bE_o)^{-2}$ and Eq. 5 can be written as a linear equation but with space varying coefficients:

$$\frac{1}{r}\frac{d}{dr}\left(r\frac{dv_z}{dr}\right) - \frac{J_o}{\eta b^2 E_o}v_z = \frac{1}{\eta}\left(\frac{\partial p}{\partial z} - \frac{J_o}{b}\right) \tag{6}$$

Homogeneous solutions to Eq. 6 are zero order modified Bessel's functions (introduced in
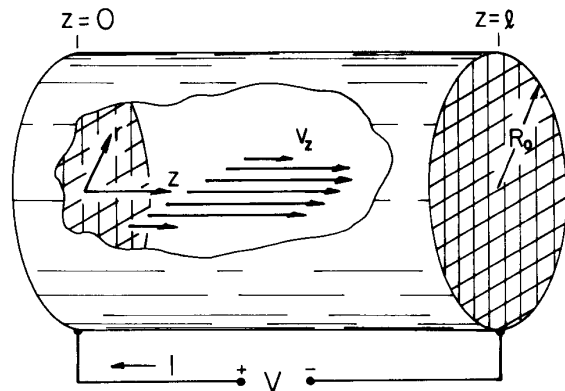

Fig. 9.12.1. Circular cylindrical conduit having insulating wall supporting screens at z = 0 and z = ℓ. Charged particles are injected at left and pulled through the fluid to provide electrohydrodynamic pumping. Flow is electric analogue of Hartmann flow.

Sec. 2.16, Eqs. 2.16.19 and 2.16.25). Because r = 0 is included in the flow, the singular solution is excluded. The particular plus homogeneous solution to Eq. 6 that makes $v_z(R_o) = 0$ is then

$$v_z = \frac{R_o^2}{\eta H_e^2} \left[\frac{J_o}{b} - \frac{\partial p}{\partial z} \right] \left[1 - \frac{I_o(H_e \frac{r}{R_o})}{I_o(H_e)} \right] \tag{7}$$

where the electric Hartmann number is $H_e \equiv \sqrt{J_o R_o^2 / \eta b^2 E_o}$. Note the analogy between this profile and that for the magnetic Hartmann flow represented by Eq. 9.10.17. Here, H_e^2 is the ratio of that part of the electric force density that is proportional to the fluid velocity to the viscous force density. An alternative interpretation comes from recognizing that $H_e = \sqrt{\tau_{mig}/\tau_{EV}}$ where $\tau_{mig} = R_o/bE_o$ (the time for a particle to migrate the radius R_o relative to the fluid) and $\tau_{EV} \equiv \eta b/J_o R_o$. The electro-viscous time, τ_{EV}, assumes the form $\eta/\varepsilon E^2$ familiar from Sec. 8.7, provided that $J_o \approx \rho_f b E_o$ and one of the E's is recognized from Gauss' law to be of the order $\rho_f R_o/\varepsilon$.

The pump characteristic is obtained by integrating Eq. 7 over the channel cross section, defining Q_v as the volume rate of flow and recognizing that the pressure rise Δp through a channel of length ℓ is $\ell(\partial p/\partial z)$ [from Eq. 2.16.26a, the integral of $xI_o(x)$ is $xI_1(x)$],

$$Q_v = \frac{2\pi R_o^4}{\eta H_e^2} \left[\frac{\Delta p}{\ell} - \frac{J_o}{b} \right] \left[\frac{I_1(H_e)}{H_e I_o(H_e)} - \frac{1}{2} \right] \tag{8}$$

The velocity profile given by Eq. 7 has the dependence on the electric Hartmann number illustrated in Fig. 9.12.2. Because $\vec{E}$ is taken as constant throughout, the force density is proportional to the charge density. With a constant current density, it is seen from Eq. 1 that the charge density is least where the velocity is the most. In spite of the viscous retarding stresses, the tendency is for elements near the wall to catch up with those nearer the center.
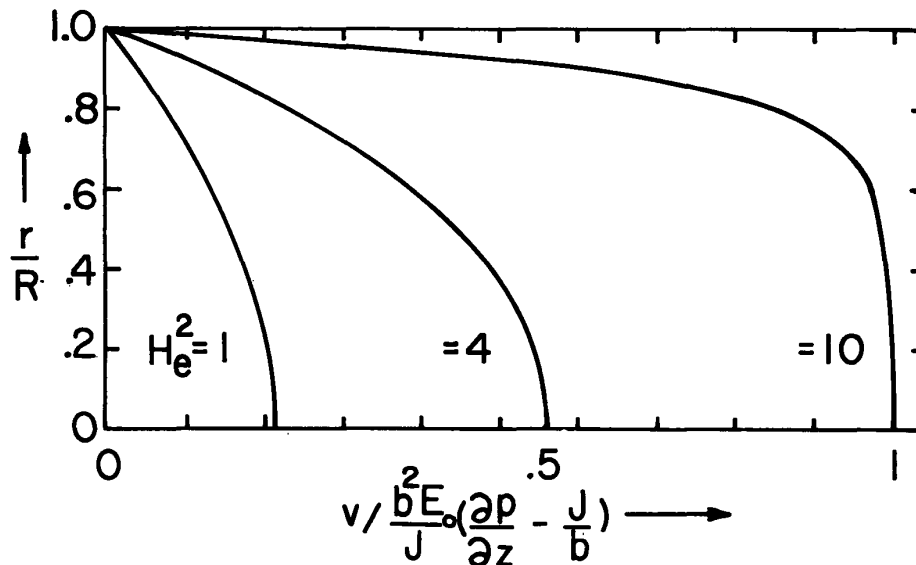

Fig. 9.12.2. Velocity profile with electric Hartmann number as a parameter for configuration of Fig. 9.12.1.

9.13 Quasi-One-Dimensional Free Surface Models

Channel flows, such as in rivers, canals and aqueducts, are a hydrodynamic example of the class of mechanical and electromechanical flow configurations considered in this and the next section. Thus, as an example, homogeneous incompressible fluid, typically water, rests on a bottom having the elevation b(z), as shown in Fig. 9.13.1. The interface at x = ξ(z,t) forms the upper "wall" of a natural conduit for the flow. Gravity confines the fluid to the neighborhood of the bottom. The height of this upper channel boundary, ξ(z,t), is itself determined by the fluid mechanics.

$$A = \xi - b \quad ; \quad f = \rho g \xi - \frac{1}{2}\epsilon_o \frac{V^2}{(a-\xi)^2}$$
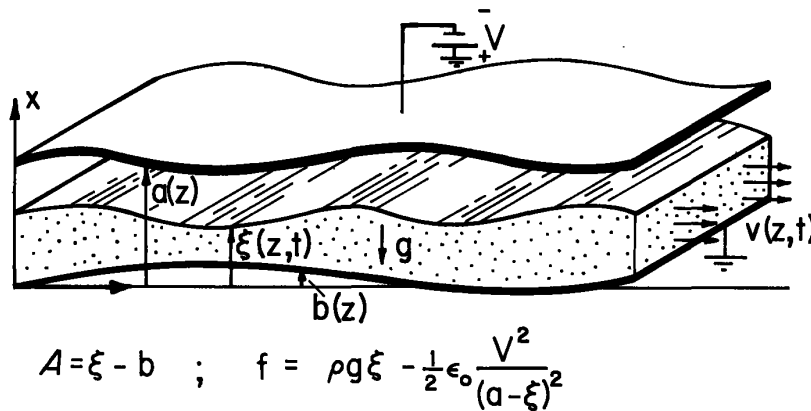
Fig. 9.13.1. Gravity flow with constant potential interface stressed by electric field. Quasi-one-dimensional model expressed by Eqs. 11 and 12 reduces to classic gravity-wave model if V = 0. The hydromagnetic flux conserving antidual of this potential conserving continuum is suggested by Sec. 8.5.

In the purely hydrodynamic context, a canoeist might ask of a long-wave model, given a downstream rock hidden at the bottom of the river [represented by b(z)], can he expect the surface he sees above the rock to be elevated or depressed? In the next section, it will be seen that the answer to such a question depends on the upstream flow conditions relative to the velocity of propagation of a gravity wave. Questions to be asked, where electric or magnetic forces alter or replace gravity, are similar. By way of illustration, an electrode is placed over the flow in Fig. 9.13.1 to impose an electric stress on the interface. The charge relaxation time in the liquid is presumed short enough that the interface can be regarded as retaining a constant potential. However, the electric surface force density is determined by not only V and a(z), but by the position of the interface as well. Of course, it is hardly on the scale of a canoe that the electric field could compete with effects of gravity. But on a scale somewhat larger than a Taylor wavelength, variations in a(z) can affect the flow in a way that depends on the upstream flow relative to a wave velocity altered by the electric field.

The electromechanical coupling due to the electric stress is typical of a wide range of electromechanical interactions that can be modeled using the prototype laws derived in this section. The configuration of Fig. 9.13.1 is typical because the fluid is subject to a volume force density (due to gravity) that can be represented as the gradient of a pressure and because the surface force density (due to the surface free-charge force density) acts normal to the interface.

Many seemingly different mechanical and electromechanical configurations have in common the following properties:

a) The dominant flow is in an axial direction, usually denoted here by z. The viscous skin depth is small compared to the transverse dimensions of the flow. Effects of viscosity are therefore ignored compared to inertial effects, and the longitudinal flow velocity is essentially independent of the transverse coordinates:

$$\vec{v} = \vec{v}_T(x,y,z,t) + v(z,t)\vec{i}_z \tag{1}$$

Because the interfaces are not subject to shear stresses, this approximation is especially appropriate for free surface flows.

b) In the absence of flow, the free surface can assume a shape such that the conditions for a static equilibrium as defined in Sec. 8.2 prevail. Thus, electrical force densities are of the form $\vec{F} = -\nabla \xi$ and surface force densities act normal to the interface.

c) Variations of the configuration with respect to the longitudinal direction are sufficiently slow that a quasi-one-dimensional model is appropriate.

A formal derivation of the canonical equations of motion for this class of flows is based on the space-rate parameter expansion introduced in Sec. 4.12 and applied to the Navier-Stokes and continuity equations (in two dimensions) in Sec. 9.7. With ℓ and d respectively representing typical dimensions in the longitudinal and transverse directions, $(d/\ell)^2 \ll 1$. What approximations are appropriate in the laws of fluid mechanics follow from a review of Eqs. 9.7.1 - 9.7.4.

Longitudinal Force Equation: First, the transverse force equation is approximated by a balance between the pressure gradient and any volume force density that is present. To first order in $(d/\ell)^2$

$$\nabla_T (p + \mathcal{E} - \rho \vec{g} \cdot \vec{r}) = 0 \tag{2}$$

as illustrated in two dimensions by Eq. 9.7.1. Here ∇_T is the gradient in the transverse directions (x,y). In the large, at the interface and in the bulk, the cross section at any given longitudinal position is in a state equivalent to a static equilibrium. Within the fluid,

$$p + \mathcal{E} - \rho \vec{g} \cdot \vec{r} = f(z,t) \tag{3}$$

where f is determined by the normal stress balance at the interface. With the presumption that the velocity takes of the form of Eq. 1, the longitudinal force equation for the fluid becomes simply

$$\rho \left(\frac{\partial v}{\partial t} + v \frac{\partial v}{\partial z} \right) + \frac{\partial f}{\partial z} = 0 \tag{4}$$

At each z-t plane, the pressure, p, and surface force density (if any) must balance. This uniquely specifies the cross-sectional geometry and f in terms of one scalar function, the transverse area $A(z,t)$:

$$p + \mathcal{E} - \rho \vec{g} \cdot \vec{r} = f(A) \tag{5}$$

This hybrid pressure function serves to evaluate Eq. 4, which then becomes one of two mechanical equations of motion in the variables (v,A). If electromechanical coupling is involved, the pressure of Eq. 5 will also be dependent on electric or magnetic variables.

Mass Conservation: All of the term in the statement of mass conservation are of the same order in $(d/\ell)^2$. (For example, see Eq. 9.7.3.) Thus, all terms are retained. Because the fluid is homogeneous and incompressible, the integral statement of mass conservation for a section on the fluid having incremental lengths Δz, shown in Fig. 9.13.2, is

$$\oint_S \vec{v} \cdot \vec{n} da = \Delta z \int_C \vec{v} \cdot \vec{n} d\ell + A(z+\Delta z) v(z+\Delta z)$$

$$- A(z)v(z) = 0 \tag{6}$$

Fig. 9.13.2

Control volume for flow with transverse boundaries S_2, S_3, and free surface S_1.

Portions of the transverse surface S_1 are bounded by rigid walls, while others are the free surface. Integrations over the cross-sectional surfaces S_2 and S_3, which have fixed locations z + Δz and z, account for the last two terms in Eq. 6. By definition, the surface S_1 deforms with the interface, so the velocity in the integrand of the first term on the right in Eq. 6 is the interfacial velocity. To first order in the incremental length Δz, the integration on S_1 is reduced to an integration around the contour C multiplied by the length Δz.

The simple geometric significance of the contour integral in Eq. 6 is seen by using the volume form of the generalized Leibnitz rule for differentiation of an integral over a time-varying volume. With $\zeta = 1$, and applied to a right cylinder having the cross section A (not the volume element of Fig. 9.13.2, but rather a right cylinder with fixed ends), Eq. 2.6.5 becomes

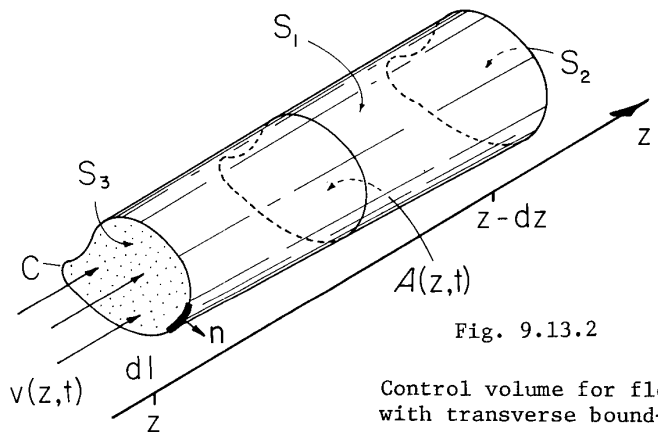$$\frac{d}{dt} \int_V dV = \Delta z \int_C \vec{v} \cdot \vec{n} d\ell \tag{7}$$

The longitudinal length of the volume in Eq. 7 is fixed, so it follows that this expression is equivalent to

$$\Delta z \left. \frac{dA}{dt} \right|_z = \Delta z \int_C \vec{v} \cdot \vec{n} d\ell \tag{8}$$

The desired quasi-one-dimensional statement of mass conservation follows by substituting the contour integral of Eq. 8 into Eq. 6 and taking the limit $\Delta z \to 0$,

$$\frac{\partial A}{\partial t} + \frac{\partial}{\partial z} (Av) = 0 \tag{9}$$

In the derivation, z has been considered a fixed quantity. Because A is not only a function of t, but of z as well, the temporal partial derivative (the time derivative holding z fixed) is now used in Eq. 9.

Gravity Flow with Electric Surface Stress: As a specific application of the long-wave model, consider the configuration of Fig. 9.13.1. In the long-wave approximation, the zero order electric field in the gap between interface and upper electrode is (see Sec. 4.12 for a formal space-rate expansion):

$$\vec{E} \simeq \vec{i}_x \frac{V}{a(z) - \xi(z,t)} \tag{10}$$

To zero order, this is also the electric field, E_n, normal to the interface. Balance of stresses at the interface requires that $p(\xi) = - \frac{1}{2} \varepsilon_0 E_n^2$, where, because the mass density of the upper fluid is much less than that below, the pressure above is defined as zero. Gravity causes the only force density in the fluid volume, so $\xi - \rho \vec{g} \cdot \vec{r} = \rho g x$. Thus, evaluation of Eq. 3 at the interface gives $f = p(\xi) + \rho g \xi$. This result makes it possible to express the longitudinal force equation, Eq. 4, in terms of (v, ξ): of (v, ξ):

$$\rho(\frac{\partial v}{\partial t} + v \frac{\partial v}{\partial z}) + \frac{\partial}{\partial z} \left[\rho g \xi - \frac{1}{2} \varepsilon_0 \frac{v^2}{(a - \xi)^2} \right] = 0 \tag{11}$$

Because the flow is independent of y, the flow area is taken as an area per unit length in the y direction, $A \to \xi - b$. Thus, Eq. 9 becomes

$$\frac{\partial \xi}{\partial t} + \frac{\partial}{\partial z} [v(\xi - b)] = 0 \tag{12}$$

With a(z) and b(z) prescribed, these last two nonlinear expressions comprise the quasi-one-dimensional model. With the removal of the voltage, they become the classic equations for gravity waves and flows.

A second configuration having a small enough scale that capillary effects dominate those due to gravity is shown in Fig. 9.13.3.[1] Here, polarization forces augment and stabilize the tendency of the capillary forces to provide a flow having most of its surface "free." Such "wall-less" flow structures provide for a gravity-independent channeling of a flowing liquid while permitting the interface to be active in heat or mass transfer processes.

It is instructive to linearize Eqs. 11 and 12. With the electrode and bottom flat, so that a and b are constants, and for perturbations from a static equilibrium in which the fluid depth is constant, the dispersion equation must agree with what is obtained from a linear (small-amplitude) theory as would develop following the approach of Sec. 8.10. Illustrated once again is the equivalence between a linearized quasi-one-dimensional model and a long-wave limit of a linearized model (Fig. 4.12.2).

Steady flow phenomena predicted by the models developed in this section are illustrated in Sec. 9.14. Nonlinear temporal transients are taken up using the method of characteristics in Chap. 11. That even steady-state phenomena depend on the causal effect of wave propagation is already evident in Sec. 9.14.

9.14 Conservative Transitions in Piecewise Homogeneous Flows

Piecewise irrotational steady flows are illustrated in this section with a quasi-one-dimensional model that can be applied to a variety of interactions with fields. Typical is the configuration shown in Fig. 9.14.1. Liquid flows in the y direction with variations in the depth $\xi(y)$ slow enough that the velocity profile is essentially independent of depth: $\vec{v} = v\vec{i}_y$. (The longitudinal coordinate is taken as y rather than the z used in Sec. 9.13.)

---

1. See T. B. Jones, Jr., and J. R. Melcher, "Dynamics of Electromechanical Flow Structures," Phys. Fluids 16, 393-400 (1973).
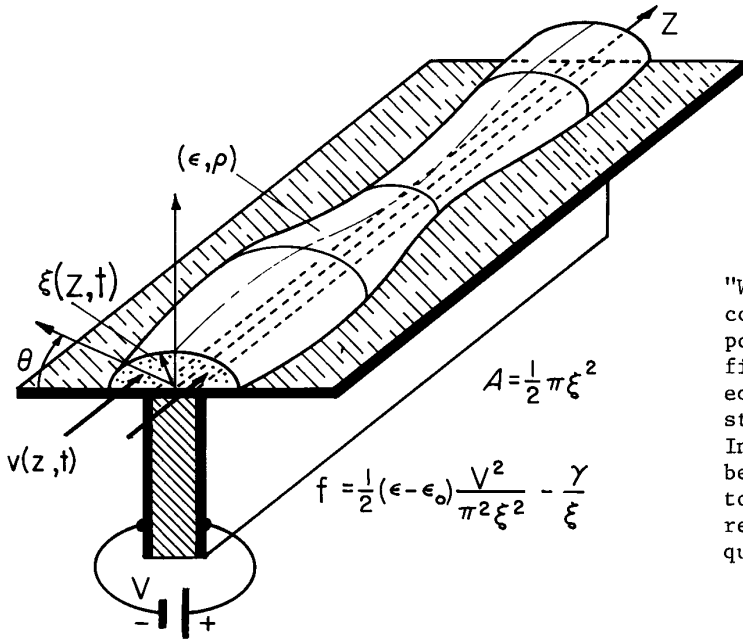
Fig. 9.13.3

"Wall-less" pipe in which fluid is confined by means of capillary and polarization forces. The electric field also stabilizes the transverse equilibrium against the pinch instability caused by surface tension. In practice the applied field should be a-c having a high enough frequency to avoid free charge and mechanical response at twice the applied frequency.

$$A = \frac{1}{2}\pi\xi^2$$

$$f = \frac{1}{2}(\epsilon - \epsilon_o)\frac{V^2}{\pi^2\xi^2} - \frac{\gamma}{\xi}$$

A magnetic field is imposed in the x-y plane. The fluid is an electrolyte or even a liquid metal, so that a uniform current density, J_o, can be imposed in the z direction. However, the flow velocity and conductivity are low enough that the magnetic Reynolds number is small. Currents induced by the motion through the imposed magnetic field can therefore be ignored. So also can the magnetic field generated by J_o.

Given the velocity v_∞ and depth ξ_∞ where the fluid enters at the left, what are these quantities as a function of y? For purposes of illustration the magnetic field is imposed by a two-dimensional magnetic dipole adjacent to the channel bottom (at the origin).

First, observe that the magnetic field and current configuration are the same as illustrated in the last part of Sec. 8.4. Thus, the magnetic force density takes the form $\vec{F} = -\nabla\mathcal{E}$ where, if J_o and $A(x,y)$ are respectively the z-directed current density and vector potential for the imposed magnetic field, $\mathcal{E} = -J_o A$ (Eq. 8.4.13). For an N-turn coil with elements having the spacing s, as shown in Fig. 9.14.1, a driving current, i, results in the vector potential

$$A = \frac{sNi}{2\pi} \frac{\sin\theta}{r} \tag{1}$$

Transformed to Cartesian coordinates, this function becomes

$$A = \frac{sNi}{2\pi} \frac{x}{x^2 + y^2} \tag{2}$$

Steady-state conservation of mass, as expressed by Eq. 9.13.9, requires that the volume rate of flow be the same over the cross section at any position y:

$$\xi v_y = \xi_\infty v_\infty \tag{3}$$

In the longitudinal force equation, Eq. 9.13.4, $-\rho\vec{g}\cdot\vec{r} = \rho g x$ and $\partial/\partial t = 0$; and, by recognizing that $v\partial v/\partial y = \partial(\frac{1}{2}v^2)/\partial y$, it follows that

$$\frac{\partial}{\partial y}[\frac{1}{2}\rho v^2 + f] = 0 \Rightarrow \frac{1}{2}\rho v^2 + f = \Pi \tag{4}$$

This is the same expression that is obtained from Bernnoulli's equation, Eq. 7.8.11, if $\vec{v} \approx v\vec{i}_y$.

At the interface there are no surface currents Also the fluid has negligible magnetizability, so there is no magnetic surface force density. Variations of the interface are on a scale long enough (compared to the Taylor wavelength, Eq. 8.9.15) that surface tension can be ignored. Thus, interfacial stress balance shows that the pressure is continuous at the interface. Because the mass density and current density above the layer are negligible, the pressure there is constant and can be defined as zero. Thus, evaluation of Eq. 9.13.3 at the interface, where $p = 0$, gives f, and Eq. 4 becomes

Fig. 9.14.1. Cross section of fluid flowing to right through imposed magnetic dipole. Uniform current density is imposed into paper.

$$\frac{1}{2}\rho v^2 + \rho g\xi + \mathcal{E}(\xi,y) = \Pi \tag{5}$$

For any given flow, the "head" Π is conserved. By using Eqs. 2 and 3, Eq. 5 is converted to an implicit expression for $\xi(y)$ as a function of y:

$$\frac{1}{2}\rho\left(\frac{\xi_\infty v_\infty}{\xi}\right)^2 + \rho g\xi - \frac{sNi}{2\pi}J_o\frac{\xi}{\xi^2 + y^2} = \Pi \tag{6}$$

The viewpoint now used to understand the implications of Eq. 6 would be familiar to a hydraulic engineer. But rather than being concerned with variations in the depth of a river, perhaps caused by an obstruction in the bottom, interest here is in the effect on the depth of the nonuniform magnetic field.

With the flow conditions, mass density, and currents i and J_o set, the left side of Eq. 6 can be plotted as a function of ξ with the longitudinal position y as a parameter. An example is shown in Fig. 9.14.2 where, because ξ measures a vertical distance, it is the ordinate. Flow conditions
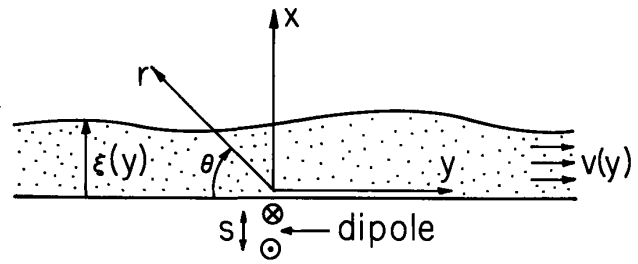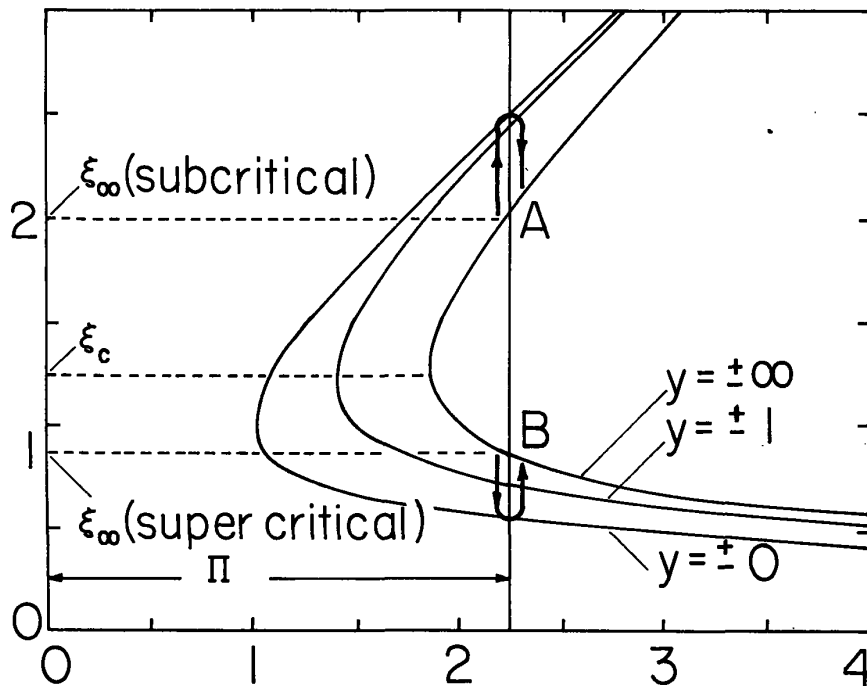

Fig. 9.14.2. Head diagram representing graphical solution of Eq. 6.
$\rho(\xi_\infty v_\infty)^2/2 = 1$, $\rho g = 1$, and $sNiJ_o/2\pi = 1$.

to the left establish Π. For the value shown, the entrance depth is either at A or B. The same head is established by a relatively deep but slowly moving entrance as by a shallower but more rapidly moving flow. The dependence of ξ on y can now be sketched by observing that flow entering at A or at B must conserve Π. Thus, entrance at depth A leads to a depth that increases between y=1 and y=0 to the values obtained by the intersections of the appropriate curves with the constant head line. Having reached the point directly over the dipole at y = 0, the depth further downstream returns to its original value at A. The result is shown in Fig. 9.14.3a.

For the entrance conditions of B in Fig. 9.14.2, the fluid depth is decreased rather than increased by the interaction. The profile is illustrated in Fig. 9.14.3b.
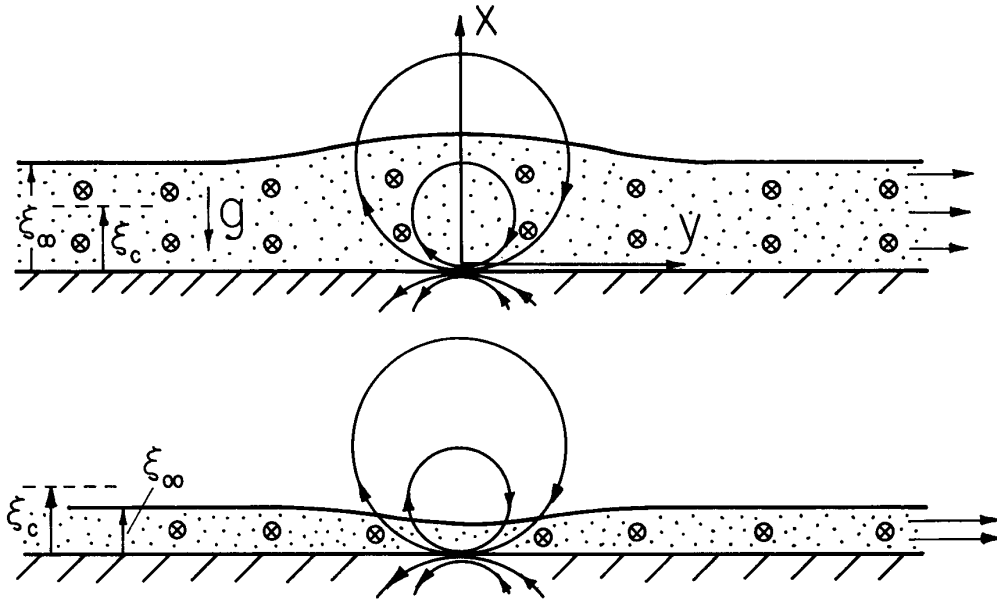

Fig. 9.14.3. Conservative transition of steady flow carrying uniform current density in z direction as it passes through field of magnetic dipole: (a) subcritical entrance; (b) supercritical entrance.

What evidently distinguishes the two entrance conditions, A and B, is their being above and below a critical depth, ξ_c, defined as the depth where the head function at y $\to$ $-\infty$ is a minimum. This critical depth is found from Eq. 6 by taking the limit y $\to$ $-\infty$, then taking the derivative with respect to ξ, setting that expression equal to zero and solving for the depth, $\xi \equiv \xi_c$. The important point is that the flow velocity obtained from Eq. 3 for this depth is

$$v = \sqrt{g\xi_c} \tag{7}$$

This is also the velocity of a shallow gravity wave on the surface of an initially stationary fluid having the depth ξ_c (see Eq. 8.9.16 with $\gamma \to 0$, $\rho_a \to 0$, and b $\to \xi_\infty$). It follows that the case of Fig. 9.14.3a is typical of what happens if the fluid enters at a velocity less than that of a gravity wave. Such an entrance flow is termed subcritical. Supercritical flow at the entrance results in a depression of the depth, as in Fig. 9.14.3b.

Shallow gravity waves propagate on the moving fluid with velocity v $\pm$ $\sqrt{g\xi}$. If the flow is subcritical, waves propagate to left and right in the entrance region and the one propagating upstream provides a mechanism for communicating the effect of the downstream field to the entrance. With supercritical flow, both gravity waves propagate to the right and there is no such mechanism. Hence, it might be expected that the steady flow established from a transient condition would depend intimately on the convection velocity relative to the wave velocity.

Any of the configurations discussed in Secs. 8.3 - 8.5 which resulted in static equilibria suggest steady flows that can be represented by quasi-one-dimensional conservative flow transitions. Examples are shown in Figs. 9.13.1 and 9.13.3.

Any of the configurations discussed in Secs. 8.3 - 8.5 which resulted in static equilibria suggest flows that can similarly undergo conservative transitions. Examples are shown in Figs. 9.13.1 and 9.13.3. If fields exist in the entrance region, there are in general electromechanical contributions to the criticality condition, reflecting the effect of the field on the propagation velocity of surface waves.

Compressible flow transitions through ducts have much in common with those described in this section. Acoustic related waves play the role of the surface waves in this section for determining the criticality conditions.

<center>GAS DYNAMIC FLOWS AND ENERGY CONVERTERS</center>

9.15 Quasi-One-Dimensional Compressible Flow Model

Gas flow through ducts having slowly varying cross-sectional areas is not only of interest in regards to understanding the performance of nozzles and diffusers, but also basic to magnetohydrodynamic and electrohydrodynamic energy conversion configurations. The basic model is developed in this section with sufficient generality that it can be applied directly to these problems in the following sections.

The duct with its rigid walls is depicted schematically in Fig. 9.15.1. In the same spirit as in Sec. 9.13 on free surface flows, the formulation is to be reduced to one involving the single independent spatial variable z. The model hinges on having a cross-sectional area $A(z)$ that varies slowly with z. Even though there is some motion transverse to the z axis, the dominant flow is in the z direction with the transverse flow of "higher order." Effects of viscosity are ignored, and hence the fluid is allowed to slip at the walls. Thus, it is assumed at the outset that the dominant velocity component, as well as the pressure and mass density, are independent of the cross-sectional position:

$$\vec{v} = v(z)\vec{i}_z; \quad p = p(z), \quad \rho = \rho(z) \tag{1}$$

The integral laws of mass, momentum and energy conservation, used in conjunction with the incremental control volume of Fig. 9.15.1, are the basis for deriving the quasi-one-dimensional differential equations. Consider first the steady form of mass conservation, Eq. 7.2.2 with $\partial\rho/\partial t = 0$ and S the surface of the incremental volume. Because there is no velocity normal to the channel walls,

$$[\rho v A]_{z+\Delta z} - [\rho v A]_z = 0 \tag{2}$$

In the limit of vanishing Δz, Eq. 2 becomes the first of the laws listed in Table 9.15.1.

Fig. 9.15.1. Schematic view of duct having slowly varying cross section $A(z)$.

The integral form of conservation of momentum, given by Eq. 7.3.3 with $\partial\vec{v}/\partial t = 0$, $\vec{F} \to -\nabla p + \vec{F}$ and $-\int_V \nabla p \, dV = \oint_S p\vec{n} \cdot d\vec{a}$, becomes

$$[\rho v^2 A]_{z+\Delta z} - [\rho v^2 A]_z + [pA]_{z+\Delta z} - [pA]_z + p\oint_C \Delta z n_z d\ell = AF_z \Delta z \tag{3}$$

Note that included is an integration over the walls of that component of the normal force acting in the z direction. An incremental section of the wall is sketched in Fig. 9.15.2. For a slowly varying cross section,

$$p\oint_C \Delta z n_z d\ell \simeq -p[A(z + \Delta z) - A(z)] \tag{4}$$

Now, substitution of Eq. 4 into Eq. 3 gives, in the limit $\Delta z \to 0$, the differential expression

$$\frac{d}{dz}(\rho v^2 A) + \frac{d(pA)}{dz} - p\frac{dA}{dz} = AF_z \tag{5}$$

The momentum conservation equation of Table 9.15.1 follows if the conservation of mass statement, Eq. (a) of the table, is used to simplify the first term. Subscripts are dropped from both v_z and F_z for convenience.
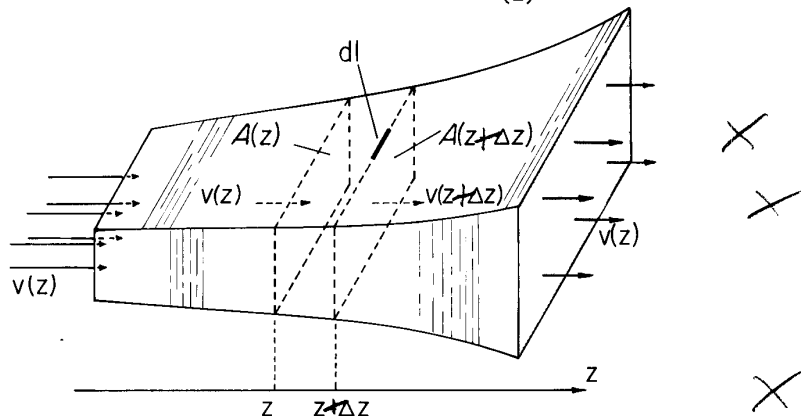
<center>9.41</center>

Table 9.15.1. Summary of quasi-one-dimensional flow equations for ideal
gas subject to force density F and power density JE.

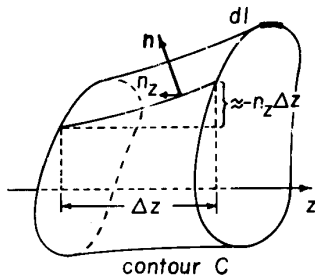| Law	Equation	
Mass conservation	$\dfrac{d}{dz}(\rho v A) = 0$	(a)
Momentum conservation	$\rho v \dfrac{dv}{dz} + \dfrac{dp}{dz} = F$	(b)
Energy conservation	$\rho v \dfrac{d}{dz}(H_T + \tfrac{1}{2}v^2) = EJ$	(c)
Mechanical state equation	$p = \rho R T$	(d)
Thermal state equation	$\delta H_T = c_p \delta T$	(e)

Fig. 9.15.2

Incremental control volume showing
normal vector $\vec{n}$ at duct walls and
cross section enclosed by contour C.

Note that the quasi-one-dimensional momentum conservation law would be correctly obtained by
simply writing the one-dimensional z component of the differential equation of motion. The misleading
inference of this finding might be that the quasi-one-dimensional model is obtained by simply writing
the one-dimensional differential laws. However, the mass conservation law gives clear evidence that
such is not the case: Eq. (a) of Table 9.15.1 is certainly not the one-dimensional form of $\nabla \cdot \rho \vec{v} = 0$
unless A is constant.

The appropriate integral form representing conservation of energy follows from integration of
Eq. 7.23.7 over the incremental volume. There is no velocity normal to the walls of the incremental
volume, and hence

$$[\rho(H_T + \tfrac{1}{2}v^2)vA]_{z+\Delta z} - [\rho(H_T + \tfrac{1}{2}v^2)vA]_z = AEJ\Delta z \qquad (6)$$

Here, E and J represent dominant components of $\vec{E}$ and $\vec{J}_f$. If the limit of vanishing Δz is taken first,
and then Eq. (a) of Table 9.15.1 exploited, Eq. (c) of that table follows.

To have a summary of the model, the mechanical and thermal equations of state for an ideal gas
are also listed in Table 9.15.1. Given the duct geometry A(z), and the field induced quantities F,
E and J, the quasi-one-dimensional model is complete.

9.16 Isentropic Flow Through Nozzles and Diffusers

By definition, a duct shaped to accelerate a gas serves as a nozzle, while one that functions as a
diffuser decelerates the flow. The actual variation of cross section depends on the gas velocity
relative to the acoustic velocity, i.e., on whether the flow is subsonic or supersonic. An immediate
objective in this section is an understanding of the relationship between duct geometry and the steady
flow evolution in a purely aerodynamic situation.

But in a broader context, the study illustrates once again how propagation effects can influence steady flow phenomena. The analogy to free surface gravity channel flows from Secs. 9.13 to 9.14 is often cited. There, gravity waves replace acoustic waves in propagating disturbances and concern is with the variation of the fluid depth ξ rather than the mass density ρ. But just as a given variation in the duct cross-sectional area A can lead to either an increased or a decreased mass density (depending on whether the flow is subsonic or supersonic), a variation in the height of the channel bottom can lead to an increased or decreased liquid depth.[1]

The wide variety of free surface electromechanical flows from Secs. 9.13-9.14 are also analogous in their behavior to the flow of compressible gas. The role of acoustic waves is played by electromechanical waves.

For the purely aerodynamic situation considered in this section, $F = 0$ and $J = 0$ in the equations of Table 9.15.1. This makes it possible to find integrals of the flow. In any case, conservation of mass as expressed by Eq. (a) of that table shows that

$$\rho v A = \rho_o v_o A_o \tag{1}$$

where subscripts o denote variables evaluated at a given position s_o. The energy conservation and thermal state equations of Table 9.15.1 show that

$$c_p T + \frac{1}{2} v^2 = c_p T_o + \frac{1}{2} v_o^2 \tag{2}$$

As a representation of momentum conservation, Eqs. (b)-(e) of Table 9.15.1 combine to give the equation of state

$$p \rho^{-\gamma} = p_o \rho_o^{-\gamma} \tag{3}$$

This manipulation is carried out without making the quasi-one-dimensional approximation with Eqs. 7.23.8-7.23.13. Recall also that the acoustic velocity is related to the local temperature by Eq. 7.23.6:

$$a = \sqrt{\gamma R T} \tag{4}$$

This last relation should be regarded only as a definition of a. Its use in the following developments in no way implies that the equations have been linearized.

The subscripts used in defining the constants of the flow are now identified with a particular position along the duct. Given v_o, p_o, T_o and ρ_o, the flow velocity, pressure, temperature and density at points downstream in the flow are to be determined. It is convenient to define the Mach number of the flow at the point o as

$$M_o = v_o/a_o = v_o/\sqrt{\gamma R T_o} \tag{5}$$

The objective is a relationship between the velocity v and the area A, with the other flow variables eliminated. Thus, from Eq. 1 the density is eliminated by writing

$$\rho = \frac{\rho_o v_o A_o}{v A} \tag{6}$$

In turn, it follows that Eq. 3 can be used to find the pressure from v and A:

$$p = p_o \left(\frac{v}{v_o}\right)^{-\gamma} \left(\frac{A}{A_o}\right)^{-\gamma} \tag{7}$$

The temperature follows from the perfect gas law and Eqs. 6-7

$$T = T_o \left(\frac{v}{v_o}\right)^{1-\gamma} \left(\frac{A}{A_o}\right)^{1-\gamma} \tag{8}$$

Now, if this last expression is introduced into Eq. 2, it can be solved for the area ratio as a function of the velocity ratio with the Mach number at the point o as a parameter:

$$\left(\frac{A}{A_o}\right) = \frac{v_o}{v} \left\{ 1 + (\gamma - 1) \frac{M_o^2}{2} [1 - \left(\frac{v}{v_o}\right)^2] \right\}^{1/1-\gamma} \tag{9}$$

---

1. For a discussion in depth, see A. H. Shapiro, Compressible Fluid Flow, Vol. I, Ronald Press Company, New York, 1953, pp. 73-105.

Given an area ratio and Mach number, Eq. 9 defines v/v_0. The remaining flow variables follow from Eqs. 6-8.

For a given gas (given γ), Eq. 9 can be represented by curves in the v/v_0 - A/A_0 plane with M_0 as a parameter. Illustrated in Fig. 9.16.1 are curves typical of flows that are supersonic and subsonic at the point o. The point (1,1) represents the flow condition at point o. Consider the subsonic flow with the Mach number at o equal to $\sqrt{0.5}$. If the area decreases, the $M_0^2 = 0.5$ trajectory requires that the velocity must increase, because the trajectory is from o to a in Fig. 9.16.1. The section behaves as a nozzle in that it increases the flow velocity. Similar arguments for trajectories b-d motivate the appearance and function of the ducts shown in Fig. 9.16.1.

Note that a supersonic flow behaves in a fashion that is just the reverse of what would be expected from simple incompressible flow concepts. An increase in the local area gives rise to an increase in the flow velocity, the duct functions as a nozzle, while the diffuser function is obtained by making a converging channel.

It is the slope of the v/v_0 - A/A_0 curve at (1,1) that determines whether the velocity increases or decreases with increasing cross-sectional area. That slope is found from Eq. 9 to be

$$\frac{d(A/A_0)}{d(v/v_0)}\bigg|_{v/v_0=1} = M_0^2 - 1 \qquad (10)$$

an expression which makes it clear that the velocity-area relationship reverses as the Mach number is increased through unity.

The trajectories of Fig. 9.16.1 make it clear that the laws used to describe the flow cannot pertain if the area is decreased by more than a critical ratio (A_c/A_0). It can be seen that as the area is reduced to this critical ratio, the flow approaches unity Mach number (see Prob. 9.16.1). The flow is then said to be choked. The existence of a greater area ratio negates the assumptions basic to the model.
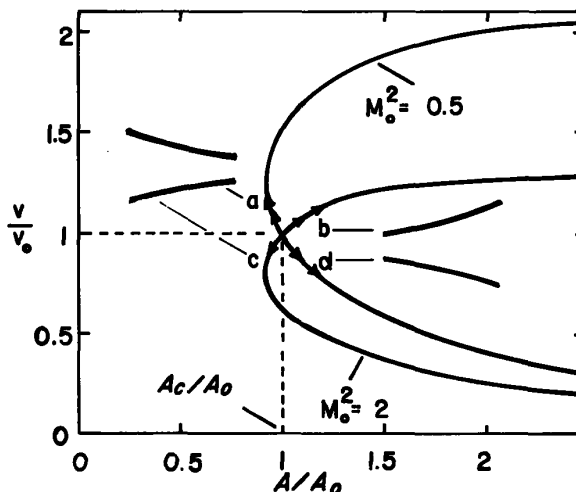

Fig. 9.16.1. Velocity-area relationship in flow transition from position "o": "a" subsonic Nozzle, "b" supersonic nozzle, "c" supersonic diffuser, and "d" subsonic diffuser. Trajectories indicated in the v/v_0 - A/A_a plane have the physical interpretation shown by the channel cross sections.

The choking crisis can be responsible for generation of shocks, highly dissipative discontinuities in the flow. To understand transitions from subsonic to supersonic flow requires combining the conservative flow transitions of this section with the shock relations to be derived in the problems.

The Laval nozzle of Fig. 9.16.2 provides the means of accelerating a stationary gas to supersonic velocities and illustrates one consequence of choking. The channel converges to a smallest cross-sectional area A_c at the throat, and then diverges. Gas enters from a large room at the left and leaves under vacuum at the right. The manometer heights record the pressure. From Eq. (b) of Table 9.15.1, it is clear that a falling pressure implies an increasing velocity and vice versa. With the pressure at the left constant, the pressure at the right is decreased by opening a valve.

The conservative transition through the channel is understood in terms of the velocity-area curves of Fig. 9.16.3. A reduction in outlet pressure causes an increase in the Mach number at the upstream position o, and hence an alteration of the curves as shown. With low pressure drop, $M_0^2 = H_0^2 < 1$, say, and the trajectory is b in the figure. The velocity first increases until the throat is reached and then decreases until the original pressure is very nearly recovered. The transition is "conservative." However, as the outlet pressure is reduced, the flow at the throat becomes sonic, as in trajectory c. It is not possible to further increase the Mach number at o. Rather a further decrease in the outlet pressure results in supersonic flow beyond the throat. This is shown, experimentally in Fig. 9.16.2c because the velocity continues to increase beyond the throat. In the supersonic region, upstream boundary conditions prevail. Hence, the supersonic region just to the right of the throat isolates the flow upstream from that downstream, and upstream flow remains essentially the same even as the outlet pressure is further reduced. But, if the supersonic region is controlled by upstream conditions, how then does the gas adjust its flow so as to match the outlet flow conditions? The shock shown to the right of the throat in Fig. 9.16.2 solves this dilemma by making an abrupt transition
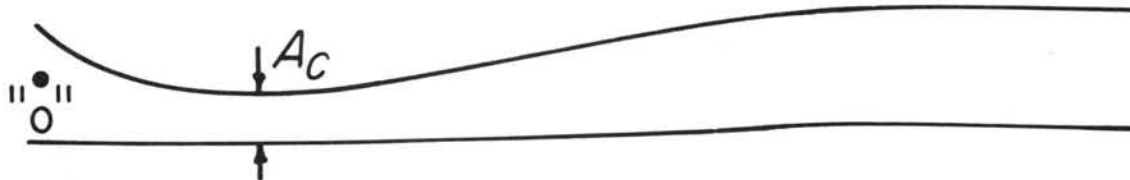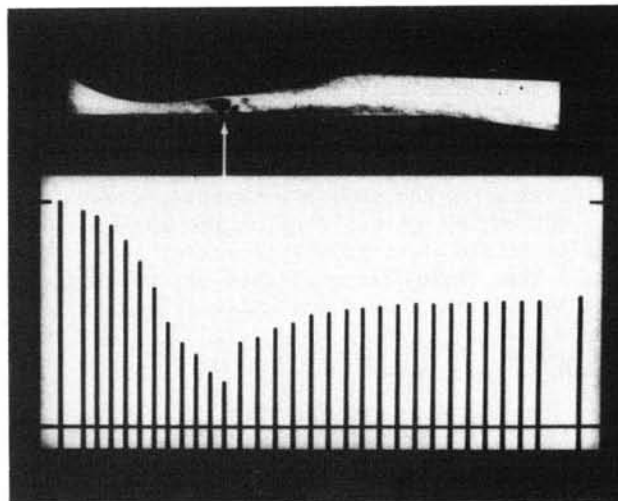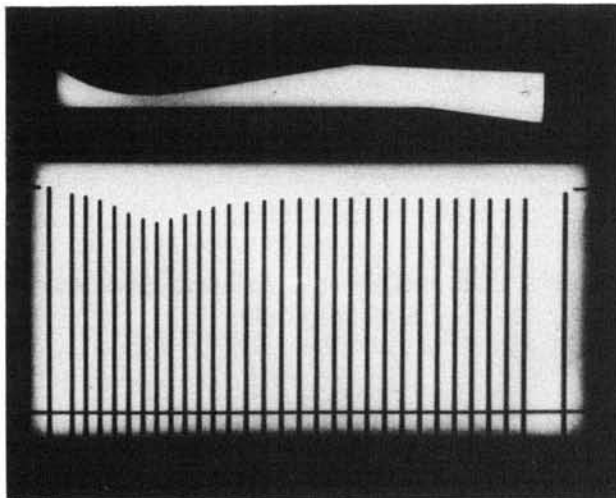
(a)

(b)   Courtesy of Education Development Center, Inc. Used with permission.   (c)

Fig. 9.16.2. Laval nozzle. (a) Cross section with flow from left to right; (b) subsonic trans-
    tion; (c) subsonic-to-supersonic transition with shock discontinuity beyond throat seen
    by Schlieren optics. From film "Channel Flow of a Compressible Fluid." (Reference 1,
    Appendix C).

from supersonic-to-subsonic flow. After the shock, the velocity decreases
rather than increases, just as is expected for a subsonic flow in a diverg-
ing section. After the shock, the channel behaves as a subsonic diffuser.
An observation to be made from the Laval nozzle is that if the flow is to
make a transition from subsonic to supersonic, then this must be done at
the throat and the flow there must be sonic.

Fig. 9.16.3. Velocity-area
    diagram showing tra-
    jectories of flow cor-
    responding to "b" and
    "c" of Fig. 9.16.2.

    Phenomena illustrated in this section have analogues in the flows
developed in Sec. 9.14. In the inhomogeneous incompressible flows,
there are also "subcritical-to-supercritical" transitions and the ana-
logue of the shock is a "jump," or sudden change in the flow accompanied
by dissipation, usually through the agent of turbulence. Shocks are taken
up in Sec. 9.20, and the analogies explored in the problems.

9.17 A Magnetohydrodynamic Energy Converter

    The magnetohydrodynamic generator shown in Fig. 9.17.1 combines the magnetic d-c interactions of
Sec. 4.10 with the compressible channel flows of Sec. 9.15. The gas is rendered electrically con-
ducting by ionization in a combustion process, and the object is to convert the thermal energy to elec-
trical form. The interaction region serves as both the turbine and the generator in a conventional
plant. From the combustion zone, the gas is accelerated to velocity v_0 at the entrance to the con-
version section by use of a nozzle, as discussed in Sec. 9.16. By virtue of its conductivity, the gas
can play the role of the armature conductors of a d-c machine as it passes through a transverse mag-
netic field imposed by an external magnet. Electrical continuity through the moving gas and an external
circuit connected to the load is provided by electrodes placed on the walls. These play the role of
brushes in a rotating d-c machine.[1]

    One of the most significant problems in making magnetohydrodynamic generators practical is the
relatively low electrical conductivities that can be attained. The conductivity is relatively small
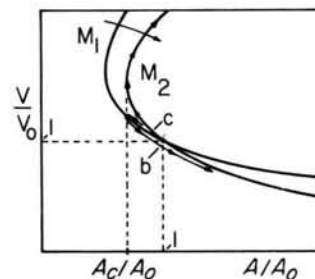
---

1. For an in-depth treatment, see G. W. Sutton and A. Sherman, Engineering Magnetohydrodynamics,
    McGraw-Hill Book Company, New York, 1965.

even at extremely high temperatures, and
although seeding of the gas and other tech-
niques are used to increase the degree of
ionization, the gas is far too low in con-
ductivity at reasonable outlet temper-
atures to make the generator a practical
substitute for existing turbine-generator
systems. As a result, such generators are
being currently developed as "topping"
units, with conventional systems used to
convert some of the significant amount of
energy remaining in the gas as it leaves
the MHD generator exit.

Fig. 9.17.1. Magnetohydrodynamic generator
configuration.

MHD Model: Because the conductivity
is relatively low, the flow can be regarded
as occurring at low magnetic Reynolds num-
ber. The effect of the flow on the mag-
netic field and current distributions is
small. The electrodes constrain the walls to
the same voltage V over the channel length:

$$\vec{E} \simeq \vec{i}_y E(z) = - \vec{i}_y \frac{V}{w(z)} \tag{1}$$

and because the upper and lower walls are magnetic surfaces, with a constant magnetomotive force
(the ampere turns driving the external magnetic circuit)

$$\vec{H} = \vec{i}_x \frac{\mathcal{F}}{d(z)} \tag{2}$$

The generator is constructed with a constant aspect ratio, so that if the width increases, so also does
the height:

$$\frac{w}{d} = \text{constant} \tag{3}$$

The objective is to determine the electrical power output, given the inlet conditions of the gas, and
either the geometry of the converter or the desired flow process. Because the power conversion den-
sity is correctly expressed as EJ, the quasi-one-dimensional model of Table 9.15.1 is applicable once
the force density F is stipulated.

The flow is at low magnetic Reynolds number so the magnetic force is essentially imposed,

$$F = -JB \tag{4}$$

Thus the magnetoquasistatic laws for the fields do not come into the formulation. However, to relate
J to E, Ohm's law for the moving fluid, as expressed by Eq. 6.2.2, is required. In terms of the model
variables,

$$J = \sigma(E + vB) \tag{5}$$

Given the voltage (or a relationship between V and the current as imposed by the external load),
E is known. Then, Eq. 5 provides the additional law needed because the additional unknown, J, is
introduced by the MHD coupling.

The electrical load connected to each pair of segments is characterized by a "loading factor" K
defined by

$$K \equiv - \frac{E}{vB} \tag{6}$$

If the object is as much electrical power output as possible, the resistance of the load on each
segment should be adjusted to make K = 1/2. This can be argued by recognizing that in terms of K,

$$J = \sigma vB(1 - K) \tag{7}$$

and hence the output power from a section of the electrodes having unit length in the z direction is

$$JVd = -J(wE)d = wd\sigma v^2 B^2(1 - K)K \tag{8}$$

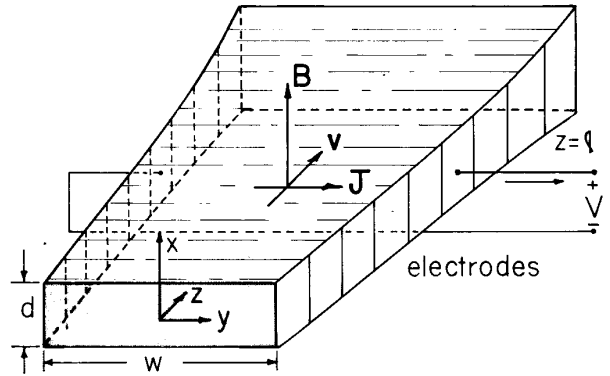With the imposed field and local flow velocity held fixed, the output power per unit length is maximum

with K = 1/2. (Note that in fact the current in turn can alter the velocity, so that the actual optimum K could be somewhat different from 1/2. Nevertheless, it is useful to think of the loading as being in the range of K = 1/2.) It is now assumed that the load is adjusted over the generator length to make K a constant.

Constant Velocity Conversion: Most likely, the geometry is considered fixed and the flow variables are to be determined. However, the generator can be designed such that one of the flow variables assumes a desired distribution throughout the generator. Following this latter approach, consider now the particular case in which the flow velocity v is to be maintained constant throughout and $A(z)$ determined accordingly.

Because $v = v_o$ = constant throughout, Eqs. (a) – (e) of Table 9.15.1 [with Eq. (b) augmented by Eqs. 4 and 6 and Eq. (c) supplemented by Eqs. 6 and 7] become

$$\rho A = \rho_o A_o \tag{9}$$

$$\frac{dp}{dz} = -\sigma v_o B^2 (1 - K) \tag{10}$$

$$\rho c_p \frac{dT}{dz} = -\sigma v_o B^2 (1 - K)K \tag{11}$$

$$p = \rho R T \tag{12}$$

The last three of these relations combine to show that ($\gamma \equiv c_p/c_v$ and $c_p - c_v = R$)

$$\frac{K dp}{p} = \frac{\gamma}{\gamma - 1} \frac{dT}{T} \tag{13}$$

Thus, integration relates the pressure and temperature:

$$\frac{p}{p_o} = \left(\frac{T}{T_o}\right)^{\gamma/[(\gamma-1)K]} \tag{14}$$

From Eq. 12, the density can be related to T:

$$\frac{\rho}{\rho_o} = \frac{p}{p_o}\frac{T_o}{T} = \left(\frac{T}{T_o}\right)^{[\gamma-(\gamma-1)K]/[(\gamma-1)K]} \tag{15}$$

In turn, the area follows from Eq. 9:

$$\frac{A}{A_o} = \frac{\rho_o}{\rho} = \left(\frac{T}{T_o}\right)^{-[\gamma-(\gamma-1)K]/[(\gamma-1)K]} \tag{16}$$

With these last three equations, it is clear that a determination of $T(z)$ would lead to a specification of all flow variables. The temperature is simply obtained from Eq. 11 which can be written as

$$\frac{dT}{dz} = - \frac{\sigma v (AB^2)(1 - K)K}{(A\rho)c_p} \tag{17}$$

and since $A\rho$ and AB^2 are constants (see Eqs 9, 2 and 3), the term on the right is constant. Integration therefore gives a linear dependence of temperature on distance:

$$\frac{T}{T_o} = 1 - (\sigma v_o \mu_o \ell)\left(\frac{\mu_o H_o^2}{\rho_o c_p T_o}\right)(1 - K)K\left(\frac{z}{\ell}\right) \tag{18}$$

The pressure, density and area then follow from Eqs. 14 – 16. With a loading factor K = 0.5 and γ = 1.5, the exponential in Eq. 15 is 5. Thus, the gas density decreases while, from Eq. 16, the channel area must be made to increase. The electrical power out per unit length is given by Eq. 8. Because B varies inversely with d and the aspect ratio is constant, the power out per unit length is independent of z. Thus the total power output is obtained by evaluating Eq. 8 at the inlet and multiplying by the channel length ℓ:

$$V \int_o^\ell dJ dz = (w_o d_o)(\ell \sigma v_o \mu_o) v_o \mu_o H_o^2 (1 - K)K \tag{19}$$

Here, the power output is written as the product of an "active" area $w_o d_o$, a magnetic Reynolds number based on the channel length, a product of magnetic pressure and velocity and a dimensionless factor representing the degree of loading. Thus, the generator output takes the form of an area-velocity-magnetic-pressure product, familiar from Sec. 4.15. The modifying factor of the magnetic Reynolds number is present because it is the alteration in magnetic stress caused by the current that accounts for the interaction with the field. The magnetic Reynolds number is the ratio of the induced-to-the-imposed magnetic field. Thus, one component of H_o^2 in the magnetic pressure term represents the imposed field, and the product of the other value of H_o and R_m represents the spatial variations in $\vec{H}$ induced by the motion.

Given the temperature T_d at the generator outlet where $z = \ell$, the electrical power output is alternatively evaluated using Eq. (c) of Table 9.15.1. The negative of the right-hand side, integrated over the generator volume, is the total electric power output, while the integral of the left side is simply mass rate of flow multiplied by the drop in specific enthalpy. Hence, because $\rho v A$ is constant

$$ V \int_o^\ell dJ dz = \rho_o v_o A_o (H_T^o - H_T^d) \tag{20} $$

where $H_T(z = \ell) \equiv H_T^d$. For an ideal gas, $H_T = c_p T$, and with the use of Eq. 18 for the temperature, Eq. 20 is identical to Eq. 19. As seen from Eq. (c) of Table 9.15.1, if the generator operates with a variable velocity, then it is the stagnation specific enthalpies $H_T^* = H_T + \frac{1}{2}v^2$ that appear in Eq. 20. Why is it that even though there is ohmic heating accounted for by $\vec{J} \cdot \vec{E}$, all of the drop in enthalpy turns up as electrical power output? The answer comes from recognizing that the electrical heating is of the gas itself. Hence, heating at one position results in thermal energy storage which can be recovered downstream. Ohmic heating in the electrodes or external conductors that is removed from the system is another matter and subtracts from the right-hand side of Eq. 20.

There is of course a price paid even for the ohmic heating of the gas itself. This can best be appreciated by inserting the generator into a thermodynamic cycle and seeing how the increase in entropy caused by the ohmic dissipation dictates an increased heat rejection and hence a diminished overall efficiency. This is discussed in Sec. 9.19.

The increase in entropy through the generator is evaluated by using the pressure and density ratios found with Eqs. 14 and 15 in the entropy equation of state for a perfect gas, Eq. 7.23.12:

$$ S_T = S_T^o - c_p \frac{(1-K)}{K} \ln \left(\frac{T}{T_o}\right) \tag{21} $$

Thus, the decrease in temperature predicted by Eq. 18 is accompanied by an increase in the specific entropy, S_T.

Fig. 9.17.2. Flow evolution through MHD generator of Fig. 9.17.3 with $A(z)$ and hence $a(z)$ designed to give constant velocity.

To summarize, the area distribution has been designed to make $v = v_o$ throughout, with the other flow conditions represented by Eqs. 14, 15, 18, and 21. Evolution of the flow is typified by Fig. 9.17.2. The temperature decreases with z in a linear fashion. For $\gamma = 1.5$ and $K = 1/2$, the area ratio A/A_o and specific volume are then proportional to $(T/T_o)^{-5}$ and hence increase with z. According to Eq. 3, this means that d/d_o is proportional to $(T/T_o)^{-5/2}$. The pressure varies as $(T/T_o)^6$ and hence drops even more rapidly than the temperature. Some of the implications of these characteristics for an energy conversion system are explored in Sec. 9.19.

Finally, observe that because the acoustic velocity is proportional to $T^{\frac{1}{2}}$ (Eq. 7.23.14) and hence increasing with z, while v is constant, the Mach number is increasing. This suggests the alternative mode of operation of Prob. 9.17.1.

9.18 An Electrogasdynamic Energy Converter

Just as the MHD convertor of Sec. 9.17 is a variation on the d-c magnetic machines of Sec. 4.10, the electrogasdynamic or EGD device of Fig. 9.18.1 is closely related to the Van de Graaff machine of Sec. 4.14.

Electromechanical coupling is through the free charge force density $\rho_f \vec{E}$. With the objective of obtaining a net space charge, and hence an electrical force density on the gas, charged particles are
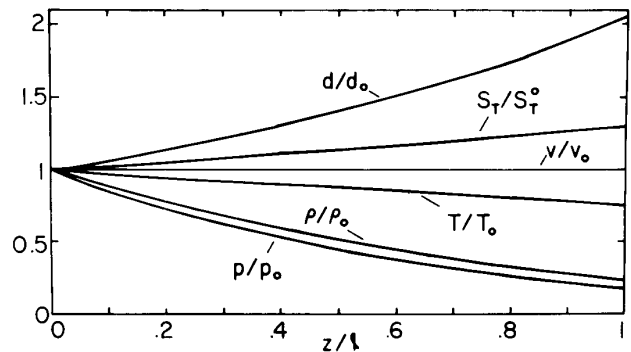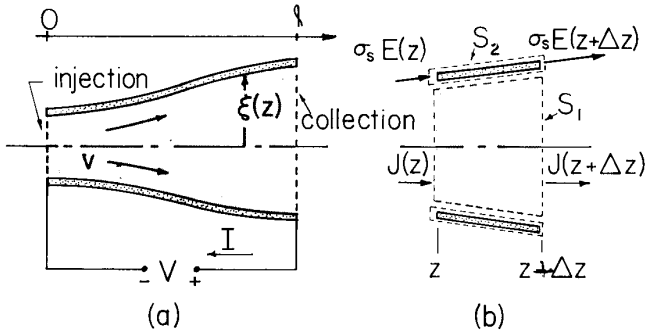
Fig. 9.18.1

Cross section of circular EGD conversion channel having walls with surface conductivity σ_s. (a) Charge is injected at the left and removed at the right. (b) Incremental volume element for deriving quasi-one-dimensional model

injected at the left and removed at the right, thus giving rise to the generator current I. Although ions can be used, charged solid particles or droplets are used to achieve small electrical losses. These particles are of sufficient size to insure that their slip velocity relative to the gas is small compared to the gas velocity. Once charged, the particles can be modeled as having a velocity proportional to the electric field intensity, with the constant of proportionality the mobility b. In the frame of the gas, the current density is $\vec{J}_f' = \rho_f b \vec{E}'$, and hence in the laboratory frame the electroquasistatic transformations give

$$\vec{J}_f = \rho_f(b\vec{E} + \vec{v}) \tag{1}$$

The first objective in this section is a substantive discussion of the electric field alternative to MHD energy conversion. A second is the illustration of how the quasi-one-dimensional modeling extends into the electrical side of the interaction when the effects of the motion on the field are dominant. Thus, by contrast to the low magnetic Reynolds number limit used in Sec. 9.17, considered here are interactions with entrained particles of sufficiently low mobility that the distribution of charge is strongly influenced by the motion. This necessitates a self-consistent electromechanical formulation and the augmentation of the quasi-one-dimensional mechanical equations formulated in Sec. 9.15. Because of limits on achievable electric pressure imposed by electrical breakdown, it is difficult to demonstrate much of a reaction on the flow from the electrical forces. Nevertheless no restrictions are made in that regard.

The EGD Model: The development of a model serves to further describe the nature of the interaction. It hinges on there being no interest in the distribution of the charge over the channel cross section. In fact, the flow is likely to be turbulent with an associated mixing that makes the charge density uniform over a given duct cross section. The generated field $E_z \equiv E(z)$ is also assumed to be constant over the cross section. The radial field E_r is defined as that evaluated adjacent and normal to the wall. The cross section is circular with radius ξ so that $A(z) = \pi\xi^2(z)$.

Conservation of charge for the control volume of incremental length Δz in Fig. 9.18.1b requires that

$$[\rho_f(bE + v)A]_{z+\Delta z} - [\rho_f(bE + v)A]_z + \rho_f bE_r 2\pi\xi\Delta z = 0 \tag{2}$$

The first two terms account for charged particles leaving and entering the volume in the z direction traveling with the velocities $bE + v$. With the last term, it is recognized that in the gas, unlike on the belt of a conventional Van de Graaff machine, a transverse electric field E_r can cause particle motion relative to the gas with as much ease as the axial field E. Thus, there is in general a current to the wall represented by the last term in Eq. 2.

To understand what determines the radial field E_r, it is necessary to specify the physical nature of the wall. Here it is modeled as having a surface conductivity σ_s, so that current carried to the wall is then carried along the walls to the electrical terminals. The conservation of charge equation, now applied to an annular volume with surface S_2 enclosing the section of wall having length Δz, requires that

$$\rho_f bE_r 2\pi\xi\Delta z = [2\pi\xi\sigma_s E]_{z+\Delta z} - [2\pi\xi\sigma_s E]_z \tag{3}$$

A further and important relation between E and the space-charge density is written using the integral form of Gauss' law for the surface S_1 of Fig. 9.18.1b:

$$[\varepsilon_o\pi\xi^2 E]_{z+\Delta z} - [\varepsilon_o\pi\xi^2 E]_z + \varepsilon_o 2\pi\xi E_r \Delta z = \rho_f\pi\xi^2\Delta z \tag{4}$$

The first two terms account for electric displacement through the surfaces with normals in the $\pm z$ directions, while the third is the net radial flux.

The differential equations describing the electrical side of the coupling are found by taking the limits $\Delta z \to 0$ of Eqs. 2-4, and are summarized now by

$$\frac{d}{dz} [\rho_f(bE + v)\xi^2\pi] + 2\rho_f bE_r\xi\pi = 0 \tag{5}$$

$$\sigma_s \frac{d}{dz} (\xi E) - \rho_f bE_r\xi = 0 \tag{6}$$

$$\frac{d}{dz} (\xi^2 E) + 2\xi E_r - \frac{\rho_f\xi^2}{\varepsilon_o} = 0 \tag{7}$$

Without raising the order of Eqs. 5 and 7, E_r is eliminated in these equations by using Eq. 6:

$$\frac{d}{dz} [\rho_f(bE + v)\pi\xi^2 + 2\pi\sigma_s\xi E] = 0 \tag{8}$$

$$\frac{d}{dz} (\xi^2 E) + \frac{2\sigma_s}{\rho_f b} \frac{d}{dz} (\xi E) = \frac{\rho_f\xi^2}{\varepsilon_o} \tag{9}$$

In addition to these two statements, representing the electrical side of the interaction, there are the mechanical relations from Table 9.15.1, with $F = \rho_f E$ and EJ reflecting the fact that the wall is thermally insulated and insulating, so that electrical heat losses in the wall are also available to the gas. Thus, the incremental volume used in deriving the quasi-one-dimensional model (Fig. 9.15.2 and Eq. 9.15.6) includes a section of wall having length Δz,

$$\frac{d}{dz} (\rho v\pi\xi^2) = 0 \tag{10}$$

$$\rho v \frac{dv}{dz} + \frac{dp}{dz} = \rho_f E \tag{11}$$

$$\rho v \frac{d}{dz} (c_p T + \frac{1}{2} v^2) = \rho_f E(bE + v) + \frac{2\sigma_s E^2}{\xi} \tag{12}$$

$$p = \rho RT \tag{13}$$

Given $\xi(z)$, these last six expressions describe the evolution of the flow in terms of the six independent variables ρ_f, E, v, ρ, p and T. The terminal variables are then given by evaluating

$$I = \rho_f(bE + v)\pi\xi^2 + 2\pi\xi\sigma_s E \tag{14}$$

$$V = - \int_o^\ell Edz \tag{15}$$

Note that according to Eq. 8, I is the same evaluated at any position, z.

In view of Eqs. 10, 14 and 15, the energy equation, Eq. 12, can be multiplied by the area $\pi\xi^2$ and integrated from the entrance to the exit to show that

$$\pi\xi_o^2\rho_o v_o[(H_T + \frac{1}{2} v^2)_{z=\ell} - (H_T + \frac{1}{2} v^2)_{z=0}] = I \int_o^\ell Edz = -VI \tag{16}$$

That is, the difference between entrance and exit enthalpy plus kinetic energy is equal to the electrical power output. Electrical heating, due to particle slip in the gas and ohmic heating in the wall, is to some extent recovered downstream. However, the ohmic heating does show up as an increase in entropy at the outlet.

Problem 9.18.3 illustrates how the equations are written in a form convenient for numerical integration. The formulation is similar to that for the MHD generator in Sec. 9.17. However, because the field variables are as much a part of the coupling as are the flow variables, E and ρ_f play roles on a par with ρ, v, etc. The channel geometry can be regarded as given and the flow determined, or the dependence of one of the field or flow variables on z can be specified and the geometry determined along with the other variables.

Electrically Insulating Walls: Physically, Eq. 8 requires that the sum of the total convection and conduction currents in the gas and the conduction current in the wall passing any position z must be the same at any other z. Equation 9 is Gauss law, written to the exclusion of E_r so as to make possible a comparison between radial and longitudinal electric fields in accounting for the space charge. If the wall equivalent conductivity σ_s/ξ is large compared to the equivalent bulk conductivity $\rho_f b$, then most of the images for the space charge are at the same axial position on the duct walls. But in the opposite extreme where

$$\frac{2\sigma_s}{\xi \rho_f b} << 1 \tag{17}$$

space charge results mainly in the divergence of an axial field E and the radial field is negligible. If, in addition to Eq. 17, the wall current is negligible compared to that in the gas,

$$\rho_f (bE + v)\xi^2 >> 2\sigma_s \xi E \tag{18}$$

then the last term in Eq. 8 is ignorable. If the wall is sufficiently electrically insulating compared to the volume that both Eqs. 17 and 18 are satisfied, then the radial electric field can be ignored in Eqs. 5 and 7. Physically, this is because a surface charge of the same polarity as the space charge builds up on the walls. This surface charge is just that required to make the electric field be tangential to the wall.

Although the quasi-one-dimensional model presumes that the channel cross section is a slowly varying function of z, it does not presume that the channel is short. Geometrically, the channel would be made to look similar to a Van de Graaff generator. But what has been learned is that using a homogeneous substance such as the gas to replace the belt of a Van de Graaff machine results in a steady-state space-charge field that is of necessity in the same direction as the generated field. This is in contrast to the Van de Graaff machine. The only way to make the space-charge field predominantly perpendicular to z is to make the wall compete for an appreciable fraction of the generated current. This may be practical for the generation of high voltages, but because it implies an electrical loss in the walls on the same order or greater than that generated, it is impractical in making bulk power.

Note that the inequality of Eq. 17 also justifies ignoring the last term in the energy equation, Eq. 12, compared to the first term on the right. Thus, for an insulating wall the appropriate model is represented by Eqs. 8-13 with $\sigma_s \to 0$.

Zero Mobility Limit with Insulating Wall: For efficient generation, it is desirable that the mobility be sufficiently small that

$$|bE| << v \tag{19}$$

in which case bE can be ignored in Eqs. 8 and 12. Limitations on wall conductivity implied by Eq. 17 become even more stringent as it is again assumed that terms in Eqs. 8, 9 and 12 proportional to σ_s are negligible.

With zero mobility, conservation of charge and mass, Eqs. 8 and 10, show that

$$\frac{\rho_f}{\rho} = \frac{I}{\rho_d \xi_d^2 \pi v_d} \tag{20}$$

where the subscript d denotes variables evaluated at the downstream end of the generator where z = ℓ. Thus, the force equation, Eq. 11, becomes

$$\frac{d}{dz} \left[\frac{1}{2} v^2 + \left(\frac{I}{\rho_d \xi_d^2 \pi v_d}\right) \Phi\right] + \frac{1}{\rho} \frac{dp}{dz} = 0 \tag{21}$$

where the potential, Φ, is defined by $E = -d\Phi/dz$. Similarly, the energy equation, Eq. 12, becomes

$$\frac{d}{dz} \left[c_p T + \frac{1}{2} v^2 + \left(\frac{I}{\rho_d \xi_d^2 \pi v_d}\right) \Phi\right] = 0 \tag{22}$$

These last two expressions make it clear that the duct flow with no electrical coupling is equivalent to that with coupling if we replace $\frac{1}{2} v^2 \to (\frac{1}{2} v^2 + I\Phi/\rho_d \xi_d^2 \pi v_d)$. Thus, the flow is isentropic, as can be seen by manipulating Eqs. 21 and 22, together with the mechanical equation of state to obtain Eq. 7.23.13:

$$\frac{p}{p_d} = \left(\frac{\rho}{\rho_d}\right)^\gamma = \frac{\rho}{\rho_d}\frac{T}{T_d} \tag{23}$$

Of course, this must be true because the rate of heat generation is zero in the limit $\sigma_s \to 0$ and then $b \to 0$.

Constant Velocity Conversion: Suppose that the channel is designed to implement a constant gas velocity $v = v_d$ throughout. Then Eqs. 8 and 10 show that

$$\rho_f \xi^2 = \rho_{fd}\xi_d^2; \quad \rho\xi^2 = \rho_d\xi_d^2 \tag{24}$$

and the right-hand side of Eq. 9, representing Gauss' law, is constant, so that that expression can be integrated to obtain

$$\xi^2 E = - \xi^2 \frac{d\Phi}{dz} = \frac{\rho_{fd}}{\epsilon_o} \xi_d^2 (z - \ell) \tag{25}$$

Here, the generator is designed (ξ prescribed) for constant velocity operation with E at the outlet adjusted to zero. This is motivated by an interest in generator operation and hence a desire to impose as large a net electric force in the $-z$ direction as possible.

The temperature is related to the area variation by combining Eqs. 23 and 24b:

$$\frac{T}{T_d} = \left(\frac{\xi_d}{\xi}\right)^{2(\gamma-1)} \tag{26}$$

The quantity in brackets in Eq. 22 is constant, and hence relates the temperature of Eq. 26 to the potential. Thus, the potential is defined as V at $z = \ell$ and also written in terms of ξ^2.

$$\Phi = V + (T_d - T)\frac{c_p \rho_d \xi_d^2 \pi v_d}{I} = V + \frac{c_p \rho_d \xi_d^2 \pi v_d T_d}{I}\left[1 - \left(\frac{\xi_d}{\xi}\right)^{2(\gamma-1)}\right] \tag{27}$$

Now, by substituting Eq. 27 for the potential in Eq. 25, an expression is obtained for the cross section as a function of z. Integration, and the condition that $\xi(\ell) = \xi_d$, gives

$$\frac{\xi^2}{\xi_d^2} = \left\{1 - \left[\frac{(\rho_{fd}\ell)^2(2-\gamma)}{2\epsilon_o \rho_d c_p T_d (\gamma-1)}\right]\left(1 - \frac{z}{\ell}\right)^2\right\}^{1/(2-\gamma)} \tag{28}$$

where the definition of $I \equiv \rho_{fd}\pi\xi_d^2 v_d$ has been used. With this result, Eqs. 24-27 give the dependence of ρ_f, ρ, E, T and Φ on z. The normalized distance upstream from the exit is $(1 - z/\ell)$. Thus, the duct radius is least at the inlet and increases to its maximum at the exit. The temperature therefore decreases in accordance with Eqs. 26 and 28, as it must if the velocity is to remain constant and yet electrical power is to be removed.

The major limitation on an electric field device is likely to be the maximum electric stress that can be developed without causing sparking. From Eq. 25 it is clear that the most critical point in this regard is at the inlet where $E = E_o$ is evaluated using Eqs. 25 and 28 with $z = 0$. From Eq. 25, it follows that $\rho_{fd} = -(\epsilon_o E_o/\ell)(\xi_o/\xi_d)^2$. Then, if that result is used in Eq. 28 also evaluated at $z = 0$, and it is recognized from Eqs. 26 and 23 that $T_d = T_o(\xi_o/\xi_d)^{2(\gamma-1)}$ and hence $\rho_d = \rho_o(\xi_o/\xi_d)^2$, it follows that the area ratio and largest electric pressure (normalized to the entrance enthalpy) are related by

$$\frac{\epsilon_o E_o^2/2}{\rho_o c_p T_o} = \left(\frac{\gamma-1}{2-\gamma}\right)\left[\left(\frac{\xi_d^2}{\xi_o^2}\right)^{2-\gamma} - 1\right] \tag{29}$$

Given the thermal entrance conditions and γ, the maximum electric field consistent with electrical breakdown serves to determine the area ratio. In turn, all of the other parameters are then determined. For example, the ratio of electrical power out to thermal power entering the duct is found from combining Eqs. 26, 27 (evaluated at $z = 0$ where $T = T_o$ and $\Phi = 0$) and 29:

$$\frac{VI}{\rho_o c_p T_o \xi_o^2 \pi v_o} = 1 - \left[\left(\frac{2-\gamma}{\gamma-1}\right)\frac{(\epsilon_o E_o^2/2)}{\rho_o c_p T_o} + 1\right]^{-\left(\frac{\gamma-1}{2-\gamma}\right)} \tag{30}$$

Thus, the entrance ratio of electric pressure to thermal energy per unit volume determines the fraction of thermal energy that can be extracted in a single stage device. To see that the electrical power output is again approximated by an area-velocity-electric-pressure product, consider the particular case where $\gamma = 1.5$ (compared to 1.4 for air). Then, Eq. 30 becomes

$$VI = \pi \xi_o^2 v_o (\tfrac{1}{2} \epsilon_o E_o^2) \left[1 + \frac{\tfrac{1}{2} \epsilon_o E_o^2}{\rho_o c_p T_o} \right]^{-1} \tag{31}$$

The factor modifying the expected form $Av(\tfrac{1}{2} \epsilon_o E_o^2)$ insures that as the electric pressure is increased, the output saturates and never exceeds the available thermal power.

In practice, even with the use of high pressures and electronegative gases to prevent sparking, the electric pressure is likely to be small compared to $\rho_o c_p T_o$. One way to scale the conversion magnitude upward in spite of this is to use many of the individual converters in series, so as to extract a reasonable fraction of the available energy. However, frictional losses (which are ignored here) are likely to give pressure drops on the order of $\tfrac{1}{2} \epsilon_o E_o^2$, and create a source of entropy that cannot easily be made manageable by multiple staging. Frictional losses are reduced if the walls are essentially removed and the charged stream is allowed to expand in a "natural" fashion. Some developments are along these lines,[1] with momentum transferred from the expanding stream to a second recirculating flow.

9.19 Thermal-Electromechanical Energy Conversion Systems

To appreciate the limitations imposed on engines that convert heat into electrical power through an electromechanical process, the converter must be seen in the overall context of a steady-state cycle. Use made of thermal energy available in a fuel depends primarily on thermodynamic considerations, and cycle refinements such as reheat loops are essential to the achievement of efficiencies such as are found in modern power systems. Objectives in this section are served by considering a basic system, with refinements a subject in itself.

In the steady state, a process can be characterized by what happens to enthalpy, volume and entropy of a given mass as it passes through its cycle. Thus, the specific extensive variables H_T, ρ^{-1} and S_T are used along with pressure, temperature and velocity to represent the state of a system at a given position in the cycle. The understanding is that the enthalpy, for example, passing a given location in time Δt is $(Av\Delta t)\rho H_T$.

Either the MHD or EGD converter can be the generator in the cycle of Fig. 9.19.1. The state of a unit mass of the fluid as it passes a given station denoted by a-e in Fig. 9.19.1 is given by the state-space trajectories of Fig. 9.19.2.

Regardless of the cycle, it is important to first recognize the relationship between variables implied by the state equation for a perfect gas. The entropy and mechanical state equations, Eqs. 7.23.12 and 7.22.1, relate T to S_T with p as a parameter, as required for the T-S_T diagram:

$$\frac{T}{T_o} = (\frac{p}{p_o})^{(\gamma-1)/\gamma} \exp\left(\frac{S_T - S_T^o}{\gamma c_v} \right) \tag{1}$$

Fig. 9.19.1. Open cycle with either MHD or EGD generator.

Hence, the lines of constant pressure shown in Fig. 9.19.2a. For Fig. 9.19.2b the same state equations are solved for the pressure as a function of the specific volume ρ^{-1} with S_T as a parameter:

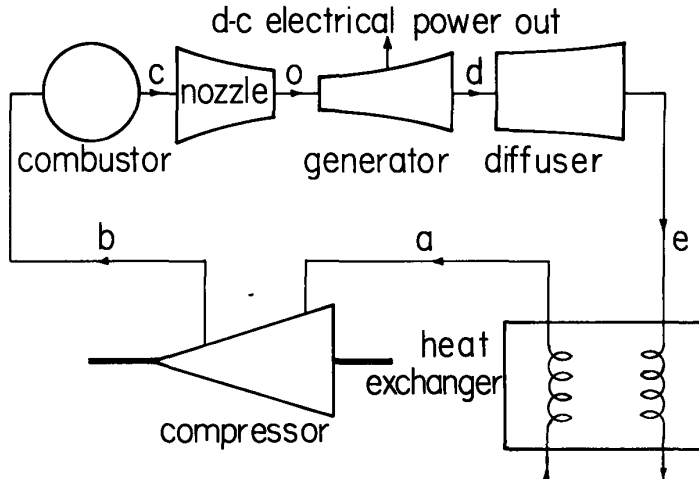$$\frac{p}{p_o} = (\frac{\rho_o}{\rho})^{-\gamma} \exp\left(\frac{S_T - S_T^o}{c_v} \right) \tag{2}$$

1. M. O. Lawson and J. A. Decaire, "Investigation on Power Generation Using Elecrofluid-Dynamic Processes," Intersociety Energy Conversion Engineering Conference, Miami Beach, Florida, August 13-17, 1967 (participating societies including ASME, IEEE and AIAA).
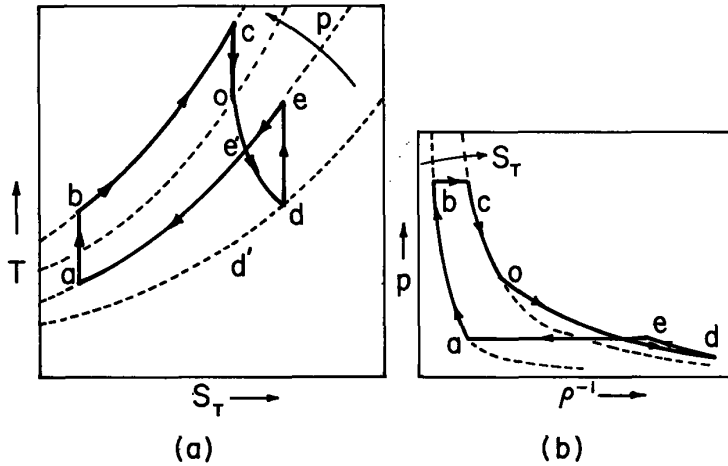
Fig. 9.19.2

(a) Temperature-specific entropy
trajectory for cycle of Fig. 9.19.1.
Broken lines are at constant pres-
sure; (b) pressure-specific volume
trajectory, broken lines are at
constant entropy.

The physical position in the cycle of a unit mass of the gas and its state at each position are
now described beginning with a. The cycle might be "open," in that ambient air is taken in at a with
temperature and pressure thereof pinned to atmospheric conditions. Open cycle or not, it is desirable
to make the compression from a to b essentially isentropic.

Combustion involves the working gas as a primary constituent and results in heat addition from
b to c. At this point the gas is essentially at rest. From c to o the nozzle converts some of the
thermal energy into kinetic form, ideally through an isentropic expansion. The developments of
Sec. 9.16 therefore describe the nozzle and, subsequently, the diffuser. According to Eq. 9.16.2,

$$H_T^c = H_T^o + \frac{1}{2} v_o^2 \tag{3}$$

where H_T^c is the "stagnation enthalpy" in the combustor and o denotes entrance conditions to the
generator (nomenclature consistent with Secs. 9.17 or 9.18).

From o to d is described in the previous two sections. For example, in the MHD interaction
the T-S_T relation through the generator is Eq. 9.17.21, and the p - ρ^{-1} relation follows from
Eqs. 9.17.14 and 9.17.15:

$$\frac{T}{T_o} = \exp \left[\frac{-(S_T - S_T^o)K}{c_p(1 - K)} \right] \tag{4}$$

$$\frac{p}{p_o} = \left(\frac{\rho^{-1}}{\rho_o^{-1}} \right)^{-\gamma/[\gamma-(\gamma-1)K]} \tag{5}$$

The thermodynamic state reflected in the plots is not the whole story. There is also a change in
kinetic energy in the transitions from c → e. Upon reaching d, the gas has a residual kinetic energy
and to complete the cycle the process by which it is brought to rest with the same ambient conditions
as a must be specified. First the gas is brought to rest, d → e, in as nearly an isentropic manner
as possible using a subsonic diffuser. Again, using Eq. 9.16.2,

$$H_T^d + \frac{1}{2} v_d^2 = H_T^e \tag{6}$$

Then, by means of a heat exchanger, or simply by expelling the gas to the atmosphere, the gas is
returned to ambient temperature and pressure. For the latter, heat rejection from e → a represents
a loss of energy and a major contribution to the overall inefficiency. A regeneration system recovering
some of the rejected heat is described in Prob. 9.19.1.

An overview of the energy conversion cycle comes from representing the system by the specific
enthalpy. To this end, note that in the steady state, the combined internal and kinetic energy con-
servation statement for a volume V enclosed by a surface S is the integral form of Eq. 7.23.7. Vis-
cous and thermal losses are neglected, so that

$$\int_V \vec{E} \cdot \vec{J}_f dV = \oint_S \rho \vec{v}(H_T + \frac{1}{2} \vec{v} \cdot \vec{v}) \cdot \vec{n} da \tag{7}$$

As derived, the left side of this expression is the sum of the total ohmic heating and work done by external forces (Eq. 7.23.1 or 7.23.2).

First, think of the ohmic heating as equivalent to the heat of combustion and apply Eq. 7 to the combustor. In the combustor, the kinetic energy is ignorable and therefore Eq. 7, divided by the mass rate of flow, becomes

$$\frac{\text{thermal energy input/unit time}}{\text{mass/unit time}} = \frac{A\rho v(H_T^c - H_T^b)}{A\rho v} = H_T^c - H_T^b \tag{8}$$

Second, Eq. 7 is applied to the converter section, where the left-hand side becomes the negative of the electrical power output:

$$\frac{\text{electrical power output}}{\text{mass/unit time}} = \frac{VI}{A\rho v} = A\rho v \frac{[(H_T^o + \frac{1}{2}v_o^2)-(H_T^d + \frac{1}{2}v_d^2)]}{A\rho v} = H_T^c - H_T^e \tag{9}$$

Here, the third equality brings in the nozzle and diffuser functions, represented by Eqs. 3 and 6.

Third, Eq. 7 is used to represent the compressor. This time, the left side represents mechanical work done by an external force density of mechanical origin:

$$\frac{\text{compressor energy input/unit time}}{\text{mass/unit time}} = H_T^b - H_T^a \tag{10}$$

Finally, with the neglect of electrical losses (other than in the MHD or EGD generator), heat transfer losses and frictional losses, the overall efficiency can be written as

$$\eta = \frac{\text{electrical power out - compressor power}}{\text{thermal power in}} = \frac{(H_T^c - H_T^e)-(H_T^b - H_T^a)}{H_T^c - H_T^b} \tag{11}$$

Written as it is in terms of the specific enthalpy, this relation is quite general. For an ideal gas $H_T = c_v T$ and Eq. 11 takes a form emphasizing the importance of having a high combustor temperature:

$$\eta = \frac{(T_c - T_e) - (T_b - T_a)}{T_c - T_b} \tag{12}$$

It is now possible to see why an entropy increase in the generator implies a loss of efficiency. If the generator operated isentropically, then points e and d in Fig. 9.19.2a would become points e' and d'; thus $T_c - T_e$ would be increased in Eq. 12 with the result an improvement in efficiency.

By writing Eq. 11 in the equivalent form

$$\eta = \frac{(H_T^c - H_T^b) - (H_T^e - H_T^a)}{H_T^c - H_T^b} = \frac{\text{heat in - heat rejected}}{\text{heat in}} \tag{13}$$

it is seen that the entropy increase requires a greater heat rejection and for that reason a decreased efficiency.

Note that the rejected heat could be put to useful purposes, for example in heating or refrigerating buildings. The high priority put on increasing the efficiency as defined by Eq. 13 reflects the presumption that the heat rejected is indeed wasted.